

Utah State University

DigitalCommons@USU

---

All Graduate Theses and Dissertations

Graduate Studies

---

5-2008

## Distributed Hydrologic Modeling for Streamflow Prediction at Ungauged Basins

Christina Bandaragoda  
*Utah State University*

Follow this and additional works at: <https://digitalcommons.usu.edu/etd>



Part of the [Civil and Environmental Engineering Commons](#)

---

### Recommended Citation

Bandaragoda, Christina, "Distributed Hydrologic Modeling for Streamflow Prediction at Ungauged Basins" (2008). *All Graduate Theses and Dissertations*. 62.  
<https://digitalcommons.usu.edu/etd/62>

This Dissertation is brought to you for free and open access by the Graduate Studies at DigitalCommons@USU. It has been accepted for inclusion in All Graduate Theses and Dissertations by an authorized administrator of DigitalCommons@USU. For more information, please contact [digitalcommons@usu.edu](mailto:digitalcommons@usu.edu).



DISTRIBUTED HYDROLOGIC MODELING  
FOR STREAMFLOW PREDICTION AT UNGAUGED BASINS

by

Christina Bandaragoda

A dissertation submitted in partial fulfillment  
of the requirements for the degree

of

DOCTOR OF PHILOSOPHY

in

Civil and Environmental Engineering

UTAH STATE UNIVERSITY  
Logan, UT

2007

## ABSTRACT

Distributed Hydrologic Modeling for Prediction  
of Streamflow at Ungauged Basins

by

Christina Bandaragoda, Doctor of Philosophy

Utah State University, 2008

Major Professor: Dr. David G. Tarboton  
Department: Civil and Environmental Engineering

Hydrologic modeling and streamflow prediction of ungauged basins is an unsolved scientific problem as well as a policy-relevant science theme emerging as a major challenge to the hydrologic community. One way to address this problem is to improve hydrologic modeling capability through the use of spatial data and spatially distributed physically based models. This dissertation is composed of three papers focused on 1) the use of spatially distributed hydrologic models with spatially distributed precipitation inputs, 2) advanced multi-objective calibration techniques that estimate parameter uncertainty and use stream gauge and temperature data from multiple locations, and 3) an examination of the relationship between high-resolution soils data and streamflow recession for use in a priori parameter estimation in ungauged catchments. This research contributes to the broad quest to reduce uncertainty in predictions at

ungauged basins by integrating developments of innovative modeling techniques with analyses that advance our understanding of natural systems.

(211 pages)

## ACKNOWLEDGMENTS

This work is dedicated to Dr. Iris Paul who, in 1998, gave me charge to bicycle down jungle footpaths to villages in rural Orissa, India, to collect information on the needs of the rural people within the service area of her small non-profit development agency. From this poignant experience I learned the foundational requirements of water for quality of life; from clean drinking water and agricultural use to the broader health, education, and economic viability which depend on water resources. Without this experience I would not have had the interest to begin this degree nor developed the fortitude needed to complete the work.

Why does it take so long to finish a PhD? It's not the actual length of time it takes to finish that is the issue, but how much longer it takes than originally planned. From my current viewpoint, I can say that I never imagined I would learn so much, but all the time it took was worth it. First, I want to recognize the triad who gave me more than I bargained for: thank you to Dr. David Tarboton for your patience, guidance, stirring conversions, and commitment to high academic standards; thank you to Dr. Mac McKee for loaning me your Water Resources Engineering classroom for a semester and first rate advice on how to engineer and educate; thank you to Dr. Ross Woods for your generous feedback, advice, and research support in New Zealand. I would also like to thank Jürgen Symanzik, Arthur Caplan, and David Bowles for their expertise and contribution to my research as supporters and committee members.

There are a few other reasons completion of this degree extended beyond optimistic deadlines. Thank you to my husband Sanjaya for starting a life with me in

Logan, even though we should have been studying; for growing raspberries, planting trees, remodeling the house and never doubting our commitment to my completion of this degree. Thank you to my parents in-law, Jayanthi and Tissa, for helping take care of our family and for providing the encouragement, brinjals, and daycare necessary since Satya Evelyn and Avani Rose have blessed our lives with their arrival. Thank you to my parents, Gail and Richard, for raising me to be a woman with persistence, creativity, love, and humor.

I will forever be indebted, professionally and emotionally, to Bethany Neilson for getting my feet wet and for sharing her field work with me. Her friendship is one variable that the equation for finishing this degree could not do without. I would have been stuck in an infinite loop without her friendship, laughter, and turkey basting.

This research was supported for two years by the GAANN fellowship. Special thanks go to the GAANN committee, and especially to Dr. Laurie McNeill for her friendship, advice, and professional example.

My friends in Logan are undoubtedly a part of the irreplaceable energy that has gone into this work. Suzann Kienast-Brown has been one of my constant companions, from the coffee breaks, through the maze of soils information I never knew I needed to know, and on the dance floor. Thank you for helping me stay balanced. Thanks to Kiran for sitting next to me and entertaining my distracting questions for so many years, and thanks to all the other 'Hard Workers' in the Hydrology Lab family -- Erkan, Jinshing, Ibrahim, and Teklu. Finally a shout out to my 400 West family for their friendship, BBQ's, kefir lime leaves, and open hearts, especially Becca, Kirk, Kristy, and Eric.

I would finally like to acknowledge William Morris Davis as important inspiration for the completion of this degree. My great-great uncle, who never completed his PhD, is known as “the father of American geography” and defined the earliest model of how rivers create landforms. Through the past few years his words have helped remind me to think both locally and globally, since "Ordinarily treated the river is like the veins of a leaf; broadly viewed it is the entire leaf."

Christina J. Bandaragoda

## CONTENTS

	Page
ABSTRACT.....	ii
ACKNOWLEDGMENTS.....	iv
LIST OF TABLES.....	ix
LIST OF FIGURES.....	xi
CHAPTER	
1. INTRODUCTION.....	1
References.....	7
2. APPLICATION OF TOPNET IN THE DISTRIUTED MODEL INTERCOMPARISON PROJECT.....	11
Abstract .....	11
2.1. Introduction.....	12
2.2. Model Description.....	14
2.3. The DMIP Experiment.....	23
2.4. Results and Analysis.....	29
2.5. Discussion and Conclusion.....	39
References.....	42
3. MULTIOBJECTIVE CALIBRATION OF SPATIALLY DISTRIBUTED HYDROLOGIC MODELS .....	68
Abstract .....	68
3.1. Introduction.....	69
3.2. Case Studies: Experimental Design.....	71
3.3. Conclusions.....	97
References.....	98
4. A PRIORI PARAMETER ESTIMATION FOR DISTRIBUTED HYDROLOGIC MODELING.....	121
Abstract .....	121



4.1. Introduction.....	122
4.2. Data and Methods.....	130
4.3. Results .....	144
4.4. Discussion .....	149
4.5. Conclusions .....	152
References.....	153
5. SUMMARY, CONCLUSIONS, AND RECOMMENDATIONS.....	175
Summary, Conclusions, and Recommendations.....	176
References.....	181
APPENDICES.....	182
A. The Indian legend and the PUB elephant.....	184
B. A solution for recession parameter $a^*$ based on linear regression.....	186
C. Coauthor Approval letters .....	188
CURRICULUM VITAE.....	192

## LIST OF TABLES

Table	Page
2.1. TOPNET Model Parameters (Multiplier Calibrated (MC)).....	45
2.2. Vegetation Parameter Values Derived from Land Cover Data from NASA LDAS Vegetation Database with IGBP Classification of 1-km AVHRR Imagery.....	46
2.3. Calibrated Parameter Multipliers and Number of Function Evaluations to Converge to the Corresponding Mean Square Error Using the Period October, 1998 - May, 1999.....	47
2.4. Calibrated and Uncalibrated Results During the June 1, 1993 – May 31, 1999 Calibration Period at Streamflow Gages Used for Calibration .....	48
2.5. Calibrated and Uncalibrated Results During the June 1, 1999 – July 31, 2000 Validation Period at Streamflow Gages Used for Calibration .....	49
2.6. Calibrated and Uncalibrated Results During the June 1, 1993 – May 31, 1999 Calibration Period at Interior Locations Modeled as “Ungaged” .....	50
2.7. Calibrated and Uncalibrated Results During the June 1, 1999 – July 31, 2000 Validation Period at Interior Locations Modeled as “Ungaged” .....	51
2.8. Baron Fork at Eldon $f$ and $K_o$ Sub-basin Parameters .....	52
2.9. Model Run Time and Calibration Time for Each of the DMIP Basins .....	53
3.1. Calibrated Parameters for the TZTS Model .....	102
3.2. Matrix of Calibration Experiments for Single Objective(SO) and Multi- Objective (MO) at Hurricane Bridge (HB) and Washington Field Diversion (WFD) for Corresponding Locations in the Main Channel (MC), Surface Storage (SS) and Sub-Surface Storage (SSS) used for Calibration (C) and Model Validation of Ungauged Performance (U).....	103
3.3. Model Results for Nash-Sutcliffe Efficiency (E) for the ‘Best’ Parameter Set.....	104

3.4	Average Nash-Sutcliffe Efficiency (AE) Results for the TZTS Model with AE Calculated Using a) Main Channel Temperatures; b) Main Channel Plus Surface Storage Locations; c) Main Channel, Surface Storage and Sub-Surface Storage Locations with Measurements at 9 cm Sediment Depth .....	105
3.5	TOPNET Model Parameters. ....	106
3.6	Matrix of Calibration Experiments for Single Objective (SO) and Multi-Objective (MO) at Illinois River at Tahlequah (T), Watts (W) and Savoy (S) Locations Used for Calibration (C) and Model Validation of Ungauged Performance (U). ....	107
3.7	The Range of Model Results for Nash-Sutcliffe Efficiency (E) for Pareto Rank One Parameter Sets .....	108
3.8	The Range of Model Results for Average Nash-Sutcliffe Efficiency (AE) for Pareto Rank One Parameter Sets .....	109
4.1	The Stratified Random Sample of HCDN Watersheds from NEON Climate Domains 1 Through 17, Excluding Domain 4 Which Is the Southern Tip of Florida.....	158
4.2	Data Used to Investigate the Relationships Between Streamflow Recessions and Soil and Watershed Properties.....	159
4.3	Porosity Based on Soil Texture from Clapp and Hornberger [1978].....	159
4.4	Correlation Statistics ( $R$ , $R^2$ , $t$ and $p$ ) between Natural Logarithms of Soil and Watershed Properties and Streamflow Recession Parameter $a^*$ . ....	160
4.5	Correlation Values ( $R$ ) Between Log Transformed Soil and Watershed Properties and the Log of Streamflow Recession Parameter $a^*$ for Watershed Data Stratified by Geography, Topography and Climate.....	161
4.6	Correlations Between Log Hydraulic Conductivity and Logs of Drainage Density, Channel Slope, Average Slope, and Slope from the Peak Elevation to the Outlet for the Entire Dataset (All) and Classified Subsets.....	162

## LIST OF FIGURES

Figure	Page
1.1 a and b. The elephant juxtaposed of different parts (1a) is used as the mascot for IAHS Decade on Predictions in Ungauged Basins (PUB): 2003-2012; (Sivapalan and Schaake, 2003; Saviodsilva, 2005).....	9
1.2. The uncertainty related to applying a model designed for use in one location to other locations: PUB mascot and Pinnawela Orphanage Elephants, Sri Lanka. ....	10
2.1. Schematic of the physical processes represented by the TOPNET modeling system. ....	54
2.2. Model element distribution for the watershed of the Illinois River at Tahlequah.....	55
2.3. DMIP river basins are located in the south central United States and range in size from 800 km <sup>2</sup> to 2500 km <sup>2</sup> .....	56
2.4. TOPMODEL wetness index for the upper portion of the Blue watershed. A histogram represents the distribution of wetness index within each sub-basin.....	57
2.5. Derivation of distributed soil based parameters from Penn State soil texture layers derived from STATSGO.....	58
2.6. Hydrograph for the Illinois River at Tahlequah for flows from January, 1997 through August, 1997.....	59
2.7. Percent bias of calibrated results by month for selected DMIP watersheds.....	60
2.8. Percent bias of uncalibrated results by month for selected DMIP watersheds.....	61
2.9. a) Peacheater Creek calibrated streamflow results, b) Peacheater Creek calibrated log streamflow results, and c) Baron Fork at Eldon log streamflow results for the 1999-2000 validation period.....	62

2.10.	Calibrated and uncalibrated simulated streamflow for Baron Fork at Eldon, November 1994.....	63
2.11.	Calibrated (-) and uncalibrated (--) watershed averaged model components for Baron Fork at Eldon, at the beginning of the water year 10/25/1994-12/20/1994.....	64
2.12.	Calibrated (-) and uncalibrated (--) direct streamflow by subwatershed for Baron Fork at Eldon, at the beginning of the water year 10/25/1994-12/20/1994.....	65
2.13.	Calibrated (-) and uncalibrated (--) depth to the water table by subwatershed for Baron Fork at Eldon, at the beginning of the water year 10/25/1994-12/20/1994.....	66
2.14.	Radar rain subwatershed averages for Baron Fork at Eldon, at the beginning of the water year 10/25/1994-12/20/1994.....	67
3.1.	Layout of Upper Virgin hydrologic cataloging unit. The portion of the river studied is below Gould's Wash (CS #1) and above Washington Fields Diversion (CS #3).....	110
3.2.	Energy balance components of the Two-Zone Temperature and Solute Model.....	111
3.3.	The tradeoff in the multi-objective calibration of the two-zone temperature and solute model using two main channel temperature locations.....	112
3.4.	Multi-objective results for calibration using main channel temperatures at Hurricane Bridge (HB) and Washington Field Diversion (WFD).....	113
3.5.	The (a) Illinois River at Tahlequah watershed and internal sub-basins used in the distributed modelling including output locations at (b) Illinois River at Watts and (c) Illinois River at Savoy.....	114
3.6.	Calibration experiment results in two dimensional space for two-objective test at a) Tahlequah and Watts, and the three-objective test using Tahlequah, Watts and Savoy comparing in two dimensions results at b) Tahlequah Watts and c) Watts and Savoy, and d) Savoy and Tahlequah.....	115
3.7.	Single objective calibration results for the Illinois River at Tahlequah.....	116

3.8	Single objective results for the Illinois River at Watts. ....	117
3.9	Single objective results for the Illinois River at Savoy. ....	118
3.10.	Results at three locations when using multi-objective calibration at two locations, Tahlequah and Watts, for the calibration period. ....	119
3.11.	Results at three locations when using multi-objective calibration at three locations, Tahlequah, Watts and Savoy, for the calibration period. ....	120
4.1.	Sample of three HCDN watersheds from each National Ecological Observatory Network (NEON) domain across the continental United States.....	163
4.2.	Hydraulic conductivity (a), soil depth (b) and porosity (c) maps for the San Casimiro Creek near Freer, Texas, in Webb County.....	164
4.3.	Hydraulic conductivity (a), soil depth (b) and porosity (c) maps for the Cartoogechaye Creek near Franklin, North Carolina in Macon County.....	164
4.4	Hydraulic conductivity (a), soil depth (b) and porosity (c) maps for Dismal River near Thedford, Nebraska in Thomas, Hooker, Grant, and Arthur Counties.....	165
4.5	The distribution of the empirically based parameter $b$ across the watersheds in the sample. The parameter $b$ is the slope of the regression line through the $\log(-dQ/dt)$ vs $\log(Q)$ scatterplot.....	166
4.6	Regression lines fit to streamflow recession for all 48 watersheds studied.....	167
4.7.	Regressions lines fit to streamflow recessions for all 48 watersheds, with the constraint $b=1$ .....	168
4.8.	Recession information extracted from USGS station 08194200, for the San Casimiro Creek near Freer, Texas in Webb County with Figure 4.8a showing three years of streamflow data on a log scale with points where recessions were selected (blue and cyan) and averaged (cyan only).....	169

4.9.	Recession information extracted from USGS station 03500240, for the for the Cartoogechaye Creek near Franklin, North Carolina in Macon County with Figure 4.9a showing three years of streamflow data on a log scale with points where recessions were selected (blue and cyan) and averaged (cyan only).....	170
4.10	Recession information extracted from USGS station 11264500, for the Merced River at Happy Isles Bridge near Yosemite California in the Yosemite National Park soil survey area, with Figure 4.10a showing three years of streamflow data on a log scale with points where recessions were selected (blue and cyan) and averaged (cyan only).....	171
4.11.	Log of streamflow recession parameter $a^*$ [ $\text{day}^{-1}$ ] versus the log of soil sensitivity, $S=K_{\text{sat}}/f$ [ $\text{m}/\text{day}$ ], for the sample watersheds classified into a) East and West, b) Low and high average hillslope (hillslope $< 0.02$ $\text{m}/\text{km}$ and hillslope $> 0.06$ $\text{m}/\text{km}$ ), and c) wet and dry (Annual precipitation threshold 1000 mm).....	172
4.12.	Log of watershed averaged saturated hydraulic conductivity versus the log of drainage density for the sample subset from the eastern United States.....	173
4.13	Log of watershed averaged saturated hydraulic conductivity versus the log of average hillslope for the sample subset from the western United States.....	174
4.14	Definition sketch for the Dupuit-Boussinesq aquifer model depicting the changing shape of the free groundwater surface through time, $h(x,t)$ , starting from saturation [adapted from Szilagyi et al. 1998, Figure 1].....	174

## CHAPTER 1

### INTRODUCTION

Streamflow prediction in ungauged basins is a policy-relevant science theme emerging as a major challenge to the hydrologic community. An international research initiative intended to promote the development of science and technology in this field is being promoted by the International Association of Hydrological Sciences (IAHS), which has declared the years 2003-2012 as the IAHS Decade on Prediction in Ungauged Basins (PUB) [Sivapalan *et al.*, 2003; Schertzer and Hubert, 2002; Franks *et al.*, 2005]. The observation network of hydrologic data is in decline around the world, yet data is needed for more efficient water resources management, flood forecasting, and policy development based on water quality and quantity modeling [Sivapalan *et al.*, 2003]. Advanced methods in hydrology are required to learn how to best use the hydrologic information that is available for streamflow prediction.

One can consider the problem of prediction of streamflow at an ungauged basin as analogous to the famous Indian legend [Saxe, 1963] where people approaching an elephant from different perspectives experience just one component of the big picture. Without combining all elements that compose the whole, it will be impossible to develop a complete representation of reality (Figure 1.1). Parts of the metaphorical elephant in this case could be considered model structure, model calibration, a priori parameterization, forcing data, and understanding of the effect of uncertainty for each of the elements as well as the resulting uncertainty of combining the elements to represent reality.



Complicating matters, we have to consider the limitations of the representation of reality in one location as it is applied to other locations. Or as is shown in Figure 1.2, we need to understand how the model designed to represent the biggest most obvious elephant (the downstream gauged location) can be expected to perform when used to represent elephants about which we have less information (smaller, internal, ungauged locations).

The definition of an ungauged basin is “one with inadequate records (in terms of both data quantity and quality) of hydrological observations to enable computation of hydrological variables of interest (both water quantity or quality) at the appropriate spatial and temporal scales, and to the accuracy acceptable for practical applications” [Sivapalan *et al.*, 2003]. Precipitation and runoff are generally the variables of interest in rainfall-runoff modeling, but if the applications are broader, they may involve erosion rates, sediment and nutrient concentrations, or stream temperature. From this perspective, all drainage basins are ‘ungauged’ to some degree and research towards understanding the application of advanced technologies to ungauged basins is applicable to all basins.

The problem of prediction in ungauged basins using distributed hydrological modeling is addressed in this dissertation. Physically based distributed modeling is based on the premise that the spatially distributed data is related to the model parameters. Improvements in distributed modeling should therefore be possible as higher resolution spatial data becomes available. This requires that the relationship between model parameters and data attributes be established. Establishment of these relationships may also advance our understanding of natural systems by providing a framework to study

heterogeneity in watersheds over space and time. The dissertation addresses the following hypotheses specifically related to distributed hydrologic modeling:

- Spatially distributed hydrologic modeling with remotely-sensed precipitation forcing data improves prediction of streamflow at ungauged basins compared to traditional modeling techniques.
- Multi-objective calibration using multiple measurement locations is effective at improving predictions at ungauged locations within or near the catchment compared to single-objective calibration at a single measurement location.
- High-resolution soils data is correlated to streamflow recession properties and can be used to quantify spatial variability in hydrologic response and to guide a priori parameter estimation for spatially distributed hydrologic models.

This dissertation includes five chapters including this introduction and a summary chapter. Three chapters are used to individually address each hypothesis listed above.

Chapter 2 presents work published in a special edition of the Journal of Hydrology, *Application of Topnet in the Distributed Model Inter-comparison Project*. This paper is a contribution to a model inter-comparison study focused on understanding the implication of using distributed hydrologic models with radar rainfall inputs for flood-forecasting [Smith et al., 2004; Reed et al., 2004; Chapter 2]. The project design, with split-sample temporal and spatial data as well as spatially distributed radar-rainfall data inputs applied in the Distributed Model Inter-comparison Project [Smith et al., 2004], provided the opportunity to assess model performance at ungauged basins. The study was designed with test datasets to model as ‘ungauged’ and results focused on diagnosis of the performance of the model structure, not simply statistical performance. Diagnosis and

inter-comparison in a performance assessment show how a spatially distributed hydrologic model can be expected to perform in an operational setting.

Chapter 3 presents a framework for the calibration of spatially distributed models using multiple measurement locations. A spatially distributed rainfall-runoff model and a spatially distributed instream temperature model are both used to test this framework. Our model uses multi-location data for understanding the effect of calibration on small nested or ungauged locations. The rainfall-runoff model locations are distributed within a catchment, the temperature model locations are distributed within the channel width and length. The use of multiple locations for automated calibration of distributed hydrologic models and the resulting implications for prediction at ungauged basins is presented. Data assimilation of temporal data, multiple streamflow timeseries, into an advanced calibration framework is shown to improve the spatial distribution of parameter values and resulting predictions at test locations.

Chapter 4 focuses on a study of the empirical relationships between soil properties and streamflow recession properties. Theoretical relationships between these properties can be used for a priori parameter estimation for distributed hydrologic models. It is critical that the theoretical relationships used are consistent with the empirical information available, especially in the case of ungauged basin modelling since streamflow data for model calibration is not available. This research compares hydrologic theory commonly used to convert soils data information to hydrologic response with empirical recession response and high-resolution soils data, SSURGO [*Soil Survey Staff, 2006*] . We found significant correlations between streamflow recession parameters and watershed sensitivity, which was defined using a combination of

hydraulic conductivity, porosity, drainage density and slope. Saturated hydraulic conductivity alone was found to explain the dominant part of the relationships that were found. When the watersheds examined were classified into subsets based on geography, topography, and climate, the correlation with hydraulic conductivity and other parameters was found to vary across the classes. A number of possible explanations for these findings, based on hillslope recession theory are presented.

In the highly cited article, *Physically Based Hydrologic Modeling 2. Is the Concept Realistic?*, Grayson et al. [1992] assert that “the most appropriate uses of process-based, distributed-parameter models are to assist in the analysis of data, to test hypotheses in conjunction with field studies, to improve our understanding of processes and their interactions and to identify areas of poor understanding in our process descriptions.” In addition to addressing questions relevant to predicting streamflow in ungauged basins, this research has approached distributed modeling as an opportunity to advance the understanding of natural systems rather than as a treatise on the good results of a particular model.

## References

- Franks, S., M. Sivapalan, K. Takeuchi, and Y. Tachikawa, ed. (2005), *Predictions in Ungauged Basins: International Perspectives on the State of the Art and Pathways Forward*, IAHS Press, Wallingford, Oxfordshire.
- Grayson, R. B., I. D. Moore, and T. A. McMahon, (1992), Physically based hydrologic modeling 2. Is the concept realistic?, *Water Resour. Res.*, 28(10), 2659-2666.
- Reed, S., V. Koren, M. Smith, Z. Zhang, F. Moreda, D. J. Seo, (2004), Overall Distributed Model Intercomparison Project Results, *J. Hydrol.*, 298(1-4), 27-60.
- Saviodsilva, (2005), African elephant, [www.saviodsilva.com](http://www.saviodsilva.com), <http://www.saviodsilva.org/gg/3/elephant/14.htm>. [Accessed November 29, 2007].

Saxe, J. G., (1963), *The Blind Men and the Elephant; John Godfrey Saxe's Version of the Famous Indian Legend*. Pictures by Paul Galdone, Whittlesey House, New York.

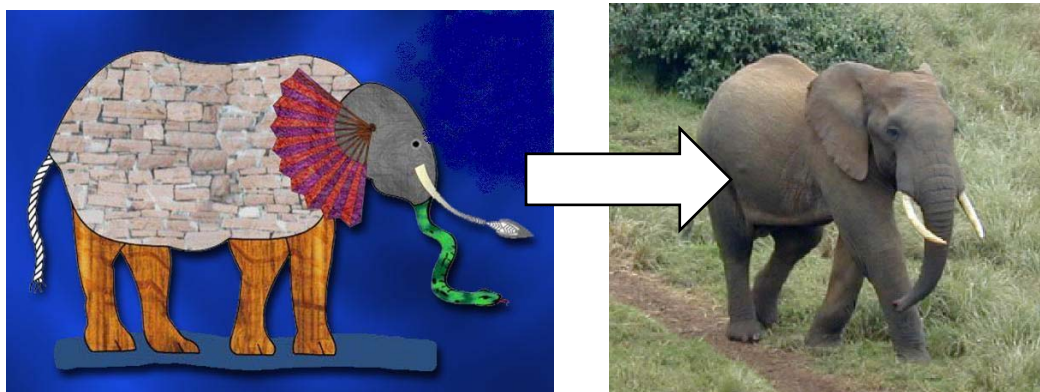
Schertzer and Hubert, (2002), IAHS PUB Programme.  
[www.cig.ensmp.fr/~iahs/archives/Paris2002/doc/PUB-Proposal-DS-PH.doc](http://www.cig.ensmp.fr/~iahs/archives/Paris2002/doc/PUB-Proposal-DS-PH.doc)  
[Accessed November 29, 2007].

Sivapalan, M. and J. Schaake, (2003), IAHS Decade on Predictions in Ungauged Basins (PUB): 2003-2012. <http://www.cig.ensmp.fr/~iahs/>. [Accessed November 29, 2007].

Sivapalan, M., K. Takeuchi, S. W. Franks, V. K. Gupta, H. Karambiri, V. Lakshmi, X. Liang, J. J. McDonnell, E. M. Mendiondo, P. E. O'Connell, T. Oki, J. W. Pomeroy, D. Schertzer, S. Uhlenbrook, and E. Zehe, (2003), IAHS Decade on Predictions in Ungauged Basins (PUB), 2003-2012: Shaping an Exciting Future for the Hydrological Sciences, *Hydrological Sciences Journal-Journal Des Sciences Hydrologiques*, 48(6), 857-880.

Smith, M. B., D. J. Seo, V. I. Koren, S. M. Reed, Z. Zhang, Q. Duan, F. Moreda, and S. Cong, (2004), The Distributed Model Intercomparison Project (DMIP): Motivation and Experiment Design, *J. Hydrol*, 298(1-4), 4-26.

Soil Survey Staff, (2006), Soil Survey Geographic (SSURGO) Database for Survey Area, Natural Resources Conservation Service, United States Department of Agriculture, <http://soildatamart.nrcs.usda.gov> [Accessed January 26, 2005].



a.

b.

**Figure 1.1 a and b.** The elephant juxtaposed of different parts (1a) is used as the mascot for IAHS Decade on Predictions in Ungauged Basins (PUB): 2003-2012; [Sivapalan and Schaake, 2003; Saviodsilva, 2005]. PUB efforts are towards combining many different modeling elements to reduce uncertainty and represent reality (1b).

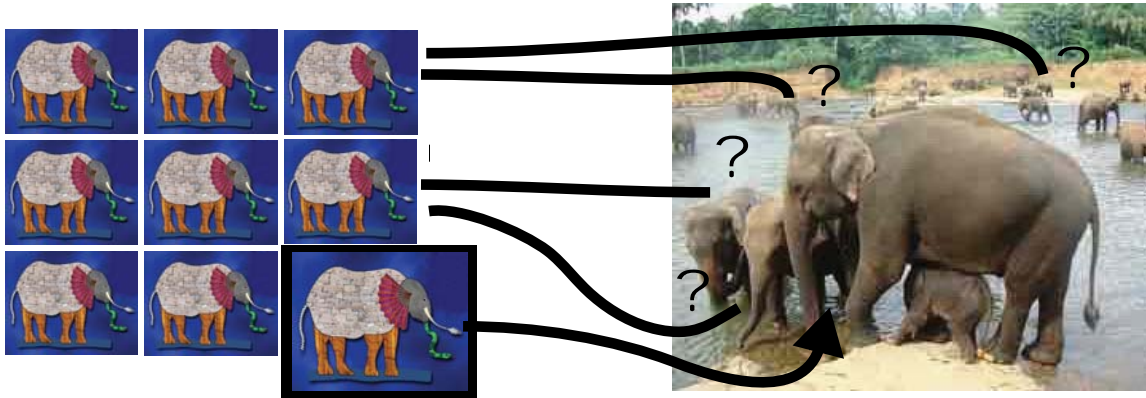


**Figure 1.2.** The uncertainty related to applying a model designed for use in one location to other locations: PUB mascot and Pinnawela Orphanage Elephants, Sri Lanka.

CHAPTER 2  
APPLICATION OF TOPNET IN THE DISTRIBUTED MODEL  
INTERCOMPARISON PROJECT<sup>1</sup>

**Abstract**

This paper describes the application of a networked version of TOPMODEL, TOPNET, as part of the Distributed Model Intercomparison Project (DMIP). The model implementation is based on a topographically derived river network with spatially distributed sub-basins draining to each network reach. The river network is mapped from the U.S. National Elevation Dataset Digital Elevation Model (DEM) using procedures that objectively estimate drainage density from geomorphic principles. Rainfall inputs are derived from NEXRAD (radar) for each sub-basin. For each sub-basin, the wetness index distribution is derived from the DEM. The initial model parameters for each sub-basin are estimated using look up tables based on soils (STATSGO) and vegetation (1-km AVHRR). These initial model parameters provide the spatially distributed pattern of parameters at the scale of each sub-basin. Calibration uses a multiplier for each parameter to adjust the parameters while retaining the relative spatial pattern obtained from the soils and vegetation data. Parameter multipliers were calibrated using the shuffled complex evolution (SCE) algorithm [Duan *et al.*, 1993] with the objective to minimize the mean square error between observed and modeled hourly streamflows. We describe the model and calibrated results submitted for all basins for the time periods involved in the DMIP study. We were encouraged by the relatively good performance of

---

<sup>1</sup> Coauthored by David Tarboton and Ross Woods



the model, especially in comparison to streamflow from smaller interior watersheds not used in calibration and simulated as ungaged basins. The limited resources used to achieve these results show some of the potential for distributed models to be useful operationally.

## 2.1 Introduction

We have applied a distributed version of TOPMODEL [*Beven and Kirkby, 1979; Beven et al., 1995a*] with a DEM-based system for delimiting channels, model components, and estimation of model parameters, to the DMIP watersheds. The implementation of TOPMODEL used is modified from the original [*Beven and Kirkby, 1979; Beven et al., 1995a*] by the addition of a potential evapotranspiration component, a canopy storage component to model interception, and the inclusion of a soil zone component that provides infiltration excess runoff generation capability through a Green-Ampt like parameterization.

To parameterize the model using physical data, we used the soil texture from each of the 11 soil depth grid layers derived from Pennsylvania State University STATSGO data [*Soil Survey Staff, 2006*] provided on the DMIP website [*Smith, 2002*], and soil hydraulic properties derived from texture using relationships provided by *Clapp and Hornberger* [1978]. We also used 1 km resolution Advanced Very High Resolution Radiometer (AVHRR) vegetation data processed through the NASA Land Data Assimilation Systems (LDAS) program with an International Geosphere-Biosphere Program (IGBP) classification system [*Eidenshink and Faundeen, 1994*]. There are a

total of nine parameters that were derived from this soils and vegetation information. We used a GIS to spatially average the parameter values for each sub-basin model element.

The calibration procedure used is designed to retain the spatial pattern provided by estimating parameters from the GIS data, while still allowing an adjustment of parameters to match observed stream flow. Parameters are adjusted through a set of multipliers that scale the parameters while maintaining the relative differences between model elements indicated from the GIS information. There is one multiplier for each parameter that is the same across all sub-basins. Subgrid variability within sub-basins is not explicitly represented apart from the spatial distribution of soil moisture that is parameterized by distribution of the TOPMODEL wetness index.

The DMIP dataset provides a unique opportunity to explore questions of location-specific radar data quality, and model performance over calibration and validation periods for different watersheds using different models. The results for our model are presented with an overview of model performance and acceptability in some watersheds, and recommendations for TOPNET model improvement in others.

We address the following questions related to the use of distributed hydrologic models. Can radar rainfall data be used for flood forecasting? Can distributed models simulate flow at uncalibrated interior locations? How applicable is a TOPMODEL representation to the DMIP watersheds? Can flows be predicted well with little or no calibration?

We found that lack of information on the uncertainty in radar rainfall inputs limits the useful interpretation of the statistical measures used to assess forecast performance. Distributed models have an advantage over lumped models in the ability to disaggregate

the source of streamflow to ungaged locations upstream of the calibration location. We found that the exponential discharge-storage response function of TOPMODEL, used to model the saturated zone, limited the ability of the model to match streamflow recessions in both high flow and low flow periods. The small difference between calibrated and uncalibrated results for TOPNET showed that, in some basins, flows can be predicted well with little or no calibration. Calibration reduced the mean square errors, improving measures such as the Nash-Sutcliffe efficiency. Matching peak flows was emphasized by this approach but this was at a cost of introducing bias and poorer representation of low flows.

The following sections of this paper include a description of our model and the methods used in the DMIP experiment. Results of the DMIP experiment are given, followed by conclusions on the model performance.

## **2.2 Model Description**

TOPNET was developed by combining TOPMODEL [Beven and Kirkby, 1979; Beven *et al.*, 1995a], which is most suited to small watersheds, with a kinematic wave channel routing algorithm [Goring, 1984] so as to have a modeling system that can be applied over large watersheds using smaller sub-basins within the large watershed as model elements. A key contribution of TOPMODEL is the parameterization of the soil moisture deficit (depth to water table) using a topographic index to model the dynamics of variable source areas contributing to saturation excess runoff. Beven *et al.* [1995a] indicate that "TOPMODEL is not a hydrological modeling package. It is rather a set of conceptual tools that can be used to reproduce the hydrological behavior of catchments in

a distributed or semi-distributed way, in particular the dynamics of surface or subsurface contributing areas."

The model we developed and applied here, TOPNET, uses TOPMODEL concepts for the representation of subsurface storage controlling the dynamics of the saturated contributing area and baseflow recession. To form a complete model we added potential evapotranspiration, interception and soil zone components. The physical processes represented in each sub-basin are illustrated in Figure 2.1. Kinematic wave routing moves the sub-basin inputs through the stream channel network. A GIS based parameterization program, TOPSETUP, has been developed to facilitate the transformation of spatial datasets into modeling parameters and the calculation of weights associated with point precipitation measurements to provide sub-basin aggregate precipitation.

In addition to streamflow, TOPNET diagnostic output for each model element consists of time series of model state variables for each sub-basin: mean water table depth, soil zone storage, and canopy storage. Diagnostic output also includes information for each sub-basin on: infiltration excess runoff, saturation excess runoff, base flow, drainage from the soil to the saturated zone (recharge), percent saturated area, potential evapotranspiration, and actual evapotranspiration.

### **2.2.1 Potential Evapotranspiration Component**

In TOPNET, potential evapotranspiration is calculated using the Priestley-Taylor equation [*Priestley and Taylor, 1972*]. This was chosen because it can be used with minimal input requirements of air temperature, dew point, date and time. *Famiglietti et al. [1992]* and *Famiglietti and Wood [1994a, 1994b]* used more complete surface energy

balance equations with TOPMODEL in developing the TOPLATS soil vegetation atmosphere transfer scheme (SVATS). Famiglietti's work focused on estimating evaporation fluxes as inputs to atmospheric models. We opted for a simpler approach here because the focus is on modeling runoff and because much of the data required to run a more complex SVATS model, such as wind and aerodynamic roughness is uncertain and difficult to estimate from the available data.

The available energy used in the Priestley-Taylor equation is calculated based on top of the atmosphere solar radiation forcing following procedures given in the Handbook of Hydrology [Shuttleworth, 1993] with atmospheric transmissivity estimated from the diurnal temperature range [Bristow and Campbell, 1984]. Temperature and dew point for each sub-basin are estimated from nearby measurements using a lapse rate and the elevation difference between the mean sub-basin elevation and measurement elevation. In the calculation of potential evapotranspiration, albedo and lapse rate are treated as parameters with albedo determined from land cover data.

### **2.2.2 Canopy Interception Component**

The canopy interception component is a new and much simpler approach than standard interception models [e.g. Rutter *et al.*, 1972]. It was developed based on the work of Ibbitt [1971] and requires only two parameters: canopy interception capacity, CC, and interception evaporation adjustment factor,  $C_r$ . Driving inputs to the canopy interception component are hourly precipitation and potential evapotranspiration. These are determined from the GIS land cover data. The state variable quantifying the amount of water held in interception storage,  $S_i$ , is used in a function  $f(S_i)$  to quantify the

proportion of precipitation that is throughfall [Ibbitt, 1971]. The remainder  $P(1-f(S_i))$ , where  $P$  is precipitation rate, is added to interception storage. The same function  $f(S_i)$  is used to quantify the exposure of water held in interception storage to potential evapotranspiration. Physically,  $f(S_i)$  could express the fraction of leaf area that is wet, relative to its maximum. Higher rates of evaporation from interception than transpiration under the same conditions, have been suggested by *Stewart* [1977] and *Dingman* [2002]. Here we represent this effect using a factor  $C_r$  quantifying the increase in evaporation losses from interception relative to the potential evapotranspiration rate [Ibbitt, 1971; *Stewart*, 1977]. The evaporation outflux from the interception store is written as  $E \cdot C_r \cdot f(S_i)$  where  $E$  is the potential evapotranspiration rate. The rate of change for interception storage is therefore given by

$$\frac{dS_i}{dt} = P(1 - f(S_i)) - E \cdot C_r f(S_i) \quad (1)$$

$f(S_i)$ , the function giving throughfall as a function of interception storage,  $S_i$ , and canopy interception capacity,  $CC$ , is given by:

$$f(S_i) = \frac{S_i}{CC} \cdot \left( 2 - \frac{S_i}{CC} \right) \quad (2)$$

Analytic integrals of equation (1) using (2) are used to solve for  $S_i$  at the end of each time step to obtain the cumulative throughfall and cumulative evaporation of intercepted water.  $C_r$  applies only to intercepted water, not soil water available for transpiration. Unsatisfied potential evapotranspiration demand is calculated as potential evapotranspiration minus cumulative evaporation of intercepted water divided by the interception enhancement factor  $C_r$ .

### 2.2.3 Soil Component

Throughfall,  $T$ , and unsatisfied potential evapotranspiration,  $E_p$ , from the interception component serve as the forcing for the soil component, which represents the upper layer of soil to the depth below which roots can no longer extract water. *Beven et al.* [1995a] indicate that two formulations that have been adopted in past TOPMODEL applications have assumed that the unsaturated flows are essentially vertical and have been expressed in terms of drainage flux from the unsaturated zone. Neither of the formulations presented by *Beven et al.* [1995a] limit the infiltration capacity, possibly due to the historical association of TOPMODEL with the saturation excess rather than the infiltration excess runoff generation mechanism. We felt it important to accommodate both saturation and infiltration excess runoff generation mechanisms and therefore developed our own soil component that combines gravity drainage and Green-Ampt infiltration excess concepts to control the generation of surface runoff by infiltration excess as well as the drainage to the saturated zone and evapotranspiration.

Parameters describing the soil store processes are depth ( $d$ ), saturated hydraulic conductivity ( $K$ ), Green-Ampt wetting front suction ( $\psi_f$ ), pore disconnectedness index soil drainage parameter ( $c$ ), drainable porosity ( $\Delta\theta_1$ ), and plant available porosity ( $\Delta\theta_2$ ). The soil parameters are estimated based on soil texture from GIS soils data using relationships from *Clapp and Hornberger* [1978].

The state variable  $S_r$  quantifies the depth of water held in the soil zone for each model element and is calculated according to

$$\frac{dS_r}{dt} = I - E_s - R \quad (3)$$

where  $I$  is the infiltration rate,  $E_s$  is soil evaporation rate and  $R$  the drainage rate or recharge to the saturated zone store from the soil store. The infiltration rate,  $I$ , is limited to be less than the infiltration capacity,  $I_c$ , modeled with a Green-Ampt formulation where we use the soil zone storage as infiltrated depth for the purposes of calculating  $I_c$ .

Unsatisfied evapotranspiration demand is given first call upon available surface water so the forcing to the soil zone is  $T - E_p$ . When this quantity is negative it represents evaporative demand on the soil component. When this quantity is positive it represents net surface water input that may infiltrate or become infiltration or saturation excess surface runoff.

Soil evapotranspiration is assumed to be at the potential rate when the soil moisture content is in excess of field capacity, but between field capacity and permanent wilting point, evapotranspiration is assumed to reduce linearly to zero as wilting point is approached. Soil evaporation is modeled as

$$E_s = \text{Min} \left( 1, \frac{S_r}{d\Delta\theta_2} \right) (E_p - T) \text{ for } E_p > T \text{ and } 0 \text{ otherwise} \quad (4)$$

where  $E_p - T$  is the unsatisfied potential evapotranspiration demand.

We assume the soil zone is comprised of two parts, the drainable part in excess of field capacity, characterized by  $\Delta\theta_1$ , and the plant available moisture, characterized by  $\Delta\theta_2$ . Drainage is estimated as gravity drainage and is modeled to only occur when the moisture content is greater than field capacity. The relative drainable saturation,  $S_{rd}$ , is defined as



$$S_{rd} = \frac{\text{Max}(0, S_r - d\Delta\theta_2)}{d\Delta\theta_1} \quad (5)$$

The drainage from the soil store and recharge to the saturated zone occurs at a rate (m/hr) given by

$$R = K S_{rd}^c \quad (6)$$

This is based upon a *Brooks and Corey* [1966] parameterization of the unsaturated hydraulic conductivity controlling the rate of drainage.

For locations with large wetness index values, the water table evaluated in the saturated zone component below may upwell into and influence the soil moisture content of the soil zone. This occurs when depth to the water table,  $z$ , is less than depth of the soil zone,  $d$ . We model the supplementary moisture in the soil zone in these cases by assuming uniform soil moisture deficit from the surface to the water table and saturated conditions from the water table to the root zone. Thus the shallow water table ( $z < d$ ) increases the soil storage to

$$S_r' = S_r + (d \cdot \theta_e - S_r) \cdot \left( \frac{d - z}{d} \right) \quad (7)$$

The soil component described here was developed independently of TOPMODEL, which we used to develop the saturated zone described in the following section.

#### 2.2.4 Saturated Zone Component

The saturated zone component is constructed using the classical TOPMODEL assumptions of 1) saturated hydraulic conductivity decreasing exponentially with depth

and 2) saturated lateral flow driven by topographic gradients at 3) steady state [Beven *et al.*, 1995a; Beven and Kirkby, 1979]. With these assumptions the local depth to the water table,  $z$ , is the following function of the wetness index  $\ln(a/\tan \beta)$ .

$$z = \bar{z} + (\lambda - \ln(a / \tan \beta)) / f \quad (8)$$

where  $\lambda$  is the spatial average of  $\ln(a/\tan \beta)$  and  $\bar{z}$  the spatial average of the depth to the water table quantifying the basin average soil moisture deficit and serving as a state variable for the saturated zone component. The parameter  $f$  quantifies the assumed decrease of hydraulic conductivity with depth. A histogram of wetness index values over each sub-basin is used to record the proportion of each sub-basin falling within each wetness index class. Locations, or wetness index classes, where  $z$  is less than 0 as calculated using equation (8) are interpreted to be saturated and represent the variable source area where surface water input ( $T-E_p$ ) becomes saturation excess runoff.

The saturated zone state equation is

$$\frac{d(\Delta\theta_1 \bar{z})}{dt} = -r_{is} + T_o e^{-\lambda} e^{-f\bar{z}} \quad (9)$$

where  $r_{is}$  is the recharge  $R$  to the saturated zone averaged across wetness index classes, recognizing that for classes where the water table impacts the soil zone  $S_r$  and hence  $R$  are impacted by  $z$  through equation (7). The last term in this equation represents the per unit area baseflow,  $Q_b$ , draining the saturated zone derived using the exponential decrease in hydraulic conductivity with depth assumed by TOPMODEL, with  $T_o$  being transmissivity,

$$Q_b = T_o e^{-\lambda} e^{-f\bar{z}} \quad (10)$$

In solving the model we do not save a state variable either for the saturated zone or soil zone for each wetness index class. Rather we only save state variables  $\bar{z}$  and  $S_r$  for each sub-basin. At each time step, equation (8) gives the depth to the water table for a specific wetness index class within a sub-basin, and equation (7) gives the modification of  $S_r$  for wetness index classes impacted by a shallow water table. This approach is different from the Beven version of TOPMODEL [Beven *et al.*, 1995b] where a separate soil zone is modeled for each wetness index class. We felt that keeping track of state variables at scales smaller than the basic sub-basin model element introduces unnecessary complexity and is unwarranted. If smaller spatial resolution is required to provide more explicit resolution of spatial variability, then smaller sub-basins can be delineated.

### **2.2.5 Routing Component**

There are three sources of runoff from each sub-basin; 1) saturation-excess runoff from excess precipitation on variable source saturated areas as determined from the topographic wetness index, 2) infiltration-excess runoff as determined from the Green-Ampt parameterization based upon soil zone storage and 3) base flow representing saturated zone drainage according to equation (10). This runoff is delayed in reaching the outlet due to the time taken by within sub-basin travel, as well as travel in the stream network to the overall watershed outlet. Within sub-basin travel is modeled assuming a constant hillslope velocity,  $V$ , which is a calibrated input parameter. A histogram of the down slope flow distances from each grid cell in each sub-basin to the first stream encountered is derived from the GIS and used to perform this routing.

Once in the stream, a kinematic wave routing algorithm [Goring, 1984] is used to route flow through the network. Sub-basin inputs to the channel network are assumed to occur at the head of first order streams and at the midpoint of internal stream reaches. Figure 2.2 gives an example of the sub-basins used to model flow in the Illinois River at Tahlequah. The inset on Figure 2.2 gives the schematic channel network with sub-basin inputs used to route flow for the portion of this network draining to the interior gage at Savoy. The parameters used in the kinematic wave channel network routing are Manning's roughness parameter  $n$ , as well as width, slope and length for each channel segment. Slope and length are determined from the GIS based upon the DEM. Channel width is determined as a power function of contributing area [Leopold and Maddock, 1953] fit to data from New Zealand rivers.

### **2.2.6 Precipitation Interpolation**

TOPNET is configured to derive aggregated sub-basin precipitation inputs as a weighted sum of point precipitation measurements. The weights associated with each gauge for each sub-basin are calculated as part of the preprocessing by TOPSETUP using linear interpolation based upon Delauney triangles. In the DMIP application, the center points of NEXRAD radar grid cells were used as precipitation gage locations. With this input, TOPSETUP determines the set of weights used to estimate sub-basin precipitation in terms of individual NEXRAD radar grid cells.

### **2.3. The DMIP Experiment**

Results were submitted to the National Weather Service (NWS) for the period June 1, 1993 to July 31, 2001 with May 1, 2000 – July 31, 2001 serving as a validation

period. Our group submitted both calibrated and uncalibrated results for all five basins, all interior locations within each of the five basins [Reed *et al.*, 2004], and over the entire calibration and validation period requested by the NWS. The difference between calibrated and uncalibrated simulations showed how simulations improved with calibration specific to a particular basin. With calibration using streamflow measurements at basin outlets, model predictions reported at interior locations can test the ability of distributed models to predict flow at ungaged locations. With model calculations performed at an hourly time step, results can be analyzed in terms of usefulness and acceptability for multiple uses, including flood forecasting.

### **2.3.1 Spatial Configuration**

To delineate streams and sub-basins we used the 30 m resolution National Elevation Dataset DEM [USGS, 2003] for this region. Software developed by *Tarboton* [2002] was used to filter the DEM, remove pits and calculate the single (D8) flow direction and contributing drainage area associated with each grid cell. The curvature based drainage network delineation method described by *Tarboton and Ames* [2001] was used to delineate streams. This method delineates the highest resolution stream network statistically consistent with empirical geomorphologic laws, specifically the constant drop property [*Broscoe*, 1959] which is related to Horton's slope and length laws and the power law relationship between stream slope and drainage area [*Flint*, 1974]. The average drainage density that resulted was  $0.4 \text{ km}^{-1}$  for the DMIP watersheds. The resulting channel network was visually checked against digital raster graph images of USGS 1:24000 topographic maps.

The DMIP stream gage and ungaged simulation point locations were all found to lie on 3<sup>rd</sup> or higher order streams. To reduce the number of model elements involved we generalized the delineated stream network by eliminating all first and second order streams. The DEM flow direction grid was then used to delineate the sub-basin draining directly to each 3<sup>rd</sup> or higher order stream reach. These sub-basins are illustrated in Figure 2.3 and were used as model elements in TOPNET. The average size of the model elements was 90 km<sup>2</sup>.

The  $D_{\infty}$  multiple flow direction algorithm [Tarboton, 1997] was used to calculate flow direction, slope ( $\tan\beta$ ) and specific catchment area,  $a$ , for each grid cell in the DEM. This method provides a better estimate of contributing area on hillsides [Tarboton, 1997]. The distribution of wetness index,  $\ln(a/\tan\beta)$ , within each sub-basin was represented using a histogram that recorded the fraction of the sub-basin within each wetness index class. Figure 2.4 illustrates the wetness index and wetness index histograms for a portion of the Blue River watershed.

### **2.3.2 Temporal inputs**

Climate inputs included precipitation at each NEXRAD Stage III radar grid location. Radar data was modeled as point rainfall measurements at the center of each 4x4 km<sup>2</sup> radar grid cell. Hourly data for air temperature and dew point temperature at each basin gage location, provided by NCDC Cooperate Observer Stations, were adjusted from the gage elevation to the basin average elevation of each sub-basin using lapse rates.

### 2.3.3 Parameter Estimation and Calibration

Parameters are time invariant and describe the unchanging properties of the sub-basins or model elements. The parameters of TOPNET are related to physical properties of the sub-basin, including soils, topography, land cover and channel geometry. These are calculated from spatial GIS data and may be spatially uniform, spatially variable and calibrated, or uncalibrated. Table 2.1 lists the TOPNET model parameters. The third column of Table 2.1 summarizes how each parameter was estimated in the DMIP experiment. Parameters  $f$ ,  $K_o$ ,  $V$ ,  $Cr$ , and  $n$ , were calibrated for the August 2002 DMIP submission.

Sub-basin model elements have their own distinct model parameters and state variables derived from the soil and vegetation data. The pattern of the spatial variability between sub-basins is maintained during calibration by using multipliers for each parameter that are the same across all sub-basins to scale the Geographic Information System (GIS) derived sub-basin parameters for each sub-basin by the same factor. The calibration procedure uses multipliers, rather than individual sub-basin parameters as its calibration variables. One multiplier value for each parameter applied uniformly to the entire watershed limits the degrees of freedom, and is a parsimonious way to maintain spatial variation between sub-basins based on GIS-derived parameter values.

To prepare TOPNET model input, soils and land cover data were interpolated to the 30 m DEM grid scale. The mapping from soil texture classes and land cover types to model parameters is through a set of value attribute lookup tables, which associate a model parameter value with each 30 m grid cell. Spatial averages of the 30 m grid cell

parameter values over the sub-basins that represent model elements are used to obtain the sub-basin parameter values.

Parameters obtained from soil data were derived using soil texture for each of the 11 standard soil depth grid layers from the Pennsylvania (Penn) State University gridding of the NRCS STATSGO database. Figure 2.5 illustrates the derivation of distributed soil based parameters from the soil database. Soil texture from 11 depth based grid layers was associated with each soil class identified using a map unit identifier. The texture of each layer was used to obtain soil parameter values based on the soil hydraulic properties given by *Clapp and Hornberger* [1978] for each layer. A depth-weighted average was used to calculate the soil class parameter values for drainable porosity, plant available porosity, and wetting front suction. Linear regression of  $\ln(K)$  versus depth  $z$  was used to fit the assumed exponential function describing decrease of hydraulic conductivity with depth and estimate saturated hydraulic conductivity at the surface,  $K_0$  and sensitivity parameter  $f$ , for each soil class. This regression did not always work because in some soil profiles, hydraulic conductivity increased with depth, or was constant. A lower bound value of  $f=0.667 \text{ m}^{-1}$  was used in these cases corresponding to a soil depth length scale of 1.5 m.

Parameter values for lapse rate, soil zone drainage sensitivity, and hydraulic geometry were left at the default values set in TOPNET, given in Table 2.1. Parameter values for land cover are given in Table 2.2. The model was run for an initialization period of 24 days before the DMIP comparison period beginning June 1, 1993, to account for lack of prior knowledge of the initial state variables.



This is the first application that uses this procedure for estimating parameters from STATSGO soil and NASA LDAS vegetation data with TOPNET. There is a scale difference between the sub-basin  $K_o$  and  $f$  parameters and the point scale parameters inferred from GIS soil texture data. Because of this scale difference, we did not have good default parameters to use in a truly uncalibrated model run and general multiplier values for  $f$  and  $K_o$  were developed to produce quasi-uncalibrated, or not formally calibrated simulations. Saturated store sensitivity,  $f$ , is related to streamflow recessions. An average  $f$  was obtained by analysis of recessions in the DMIP basins and divided by the average  $f$  from the soil data to obtain the default  $f$  multiplier for the uncalibrated model runs. Conceptually, the multiplier value relates the average soil  $f$  to the average recession  $f$ . We had hoped to develop an empirical relationship between soil  $f$  and recession  $f$  using values from each gaged basin, but were unsuccessful. The default multiplier value for surface saturated hydraulic conductivity,  $K_o$ , was selected by trial and error so that, on average, peak flows were of the correct order of magnitude for the DMIP basins. The multiplier values used for uncalibrated model simulations were: 1) saturated store sensitivity,  $f$ : 6.67, and 2) surface saturated hydraulic conductivity,  $K_o$ : 1000. The multipliers for other parameters were held at 1 for uncalibrated model simulations.

Although the official calibration period for the DMIP experiment was June 1993 to May 1999 with a validation period to July 2001, we used a shortened calibration period and calibrated to observed stream flow at the gaged basins for the time period of October 1998- May 1999. We hoped that calibrating to the end of the dataset up to the validation period would avoid incorporating the bias noted in the rainfall prior to 1997 [Seo *et al.*, 1997].

We used the Shuffled Complex Evolution (SCE) algorithm [Duan *et al.*, 1993] implemented in NLFIT [Kuczera, 1983a, b; 1994] to calibrate five selected parameters, 1) saturated store sensitivity,  $f$ , 2) surface saturated hydraulic conductivity,  $K_o$ , 3) canopy capacity,  $CC$ , 4) Manning's  $n$ , and 5) overland flow velocity,  $V$ . NLFIT is a software package that allows the user to choose parameters for optimization and runs the model for a range of parameter values chosen by the SCE algorithm using a global probabilistic search. We used this method to search for multiplier values for each of the calibrated parameters. The unique GIS-derived parameters for each sub-basin were uniformly scaled up or down using the multiplier value derived for the entire watershed. The objective function used in calibration was the mean square error between modeled and observed hourly streamflow. Lack of time and resources limited experiments with different objective functions. The remaining 10 parameters were left uncalibrated due to the model being less sensitive to these parameters and to keep the calibration parsimonious recognizing concerns regarding over parameterization of distributed models.

## **2.4. Results and Analysis**

The model was calibrated using streamflow, once for each of the five DMIP experiment gaged flow locations. The calibration for each DMIP basin used only the downstream gaged location and reserved the interior gaged locations for validation. The number of function evaluations for the search algorithm to minimize the mean square error was as low as 916 for the Elk Basin and as high as 2668 for the Blue Basin.

Results are separated by calibration and validation periods in order to compare the model performance of the two periods, as well as to compare the model performance of calibrated and uncalibrated simulations. The values for calibrated parameter multipliers are given in Table 2.3 for the five parameters that we calibrated for each DMIP basin, with the corresponding number of function evaluations and the mean square error for our shortened calibration period. We were able to obtain convergence in all cases, an indication of the robustness of the SCE algorithm. This limited study leaves open future exploration of alternative calibration objectives, improvements in parameter estimation schemes, exploration of non-uniqueness of parameter values and uncertainty in model predictions due to multiple behavioral parameter sets.

#### **2.4.1 Flow Prediction**

Statistical analyses of the simulations at the calibration streamflow gages are presented in Table 2.4 for the calibration period and in Table 2.5 for the validation period. Tables 2.6 and 2.7 give statistics at the internal locations not used in calibration. Statistical measures included: modeled average flow, hourly root mean square, mean absolute error, absolute maximum error, Nash-Sutcliffe efficiency measure (NSC), percent bias, and peak difference. Equations for statistical measures are available in [Gupta *et al.*, 1998]. Measured average flows are included to provide a reference scale for the results.

Figure 2.6 gives a hydrograph comparison for the Illinois River at Tahlequah in 1997. Rainfall is shown as basin average daily totals from NEXRAD data, and hydrograph plots include observed streamflow, simulated streamflow with calibration and

simulated streamflow without calibration. This figure is typical of many of the hydrograph comparisons obtained and illustrates some of the challenges faced in this modeling experiment. In some cases, the uncalibrated flows matched peaks better than the calibrated flows; see dates 2/20, 6/1, 7/10, and 8/12 in Figure 2.6. Looking at intermediate model outputs (not shown here) reveals that the baseflow from the uncalibrated model tends to better match the observed streamflow. The difference between model and observed baseflow after calibration is a significant contributor to the bias reported in Tables 2.4 – 2.7. There are also peaks in the simulated streamflow due to what appear to be significant basin average daily rainfall totals in excess of 20 mm, where little or no observed streamflow peak occurs. These may be due to the radar overestimating the rainfall input, or to snow, which had not been incorporated into TOPNET at the time of these model simulations, or due to limitations in the models ability to represent antecedent conditions and discern whether or not the basin is primed to respond to rainfall.

The values for the Nash-Sutcliffe efficiency reported in Tables 2.4 and 2.5 (parent basins) and Tables 2.6 and 2.7 (interior locations) are different from the values in Table 9 of *Reed et al.* [2004] since our statistical measures are reported for the calibration and validation periods separately. Using the Nash-Sutcliffe efficiency, where a value of 1 represents a perfect fit and values less than 0.7 are generally considered unacceptable, one can see that many of our simulations would be deemed unacceptable. One can also see that both our calibrated and uncalibrated model simulations are better in the validation period than over the calibration period, with the exception of the Blue River. The improved model performance in the validation period is possibly due to the fact that

we calibrated our models only to the portion of the streamflow record immediately before the validation period that is more similar to the validation period than the entire calibration period. There is also variability in model performance measures due to the differences in precipitation and streamflow patterns between calibration and validation periods.

In Tables 2.4 and 2.5, there is a notable difference in the relatively better performance at Illinois at Tahlequah, Illinois at Watts, and the Baron Fork at Eldon compared to the poor performance at the Elk River watershed and Blue River, Oklahoma. Looking at the Nash-Sutcliffe efficiency and bias results, one can see that the Nash-Sutcliffe efficiency is improved by calibration. This is expected with the use of mean-square error as an objective during calibration. This improvement in mean square error comes at a cost however, in terms of increased bias associated with the calibrated flows. The statistical improvement does not therefore necessarily reflect an improvement in terms of simulated hydrographs. This was evident in Figure 2.6 where, although the calibration resulted in better fitting of some high peak flows which dominate the mean square error differences, calibration resulted in an overall increase in modeled flows and decreased the quality of model performance during average and low flow periods.

The percent bias, calculated for the entire experimental period (calibration and validation periods), is presented in Figures 2.7 and 2.8, where the calibration (Figure 2.7) created a model that fits the high spring flows, but that causes over-prediction during the rest of the year, during lower flow periods. The uncalibrated results (Figure 2.8) show the tendency of the model to over-predict streamflow in the first three months of the water year, and then to under-predict during the higher flow periods.

#### 2.4.2 Using Distributed Models to Simulate Flow at Uncalibrated Interior Locations

There are three DMIP interior locations that were modeled as “ungaged” but have measured streamflow to use for testing model results. The comparison of model performance in the additional five ungaged locations are presented using the coefficient of variation to compare with the models in *Reed et al.* [2003]. Tables 6 and 7 present the statistical results for the interior locations with measured streamflow not available for calibration. Using the Nash-Sutcliffe coefficient as a measure, the calibrated model did well modeling the high flows at Peacheater Creek, especially during the validation period. This result is encouraging since the June flood event was greater than 100 times the average low flows in the creek (Figure 2.9a). However, the effect of calibration on the peak flows can be seen when a log scale is used, Figures 2.9b,c. Figure 2.9c shows the streamflow for this period in the Baron Fork at Eldon. This is the streamflow location used in calibration. High flows dominate the mean square error objective and Nash-Sutcliffe efficiency measure. The high flows in Figure 2.9c are well matched, suggesting that the physical processes involved in the generation of high flows have been sufficiently captured by the model to carry over into an out of sample validation period. This matching of high flows also carries over to the interior Peacheater Creek location.

The low flow recessions are not modeled well, either at Baron Fork (Figure 2.9c) or Peacheater Creek (Figure 2.9b). TOPMODEL has a single function that models baseflow recession, equation (10). The calibration has resulted in the adjustment of the sensitivity parameter  $f$  to match high flow recessions rather than low flow recessions.

*Jakeman and Hornberger* [1993] identified the need for rainfall runoff models to include

both a quick flow and slow flow response. In TOPMODEL, as it is functioning in the subsurface storage component of TOPNET, the response is being controlled by the single exponential discharge-storage function that is unable to represent both high and low flow recessions. Furthermore the recessions in Figures 2.9b and c on the log scale appear close to linear suggesting that linear discharge-storage, rather than exponential discharge-storage functions may be better for this watershed. These results indicate that if the full range of streamflow is to be simulated successfully a more flexible parameterization of the discharge-storage function is required, perhaps along the lines of *Lamb and Beven* [1997] or *Duan and Miller* [1997]. Using validation periods and interior locations for testing model performance of distributed models has helped us test our model assumptions and their impact on simulation of streamflow. The DMIP intercomparison experiment has proven to be a valuable and important framework for assessment of model performance before operational or other model applications are implemented.

### **2.4.3 Using Radar Rainfall for Distributed Modeling**

The propagation of radar-rainfall estimation errors through runoff predictions should be estimated. Unfortunately, because all available rain gage data was used in the generation of NEXRAD Stage III data, there is no independent data to assess the accuracy of this data [*Young et al.*, 2000]. Examples of limitations are well documented in the literature [*Smith et al.*, 1996; *Young et al.*, 2000]. Lack of information on the uncertainty in radar rainfall inputs does limit the interpretation of model performance based on statistical measures, especially over time-scales longer than the single event.

#### **2.4.4 Diagnosis of TOPNET Using DMIP Results**

One of the benefits of distributed hydrologic modeling is the spatial variation of intermediate calculations and model results. Participation in the DMIP experiment has provided a good way to test the strengths and weaknesses of TOPNET and point towards directions for model improvements. In Figures 2.10 through 2.14, we use November-December data from 1994 for the Baron Fork at Eldon as an example of how we perform model diagnosis using the different modeled responses captured by calibrated and uncalibrated results. This time period is presented since the temporal shift in bias with over-prediction in the early part of the water year was of special interest. We wanted to check whether this bias is a function of radar input bias, model structure, or soil parameterization.

In Figure 2.10, the hydrograph for the time period shows that the calibrated result fits the peak event in the beginning of November, and the uncalibrated result over-estimates the peak flow. Figure 2.10 also shows that the calibrated result over-predicts the low flows while the uncalibrated flow fits the low flows and recessions better. An investigation of how the model is partitioning the flows can be conducted by checking the basin averaged model component results during the time period. Figure 2.11 shows the averages of sub-basin outputs for some TOPNET diagnostic variables, this is an aggregate view of model response. The calibrated and uncalibrated models have different basin averaged flow, baseflow, saturation excess runoff, depth to the water table,  $\bar{z}$ , and soil zone storage. Canopy storage, evapotranspiration, and infiltration



excess were also investigated but these results are not shown because the calibrated and uncalibrated modeling of these components was not significantly different.

Figure 2.12 shows the streamflow originating from each individual sub-basin, indicating that the difference in modeled response can be traced to specific sub-basins. Sub-basin one does not contribute to the difference in flow between calibrated and uncalibrated simulations while all the other sub-basins do, to a varying degree. The parameters to which basin response is most sensitive are  $K_o$  and  $f$ . These are reported in Table 2.8 for each sub-basin within the Baron Fork at Eldon watershed. This table also presents the calibration and default (uncalibrated) multipliers that were used to obtain these parameters from those derived directly from the soils data. Most notable is that overall the  $f$  parameter is larger for the uncalibrated than for the calibrated simulations.

The streamflow response in these model simulations is dominated by baseflow and saturation excess runoff. Baseflow responds at short time scales representing the subsurface streamflow response. Saturation excess is due to precipitation on saturated areas where the wetness index is large. The simulated extent of saturated area is related to the simulated depth to the water table and increases as the depth to the water table decreases. Figure 2.13 shows the depth to the water table modeled in each basin. A large  $f$ , acting through equation (10), makes the baseflow from a sub-basin more sensitive to changes in depth to water table and hence more sensitive to precipitation inputs. This is the main reason why, in general, the uncalibrated simulations are flashier. However, because of the nonlinear exponential form of equation (10), sensitivity to  $\bar{z}$  depends upon changes in  $\bar{z}$  in a multiplicative, rather than additive way. A change in  $\bar{z}$  by  $\Delta\bar{z}$  results

in multiplication of baseflow by a factor  $e^{-f\Delta\bar{z}}$ . If baseflow is small, the change is still small in absolute terms. If, however, baseflow is large, the change is large.

The specific degree to which a sub-basin is more or less flashy in uncalibrated versus calibrated simulations depends upon the juxtaposition of precipitation, antecedent precipitation and basin parameters. Figure 2.14 shows the sub-basin rainfall in each sub-basin with the three-day storm totals associated with the 11/6/94 and 12/9/94 events, as well as the prior 3-month antecedent precipitation. Sub-basin one has the smallest rainfall totals for this two-month period. Initial depth to water table is largest with the result that increases in soil moisture do not significantly increase the saturated area. The baseflow response from sub-basin one in both simulations is relatively minor due to the sensitivity multiplier being applied to a small number. Sub-basins five and six have different soils that result in them having different  $f$  and  $K_o$  parameters. The larger values of  $f$  should imply large sensitivity, but the large sensitivity results in the saturated zone adjusting rapidly to accommodate inputs. As soon as  $\bar{z}$  decreases due to water entering the saturated zone, the baseflow increases modulating the reduction in  $\bar{z}$ . This effect limits the range over which  $\bar{z}$  varies for these sub-basins, as indicated in Figure 2.13. The  $f$  values for sub-basins five and six are sufficiently large that this behavior is similar for both calibrated and uncalibrated simulations. In the remaining sub-basins, the depth to water table is such that streamflow is quite sensitive to decreases in  $\bar{z}$ . The sub-basins with the largest precipitation inputs (two, three and seven) that follow the largest antecedent precipitation inputs are most sensitive and exhibit the largest differences between calibrated and uncalibrated results.

We do not know, for these watersheds, how much of this model behavior is representative of reality. We also do not know whether the rainfall inputs are sufficiently resolved at the scale of sub-basins to meaningfully drive differences in sub-basin response. Distributed modeling studies like this stimulate questions and hypotheses that can be pursued further in the ongoing effort to better understand and model the hydrologic response of watersheds. We have confirmed that for TOPNET, with TOPMODEL controlling subsurface flow, the parameter  $f$  is highly sensitive and its derivation from GIS soils information and careful calibration of the multiplier value is important for accurate streamflow simulations.

#### **2.4.5 Model Run-Time**

Computer and time resources remain a limiting factor to the operational use of distributed models. Our computer system for the work was an AMD athlon XP 1900+ with 512 MB RAM, 1.4 GHz, and Windows 2000 platform. Run-time for one seven-year model run of 63,000 hourly timesteps was 4-9 minutes for a range of 9-21 model elements. Time for parameter calibration by the SCE algorithm incorporated in the NLFIT software for five parameters took between 6-9 hours. See Table 2.9 for computer run times required to model each of the DMIP basins.

#### **2.5. Discussion and Conclusion**

For both calibration and validation periods, we found that for our model calibrated flows using the mean square error objective function improved the matching of the peak streamflows, at the cost of over-predicting the low flows and introducing bias into the cumulative water balance, shown in the different results for calibrated and

uncalibrated simulations. Statistics based on the square of the error term are highly sensitive to differences between model and measured flow during peak flood flows. Overall, the model performed as well, or better in some cases, in the validation period as in the calibration period. Lack of information on the uncertainty in radar rainfall inputs limited the interpretation of statistical performance measures used in DMIP to verify the quality of flood simulations. Similarly, this lack of information would limit the useful interpretation of statistical performance measures used to verify the quality of flood forecasts in applications beyond the scope of this project.

The use of distributed models to simulate flow at ungaged interior locations was highlighted with the model results in Peacheater Creek at Christie, Oklahoma. Our model simulations with calibration were as good at interior locations, especially during the validation period, as in the larger scale basins. Understanding the reasons for the difference in relative performance in larger basins and in interior locations compared to the distributed Sacramento models will help us improve our model simulations for all basin scales. Comparative studies between the model structures for simulating the subsurface (TOPMODEL vs. Sacramento), treatment of radar rain sub-basin averaging, and soil parameterization should be conducted.

The exponential functional form of baseflow discharge-storage response limits the capability of our model to match recessions in both low and high flow scenarios and a single value per sub-basin for the  $f$  parameter may not be appropriate. If the full range of streamflow is to be simulated successfully a more flexible parameterization of the discharge-storage function is required, perhaps including separate quick flow and slow flow functionality [Jakeman and Hornberger, 1993] or development of a generalized

discharge-storage function from actual recession curve analysis [*Lamb and Beven, 1997*], or by generalizing the discharge-storage function [*Duan and Miller, 1997*].

The small difference between calibrated and uncalibrated results for TOPNET showed that, in some basins, flows could be predicted well with little or no calibration. Interior gages were modeled comparatively as well as calibrated gages and show the benefit of distributed models for simulating uncalibrated interior monitoring point locations. In future work we intend to investigate model element scale questions and sensitivity to the spatial data resolution of soil and vegetation data. We would like to increase the number of model elements to see if smaller element size improves model performance. Since the submission of DMIP results in August 2000, we have added an impervious area parameter to the model structure and will be testing this functionality in urban and disturbed watersheds.

## References

- Beven, K., R. Lamb, P. Quinn, R. Romanowicz and J. Freer, (1995a), Topmodel, *Computer Models of Watershed Hydrology*, Edited by V. P. Singh, 627-668, Water Resources Publications, Highlands Ranch, CO.
- Beven, K., P. Quinn, R. Romanowicz, J. Freer, J. Fisher and R. Lamb, (1995b), *Topmodel and Gridatb, a Users Guide to the Distribution Versions (95.02)*, CRES technical Report TR110, Centre for Research on Environmental Systems and Statistics, Institute of Environmental and Biological Sciences, Lancaster University, Lancaster LA 1 4YQ, UK.
- Beven, K. J. and M. J. Kirkby, (1979), A physically based variable contributing area model of basin hydrology, *Hydrol. Sci. Bull.*, 24(1). 43-69.
- Bristow, K. L. and G. S. Campbell, (1984), On the relationship between incoming solar radiation and the daily maximum and minimum temperature, *Agricultural and Forest Meteorology*, 31, 159-166.
- Brooks, R. H. and A. T. Corey, (1966), Properties of porous media affecting fluid flow, *J. Irrig. and Drain., ASCE*, 92(IR2), 61-88.
- Broscoe, A. J., (1959), Quantitative Analysis of Longitudinal Stream Profiles of Small Watersheds, Office of Naval Research, Project NR 389-042, Technical Report No. 18, Department of Geology, Columbia University, New York.
- Clapp, R. B. and G. M. Hornberger, (1978), Empirical equations for some soil hydraulic properties, *Water Resour. Res.*, 14:,601-604.
- Dingman, S. L., (2002), *Physical Hydrology*, 2nd Ed. Prentice Hall, Upper Saddle River, NJ.
- Duan, J, and N.L. Miller, (1997), A generalized power function for the subsurface transmissivity profile in TOPMODEL, *Water Resour. Res.*, 33, 2559–2562.
- Duan, Q., V. K. Gupta and S. Sorooshian, (1993), A shuffled complex evolution approach for effective and efficient global minimization, *Journal of Optimization Theory and Its Applications*, 61(3), 501-521.
- Eidenshink, J. C. and J. L. Faundeen, (1994), The 1-Km Avhrr global land data set: First stages in implementation, *International J. of Remote Sensing*, 15, 3443-3462.
- Famiglietti, J. S. and E. F. Wood, (1994a), Application of multiscale water and energy balance models on a tallgrass prairie, *Water Resour. Res.*, 30(11), 3079-3093.

- Famiglietti, J. S. and E. F. Wood, (1994b), Multiscale modeling of spatially variable water and energy balances, *Water Resour. Res.*, 30(11), 3061-3078.
- Famiglietti, J. s., E. F. Wood, M. Sivapalan and D. J. Thongs, (1992), A catchment scale water balance model for Fife, *J. of Geophysical Research*, 97(D17), 18,997-19,007.
- Flint, J. J., (1974), Stream gradient as a function of order, magnitude and discharge, *Water Resour. Res.*, 10(5), 969-973.
- Goring, D. G., (1984), Flood routing by a linear systems analysis technique, *J. Hydrol.* 69, 59-76.
- Gupta, H. V., S. Sorooshian and P. O. Yapo, (1998), Toward improved calibration of hydrologic models: Multiple and noncommensurable measures of information, *Water Resour. Res.*, 24(4), 751-763.
- Ibbitt, R., (1971), Development of a conceptual model of interception, Unpublished Hydrologic Research Progress Report No. 5, Ministry of Works, New Zealand.
- Jakeman, A. J. and G. M. Hornberger, (1993), How Much Complexity Is Warranted in a Rainfall-Runoff Model, *Water Resour. Res.*, 29(8), 2637-2649.
- Kuczera, G., (1983a), Improved parameter inference in catchment models. 1 Evaluating Parameters, *Water Resour. Res.*, 19(5), 1151-1162.
- Kuczera, G., (1983b), Improved parameter inference in catchment models. 2 Combining different kinds of hydrologic data and testing their compatibility, *Water Resour. Res.*, 19(5), 1162-1172.
- Kuczera, G., (1994), *Nlfit, a Bayesian nonlinear regression program suite*, Version 1.00g, Department of Civil Engineering and Surveying, University of Newcastle, NSW, 2308, Australia.
- Lamb, R. and K. Beven, (1997), Using interactive recession curve analysis to specify a general catchment storage model, *Hydrology and Earth Systems Sci.*, 1, 101-113.
- Leopold, L. B. and T. Maddock, (1953), The hydraulic geometry of stream channels and some physiographic implications, *U. S. Geol. Surv. Prof. Paper*, No. 252.
- Priestley, C. H. B. and R. J. Taylor, (1972), On the assessment of surface heat flux and evaporation using large-scale parameters, *Monthly Weather Review*, 100(2), 81-92.

- Reed, S., Koren, V., Smith, M., Zhang, Z., Moreda, F., Seo, D.-J. & DMIP participants, (2004), Overall distributed model intercomparison project results, *J. Hydrol.*, 298 (1-4), 27-60.
- Rutter, A. J., K. A. Kershaw, P. C. Robins and A. J. Morton, (1972), A predictive model of rainfall interception in forests, 1. Derivation of the model from observations in a plantation of corsican pine, *Agricultural Meteorology*, 9, 367-384.
- Seo, D. J., R. A. Fulton and J. P. Breidenbach, (1997), Final Report for Interagency MOU among the Nexrad Program, WSR-88D OSF and NWS/OH/HRL, NWS/OH/HRL, Silver Spring, MD.
- Shuttleworth, W. J., (1993), Evaporation, in *Handbook of Hydrology, Chapter 4*, Edited by D. R. Maidment, McGraw-Hill, New York.
- Smith, J. A., D. J. Seo, M. L. Baek and M. D. Hudlow, (1996), An Intercomparison Study of Nexrad Precipitation Estimates, *Water Resour. Res.*, 32, 2035-2045.
- Smith, M., (2002), Distributed Model Intercomparison Project (DMIP), National Weather Service. Retrieved October, 2001 from the World Wide Web:  
<http://www.nws.noaa.gov/oh/hrl/dmip/>.
- Soil Survey Staff, (2006), Soil Survey Geographic (SSURGO) Database for Survey Area, Natural Resources Conservation Service, United States Department of Agriculture, <http://soildatamart.nrcs.usda.gov> [Accessed January 26, 2005].
- Stewart, J. B., (1977), Evaporation from the wet canopy of a pine forest, *Water Resour. Res.*, 13(6), 915-921.
- Tarboton, D. G., (1997), A New Method for the Determination of Flow Directions and Contributing Areas in Grid Digital Elevation Models, *Water Resour. Res.*, 33(2): 309-319.
- Tarboton, D. G., (2002), Terrain Analysis Using Digital Elevation Models (Taudem), Utah Water Research Laboratory, Utah State University,  
<http://www.engineering.usu.edu/dtarb>.
- Tarboton, D. G. and D. P. Ames, (2001), Advances in the Mapping of Flow Networks from Digital Elevation Data, World Water and Environmental Resources Congress, Orlando, Florida, May 20-24, ASCE.
- USGS, (2003), The National Map Seamless Data Distribution Server, EROS Data Center,  
<http://seamless.usgs.gov/>.



Young, C. B., A. A. Bradley, W. F. Krajewski and A. Kruger, (2000), Evaluating Nexrad multisensor precipitation estimates for operational hydrologic forecasting, *J. of Hydrometeorology*, 1(June), 241-254.

**Table 2.1.** TOPNET Model Parameters (Multiplier Calibrated (MC))

<b>Sub-Basin</b>	<b>Name</b>	<b>Estimation</b>
$f$ ( $m^{-1}$ )	Saturated store sensitivity	From soils. <b>MC</b>
$K_o$ (m/hr)	Surface saturated hydraulic conductivity	From soils. <b>MC</b>
$\theta\Delta_1$	Drainable porosity	From soils
$\theta\Delta_2$	Plant available porosity	From soils
$d$ (m)	Depth of soil zone	depth = $1/f$ From soils
$c$	Soil zone drainage sensitivity	1
$\psi_f$ (m)	Wetting front suction	From soils
$V$ (m/hr)	Overland flow velocity	360 <b>MC</b>
$CC$ (m)	Canopy capacity	From vegetation
$Cr$	Intercepted evaporation enhancement	From vegetation. <b>MC</b>
$\alpha$	Albedo	From vegetation
Lapse ( $^{\circ}C/m$ )	Lapse rate	0.0065

<b>Channel parameters</b>		
$n$	Mannings $n$	0.024 <b>MC</b>
$a$	Hydraulic geometry constant	0.00011
$b$	Hydraulic geometry exponent	0.518

<b>State variables</b>		<b>Initialization</b>
$\bar{z}$ (m)	Average depth to water table	Saturated zone drainage matches initial observed flow
SR (m)	Soil zone storage	0.02
CV (m)	Canopy storage	0.0005

**Table 2.2.** Vegetation Parameter Values Derived from Land Cover Data from NASA LDAS Vegetation Database with IGBP Classification of 1-km AVHRR Imagery

<b>VEG CLASS</b>	<b>CC (m)</b>	<b>CR</b>	<b>Albedo</b>	<b>Description</b>
0	0	1	0.23	unclassified
1	0.003	3	0.14	Evergreen Needleleaf Forest
2	0.003	3	0.14	Evergreen Broadleaf Forest
3	0.003	3	0.14	Deciduous Needleleaf Forest
4	0.003	3	0.14	Deciduous Broadleaf Forest
5	0.003	3	0.14	Mixed Forest
6	0.002	2	0.2	Closed Shrublands
7	0.0015	1.5	0.2	Open Shrublands
8	0.0015	1.5	0.2	Woody Savannah
9	0.0015	1.5	0.2	Savannahs
10	0.001	1	0.26	Grasslands
11	0.001	1	0.1	Permanent Wetlands
12	0.001	1	0.26	Croplands
13	0.001	1	0.3	Urban/Developed
14	0.0015	1.5	0.2	Natural Vegetation

**Table 2.3.** Calibrated Parameter Multipliers and Number of Function Evaluations to Converge to the Corresponding Mean Square Error Using the Period October, 1998 to May, 1999

	<b>f</b>	<b>K</b>	<b>V</b>	<b>Cr</b>	<b>n</b>	<b># Function Evaluations</b>	<b>Mean Sq. Error (mm/hr)<sup>2</sup></b>
<b>Baron</b>	2.9	411.9	3.2	0.8	5.0	1657	0.0023
<b>Blue</b>	1.7	79.9	2.4	1.1	2.4	2668	0.0017
<b>Elk</b>	1.6	187.6	1.8	0.8	3.6	916	0.0020
<b>Tahl</b>	1.8	102.7	1.8	1.0	2.8	1551	0.0011
<b>Watt</b>	1.5	134.3	3.3	0.9	4.4	2536	0.0015

**Table 2.4.** Calibrated and Uncalibrated Results During the June 1, 1993 – May 31, 1999 Calibration Period at Streamflow Gages Used for Calibration

	Calibration Period: June 1, 1993 - May 31, 1999									
	Illinois at Tahlequah		Illinois at Watts		Baron Fork at Eldon		Blue River		Elk River	
(m <sup>3</sup> /s)	Calibrated	Unclb	Calibrated	Unclb	Calibrated	Unclb	Calibrated	Unclb	Calibrated	Unclb
Measured Ave Flow	30.38	30.38	20.92	20.92	11.78	11.78	9.83	9.83	28.89	28.89
Modeled Ave Flow	35.49	32.74	24.60	22.34	13.19	12.23	15.21	13.74	38.80	35.33
Hourly RMS	25.11	32.91	20.11	29.72	14.73	18.82	17.24	21.93	38.65	56.74
Mean Abs. Error	12.99	15.03	10.15	12.09	5.29	5.82	9.31	8.90	20.35	19.76
Abs. Max Error	358.65	399.12	331.90	404.38	811.03	712.24	310.71	357.47	1398.59	1075.51
NSC	0.71	0.51	0.68	0.31	0.71	0.53	0.53	0.25	0.53	-0.02
%Bias	-48.59	7.72	-56.44	8.33	-68.58	-2.28	-238.50	-118.24	-135.08	-27.83
Peak Difference	168.12	3.38	191.57	108.04	103.12	164.14	-98.27	-117.54	1381.22	285.72

**Table 2.5.** Calibrated and Uncalibrated Results During the June 1, 1999 – July 31, 2000 Validation Period at Streamflow Gages Used for Calibration

	Validation Period: June 1, 1999 - July 31, 2000									
	Illinois at Tahlequah		Illinois at Watts		Baron Fork at Eldon		Blue River		Elk River	
(m <sup>3</sup> /s)	Calibrated	Unclb	Calibrated	Unclb	Calibrated	Unclb	Calibrated	Unclb	Calibrated	Unclb
Measured Ave Flow	30.91	30.91	19.63	19.63	9.59	9.59	2.25	2.25	19.05	19.05
Modeled Ave Flow	38.25	34.30	24.69	21.57	10.53	9.34	9.04	6.60	36.89	31.69
Hourly RMS	34.73	34.11	26.79	32.75	17.94	26.22	9.83	11.32	28.46	44.62
Mean Abs. Error	15.63	12.79	10.81	10.59	4.33	4.72	6.83	4.73	20.15	15.65
Abs. Max Error	416.95	666.95	459.10	421.72	828.58	944.58	171.59	169.35	391.99	488.90
NSC	0.81	0.81	0.78	0.67	0.84	0.67	-13.64	-18.44	0.59	-0.02
%Bias	-57.56	10.52	-55.39	15.94	-56.26	14.59	-381.56	-172.77	-199.08	-31.57
Peak Difference	181.69	-299.57	195.47	13.66	547.44	823.33	-135.42	-133.16	251.36	-226.43

**Table 2.6.** Calibrated and Uncalibrated Results During the June 1, 1993 – May 31, 1999 Calibration Period at Interior Locations Modeled as “Ungaged”

(m <sup>3</sup> /s)	Calibrated at Tahlequah				Calibrated at Eldon	
	Illinois at Watts		Flint Creek		Peachester Creek	
	Calibrated	Unclb	Calibrated	Unclb	Calibrated	Unclb
Measured Ave Flow	20.92	20.92	3.28	3.28	0.70	0.70
Modeled Ave Flow	23.97	22.10	3.88	3.57	1.03	0.96
Hourly RMS	20.90	30.26	4.25	5.61	1.25	1.93
Mean Abs. Error	9.55	12.34	1.71	2.04	0.50	0.53
Abs. Max Error	395.39	415.29	231.66	249.85	37.68	57.21
NSC	0.66	0.28	0.51	0.15	0.26	-0.75
%Bias	-41.69	8.76	-44.73	8.02	-49.58	-39.31
Peak Difference	240.23	165.38	203.54	173.77	5.70	-10.42

**Table 2.7.** Calibrated and Uncalibrated Results During the June 1, 1999 – July 31, 2000 Validation Period at Interior Locations Modeled as “Ungaged”

(m <sup>3</sup> /s)	Calibrated at Tahlequah				Calibrated at Eldon	
	Illinois at Watts		Flint Creek		Peachester Creek	
	Calibrated	Unclb	Calibrated	Unclb	Calibrated	Unclb
Measured Ave Flow	19.63	19.63	3.86	3.86	0.61	0.61
Modeled Ave Flow	24.38	21.78	4.55	4.14	0.91	0.81
Hourly RMS	28.33	35.01	12.76	14.60	1.54	2.41
Mean Abs. Error	10.46	11.13	2.40	2.92	0.42	0.45
Abs. Max Error	457.69	413.40	459.65	478.14	63.51	71.97
NSC	0.75	0.62	0.45	0.28	0.80	0.50
%Bias	-40.53	13.87	-46.42	7.97	-48.70	-31.54
Peak Difference	257.61	96.85	429.57	410.78	59.76	63.95



**Table 2.8.** Baron Fork at Eldon  $f$  and  $K_o$  Sub-basin Parameters

	calibrated		uncalibrated	
multipliers	2.9	411.9	6.7	1000
Sub-basin	$f$ ( $m^{-1}$ )	$K_o$ (m/hr)	$f$ ( $m^{-1}$ )	$K_o$ (m/hr)
1	3.76	12.4	8.69	30.0
2	3.80	12.4	8.78	30.2
3	4.02	12.4	9.29	30.0
4	4.57	12.9	10.57	31.4
5	7.93	22.8	18.31	55.4
6	6.72	20.4	15.53	49.6
7	3.73	12.4	8.63	30.0
8	4.19	12.3	9.68	29.8
9	4.14	12.4	9.57	30.2

**Table 2.9.** Model Run Time and Calibration Time for Each of the DMIP Basins

<b>Basin</b>	<b>model elements</b>	<b>run-time minutes/ model run</b>	<b>parameter calibration* (hrs)</b>
<b>Baron</b>	<b>9</b>	<b>4</b>	<b>6</b>
<b>Blue</b>	<b>9</b>	<b>7</b>	<b>6</b>
<b>Elk</b>	<b>16</b>	<b>6</b>	<b>8</b>
<b>Tahl</b>	<b>21</b>	<b>9</b>	<b>9</b>
<b>Watt</b>	<b>15</b>	<b>7</b>	<b>7</b>

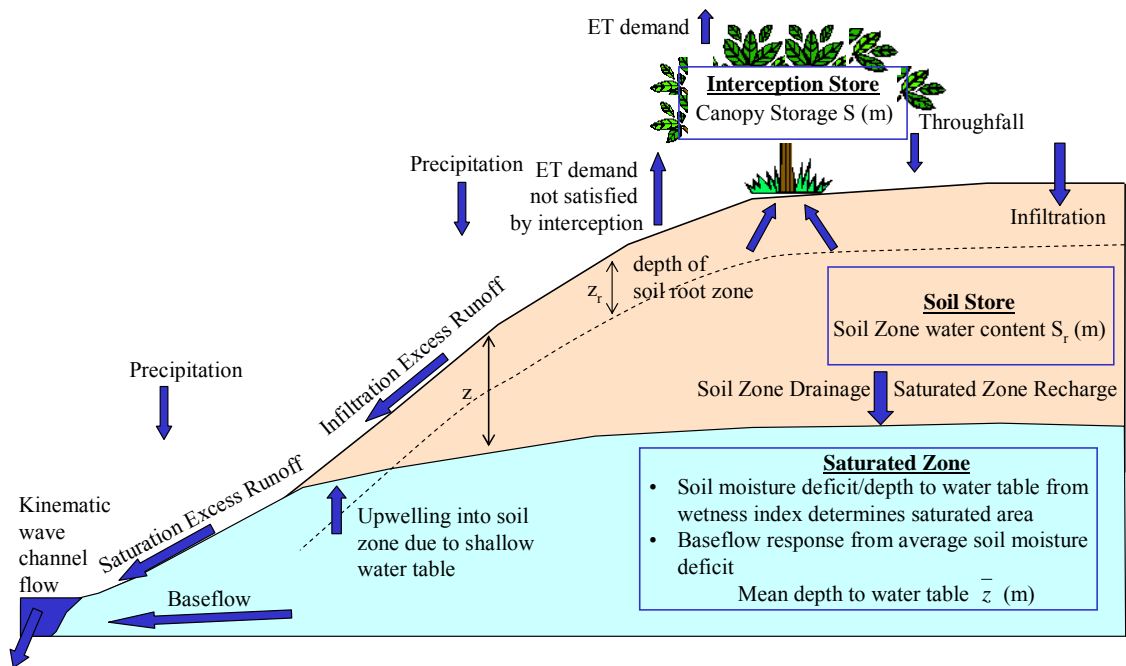


**Figure 2.1.** Schematic of the physical processes represented by the TOPNET modeling system.

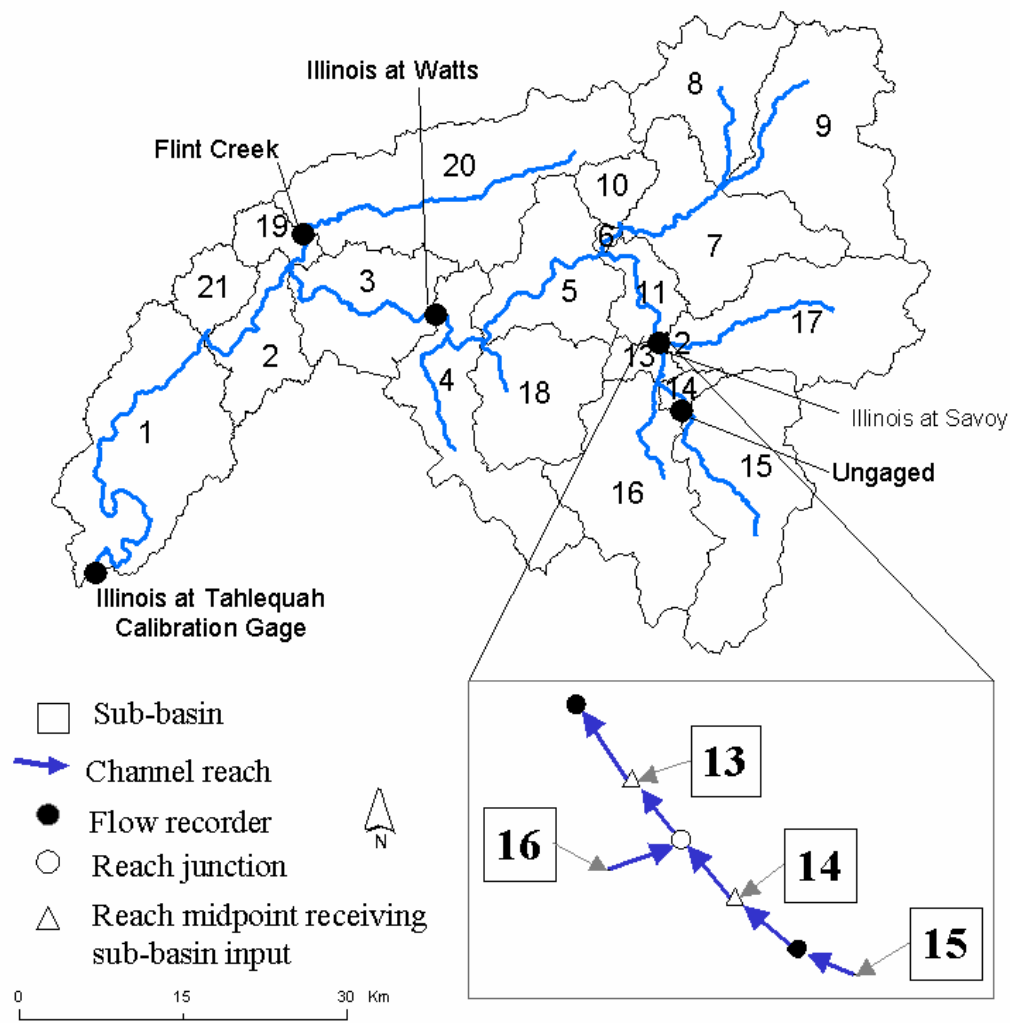


**Figure 2.2.** Model element distribution for the basin of the Illinois River at Tahlequah. Channel routing of flow from sub-basins through the channel system is displayed for the interior gage at Savoy.

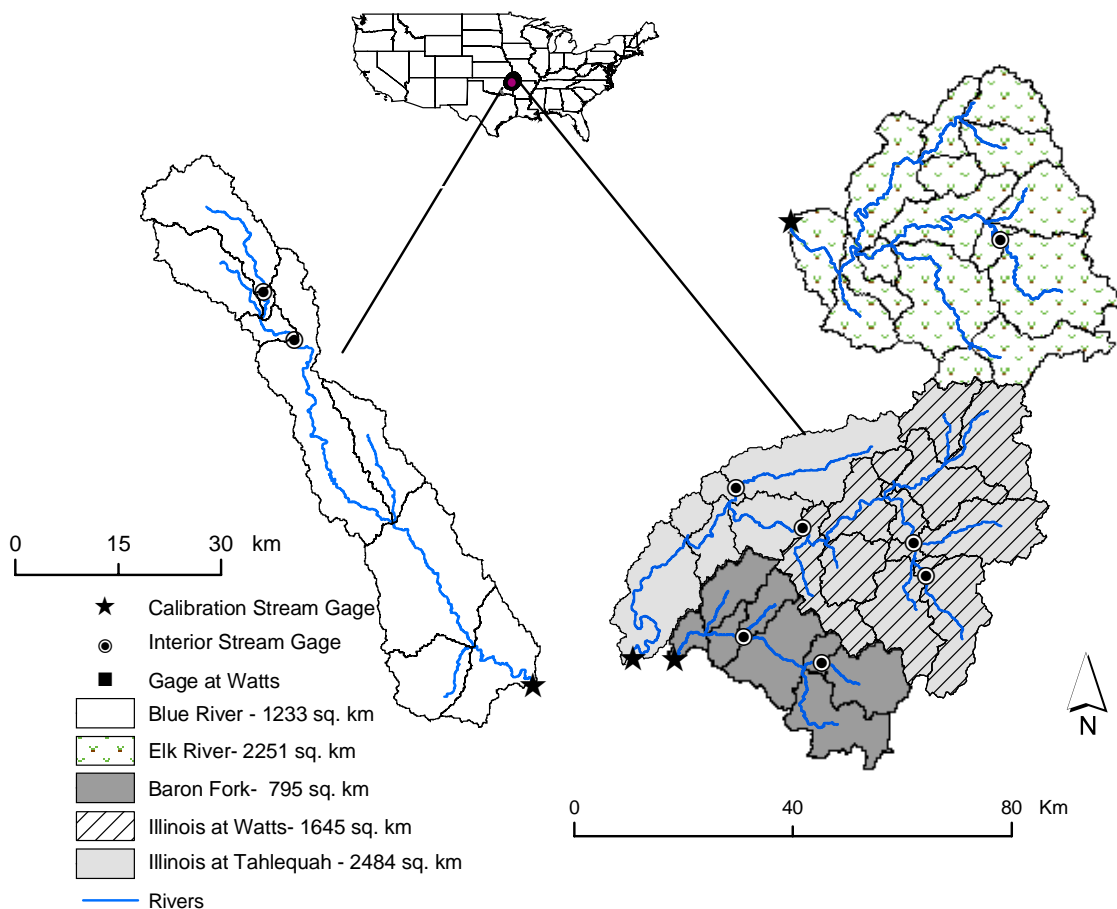


**Figure 2.3.** DMIP river basins are located in the south central United States and range in size from  $800 \text{ km}^2$  to  $2500 \text{ km}^2$ . Interior gaged locations were modeled as “ungaged” for the experiment. The Illinois at Tahlequah basin includes the Illinois at Watts basin. The Illinois at Watts streamgage location was used once as an interior “ungaged” location for modeling Illinois at Tahlequah, and secondly for the calibration of Illinois at Watts.

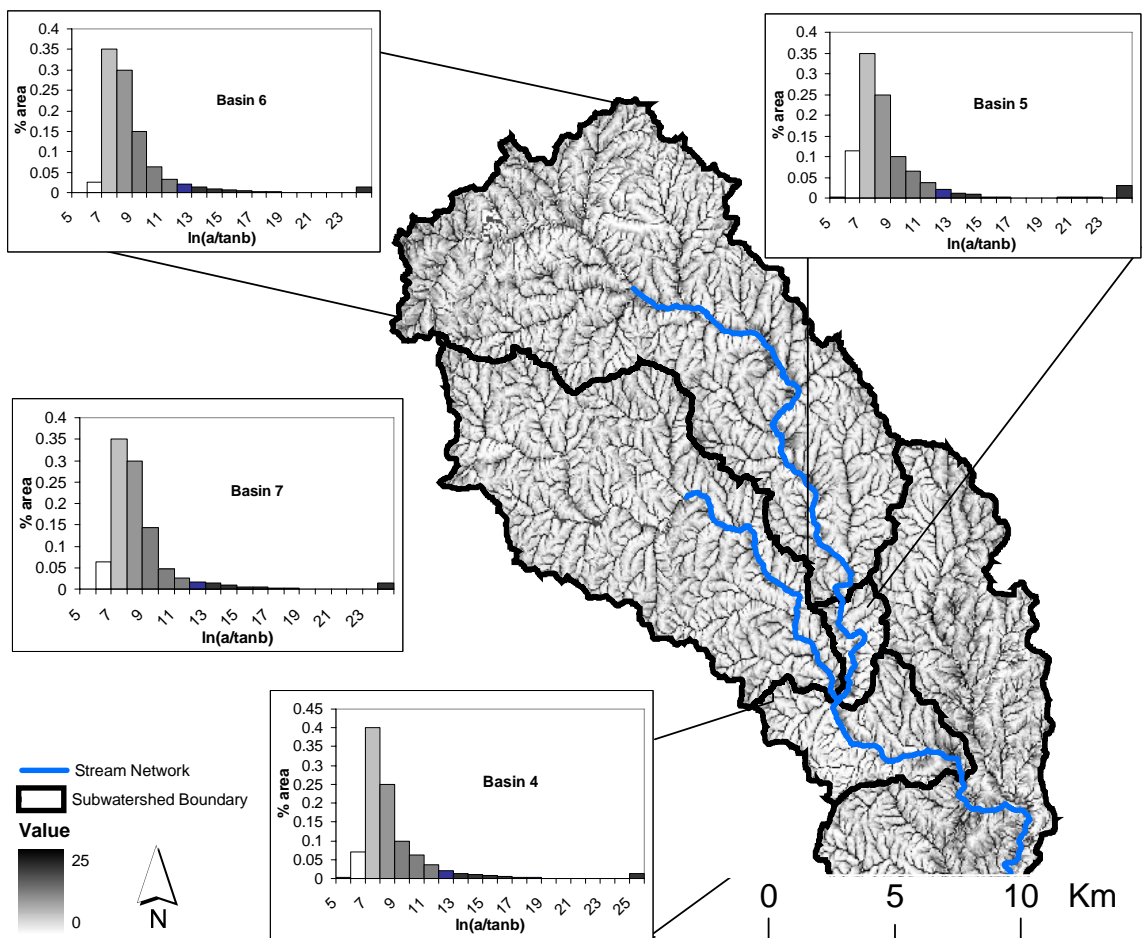


**Figure 2.4.** TOPMODEL wetness index for the upper portion of the Blue basin. A histogram represents the distribution of wetness index within each sub-basin.

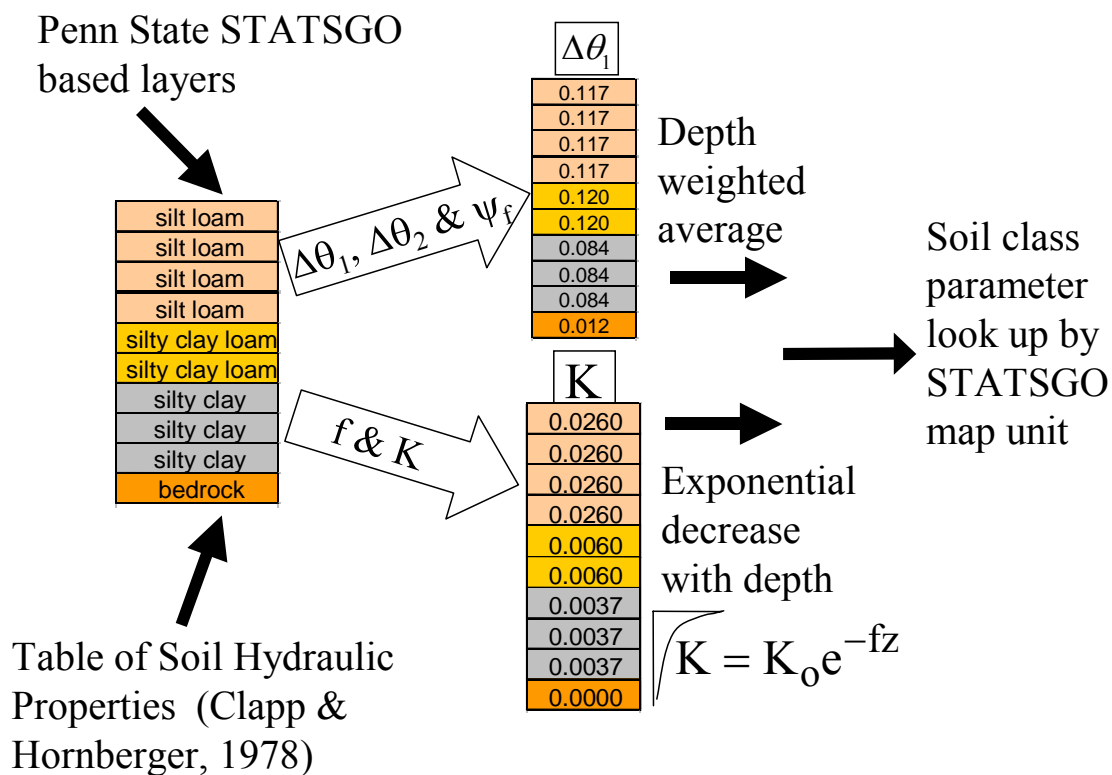


**Figure 2.5.** Derivation of distributed soil based parameters from Penn State soil texture layers derived from STATSGO.

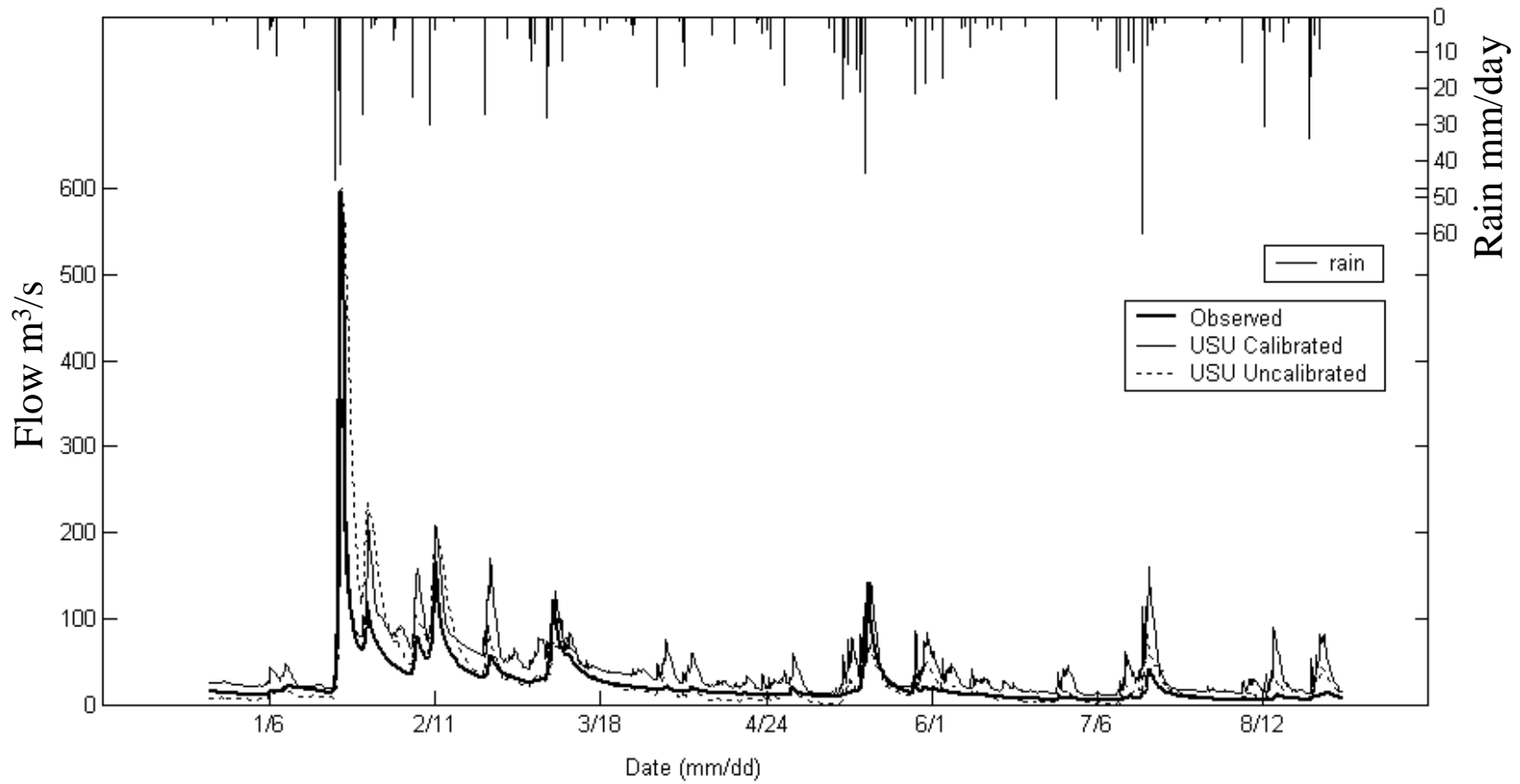


**Figure 2.6.** Hydrograph for the Illinois River at Tahlequah for flows from January, 1997 through August, 1997.



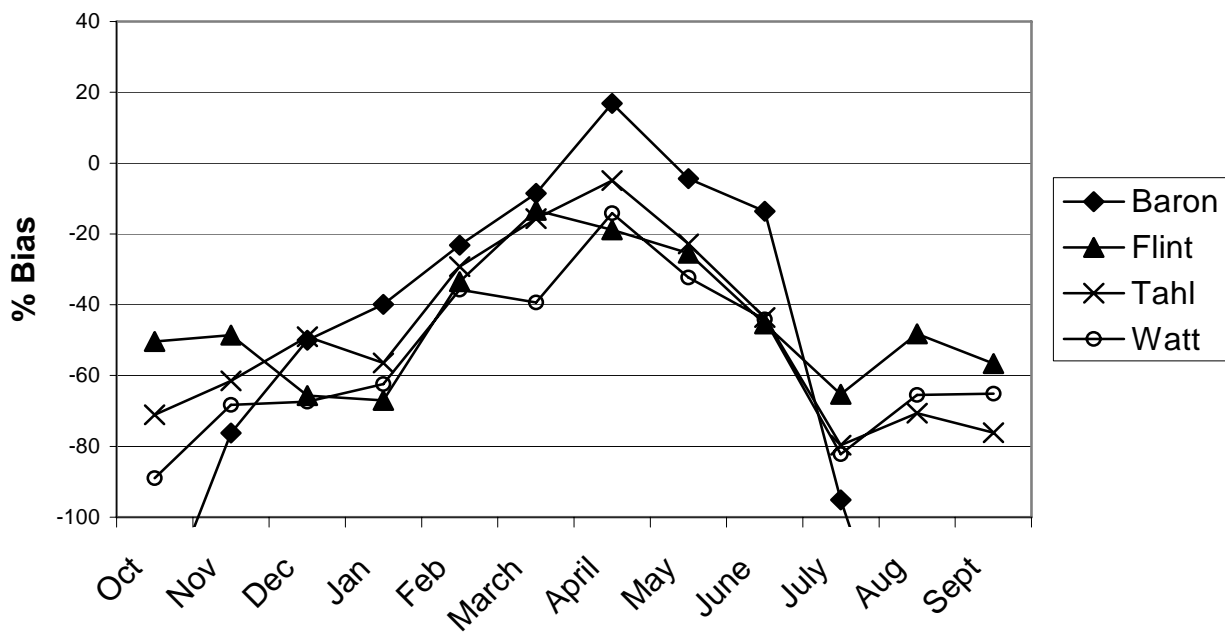


**Figure 2.7.** Percent bias of calibrated results by month for selected DMIP watersheds.

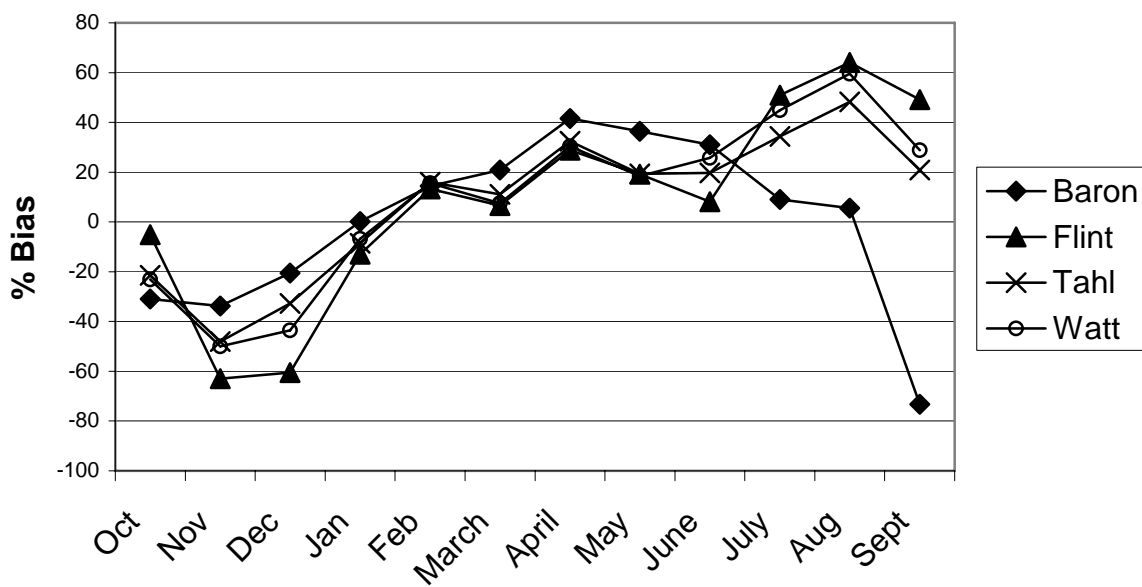


**Figure 2.8.** Percent bias of uncalibrated results by month for selected DMIP watersheds.

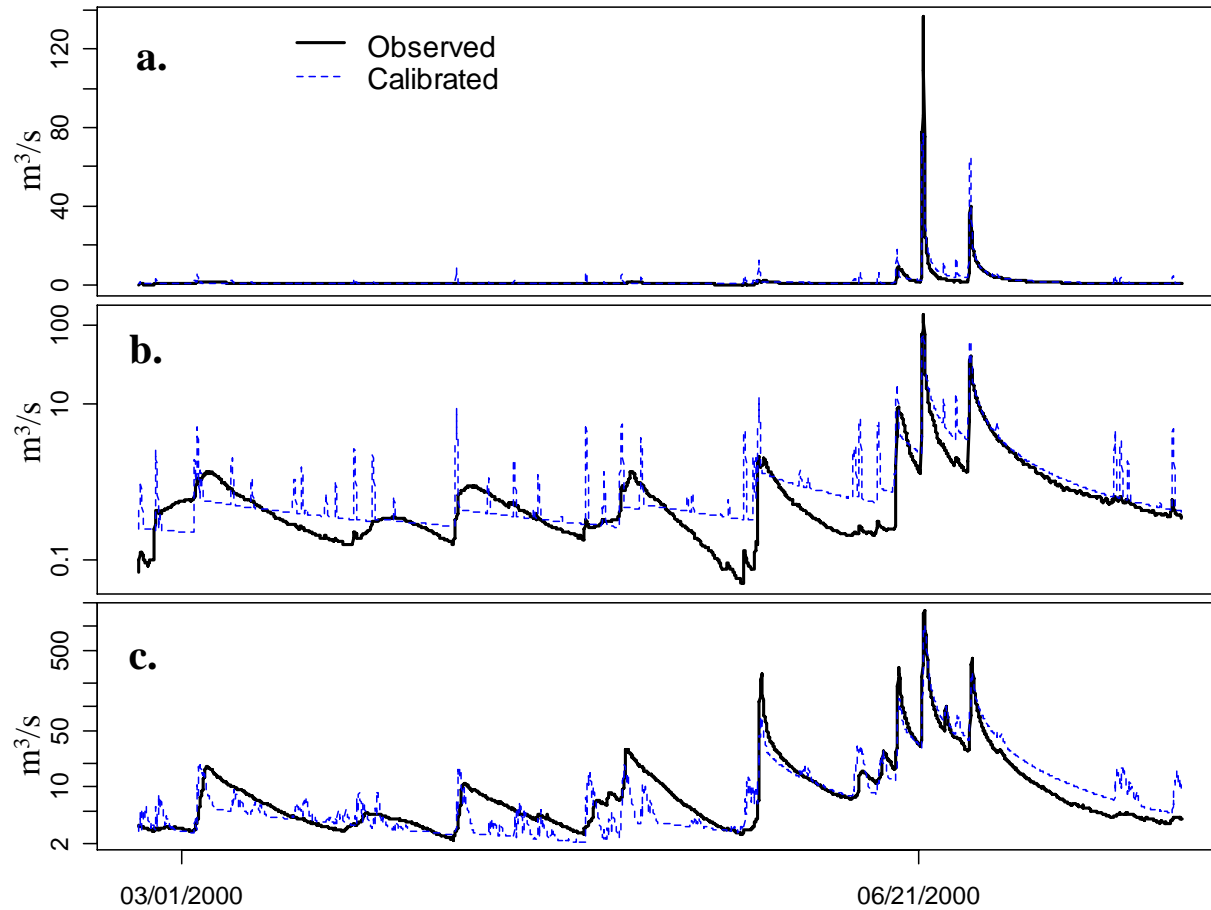


**Figure 2.9.** a) Peacheater Creek calibrated streamflow results, b) Peacheater Creek calibrated log streamflow results, and c) Baron Fork at Eldon log streamflow results for the 1999-2000 validation period.

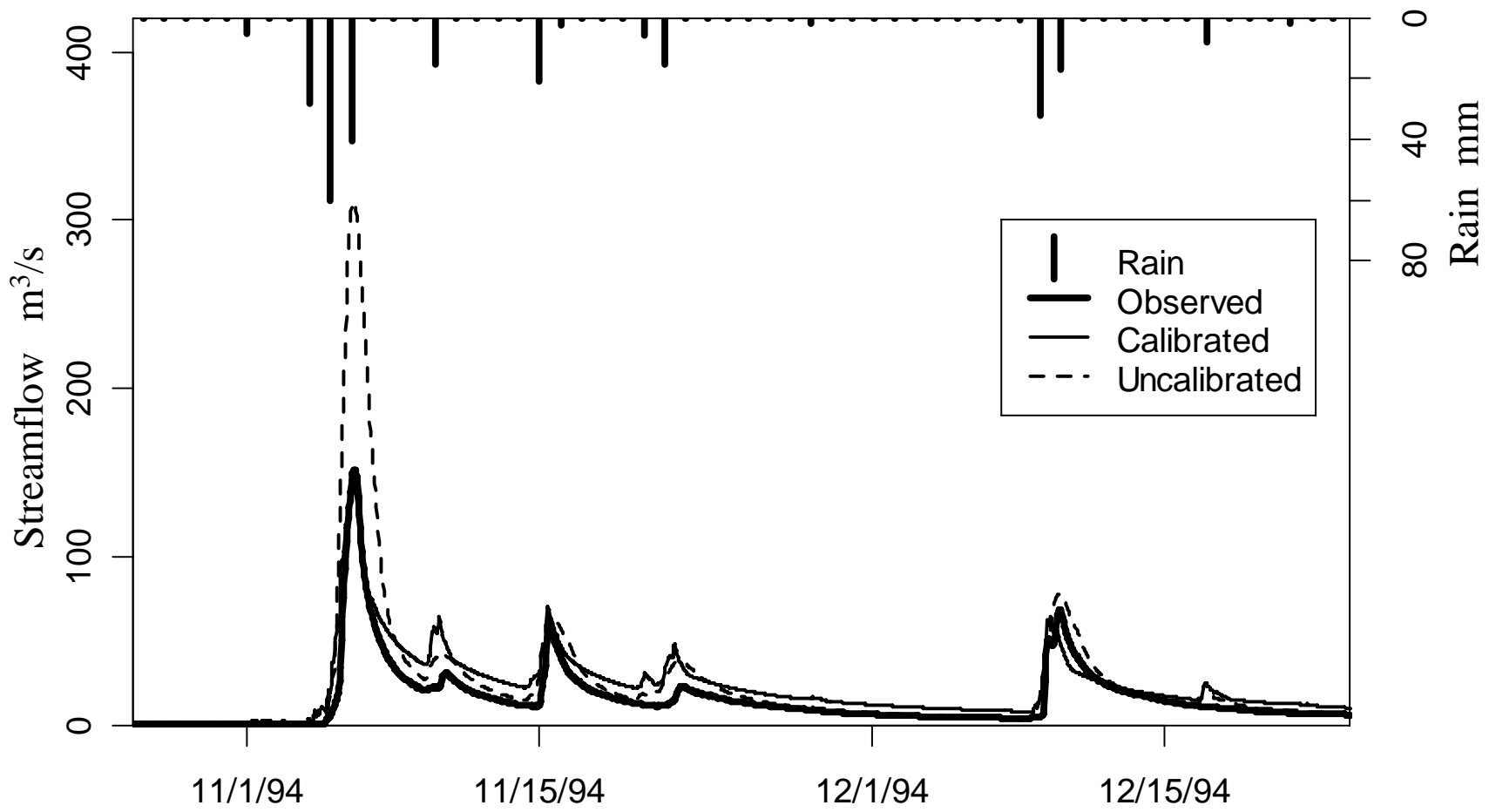


**Figure 2.10.** Calibrated and uncalibrated simulated streamflow for Baron Fork at Eldon, November 1994.

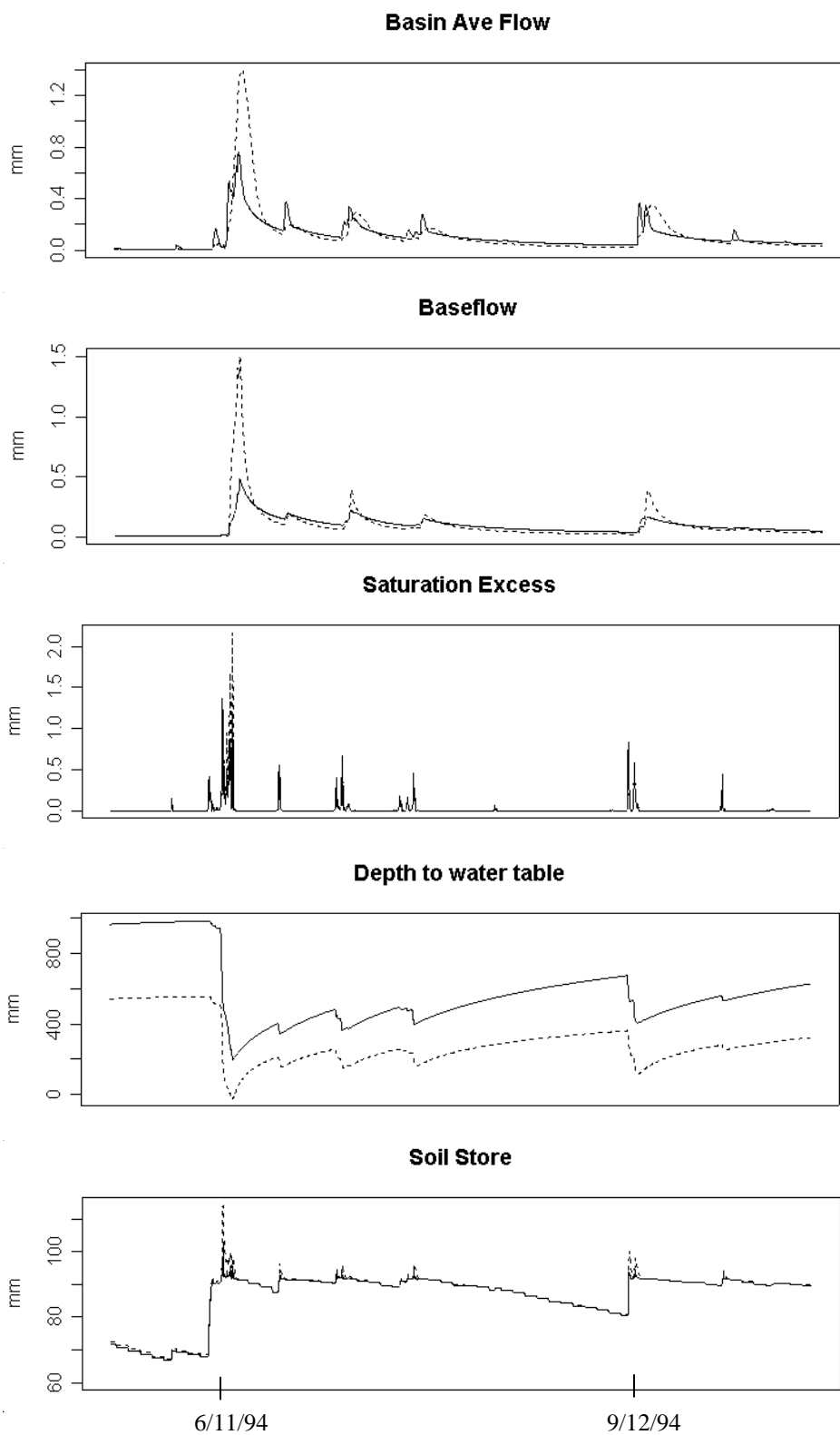


**Figure 2.11.** Calibrated (-) and uncalibrated (--) watershed averaged model components for Baron Fork at Eldon, at the beginning of the water year 10/25/1994-12/20/1994.

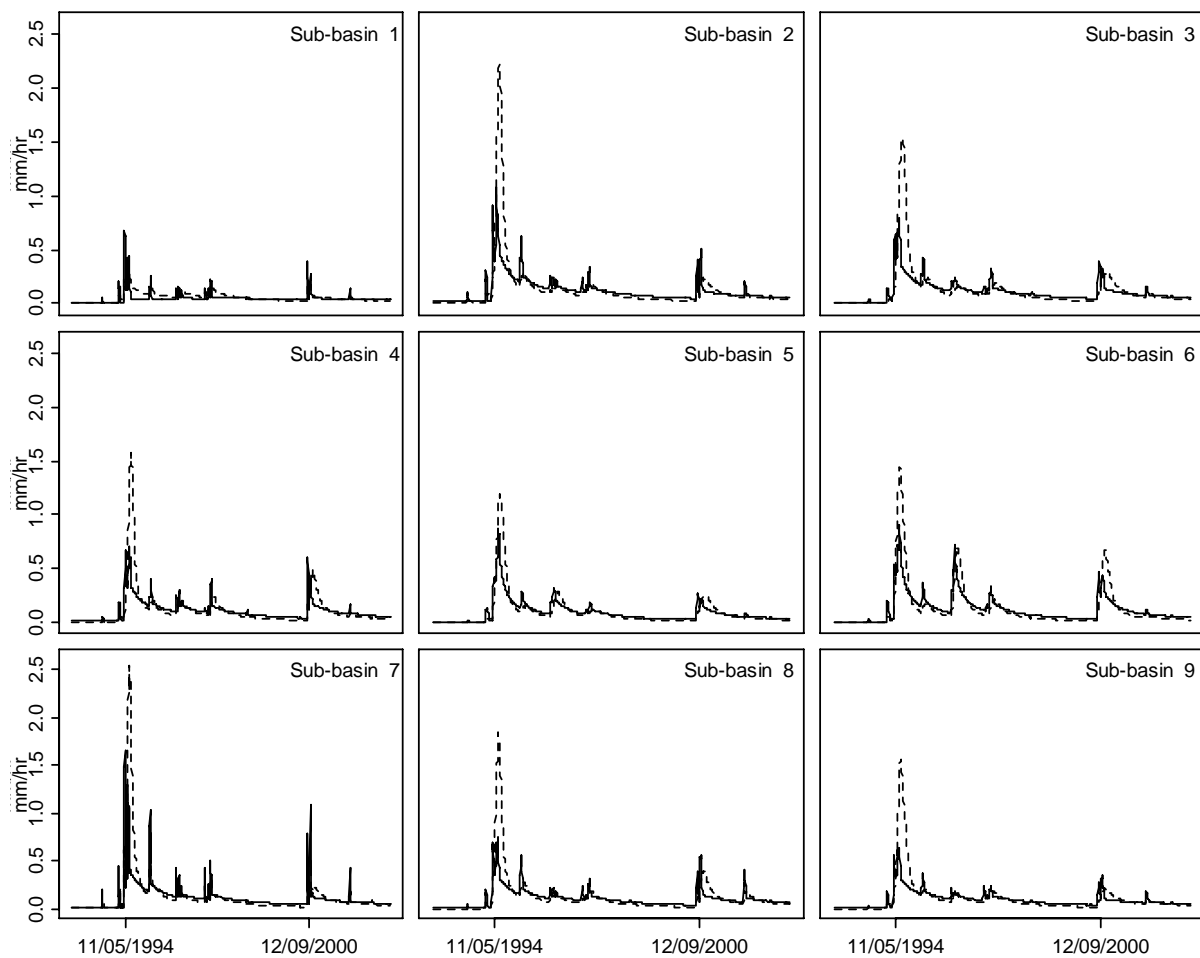


**Figure 2.12.** Calibrated (-) and uncalibrated (--) streamflow by subwatershed for Baron Fork at Eldon, at the beginning of the water year 10/25/1994-12/20/1994.

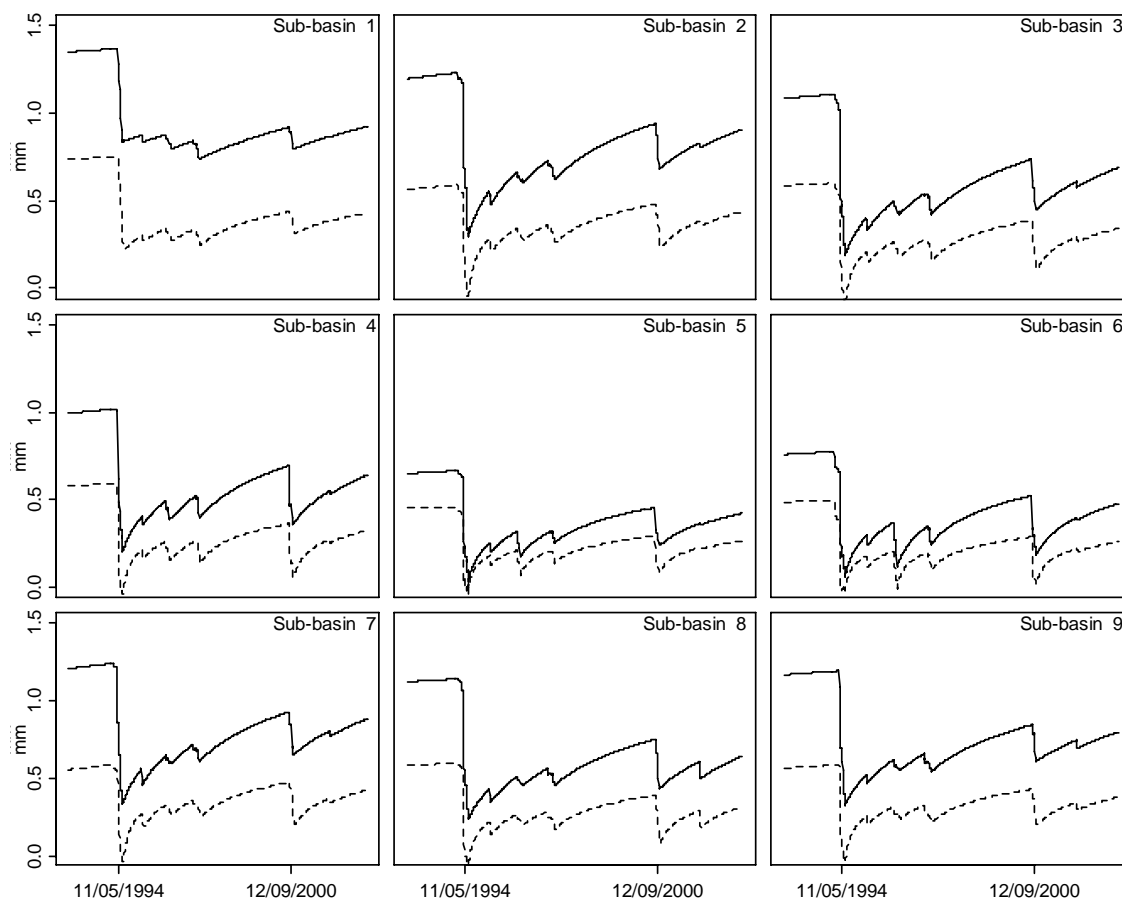


**Figure 2.13.** Calibrated (-) and uncalibrated (--) depth to the water table by subwatershed for Baron Fork at Eldon, at the beginning of the water year 10/25/1994-12/20/1994.

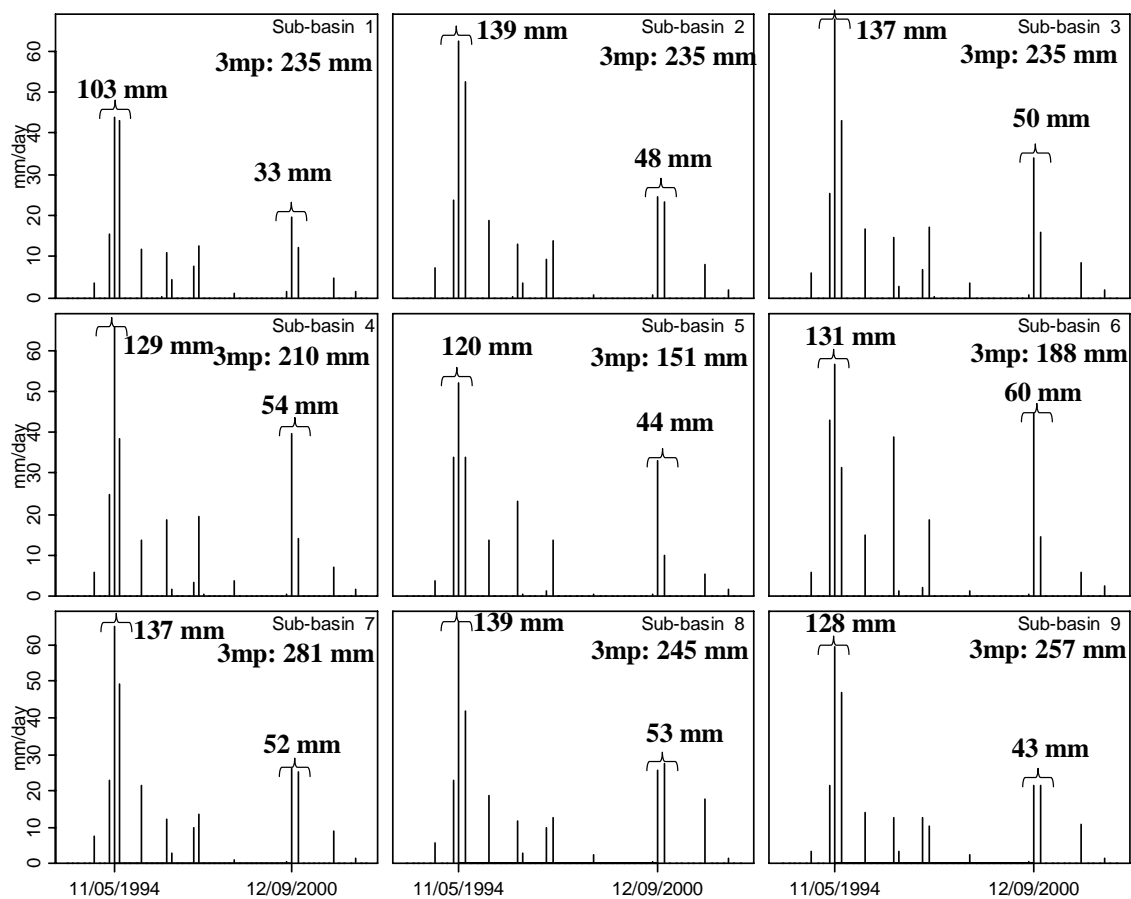


**Figure 2.14.** Radar rain subwatershed averages for Baron Fork at Eldon, at the beginning of the water year 10/25/1994-12/20/1994.



CHAPTER 3  
MULTI-OBJECTIVE CALIBRATION OF  
SPATIALLY DISTRIBUTED MODELS<sup>1</sup>

**Abstract**

Unlike calibrating a hydrologic model at a gauged basin using measured data at that location, a model for an ungauged basin only has measured information available for calibration at locations other than where the prediction is being made. This paper tests the impact on spatially distributed models using calibration of model components at one location compared to calibration using multiple locations. This paper uses two kinds of distributed models to test the calibration framework: 1) in-stream temperature and solute model and 2) a rainfall-runoff model. For this work, ungauged basins are considered basins with there is generally no measured data to compare with model results; specifically, in-stream temperature and streamflow, for the two models tested. In both cases, incorporating information from multiple locations in the calibration scheme improves the model performance over the spatial extent of the watershed compared to an optimization approach of calibrating the distributed model at one downstream location while making predictions at multiple locations upstream.

---

<sup>1</sup> Coauthored by Bethany Neilson and David Tarboton

### 3.1 Introduction

Typically, the calibration of models involves fitting model results to either single or multiple variables or error measures at a single location or combining information from multiple locations. One approach to combining information from more than one location or error measure is to use weighting schemes to merge error measures into a single objective [Madsen and Kristensen, 2002; Parada et al., 2003; Vrugt et al., 2003a; Schoups et al., 2005b]. Another approach is to use Pareto ranking to quantify the trade-off involved with multiple objectives [Schoups et al., 2005a, b; Vrugt et al., 2003a; Gupta et al., 1998]. This paper explores the effect of single location calibration schemes on model performance at ungauged locations within the model area and presents an alternative multi-objective calibration scheme for incorporating multi-location information in the modeling framework. We use two different types of distributed models to test the hypothesis that spatial multi-objective calibration provides useful information for modeling ungauged components of the hydrologic system.

For this work, we are adopting the definition of an ungauged basin as “one with inadequate records (in terms of both data quantity and quality) of hydrological observations to enable computation of hydrological variables of interest (both water quantity or quality) at the appropriate spatial and temporal scales, and to the accuracy acceptable for practical applications” [Sivapalan et al., 2003]. Precipitation and runoff are generally the variables of interest in rainfall-runoff modeling, but if the applications are broader they may involve erosion rates, sediment and nutrient concentrations, or stream temperature. From this perspective, all drainage basins are “ungauged” to some

degree and research towards understanding the application of advanced technologies to ungauged basins is applicable to all basins.

Use of distributed models for prediction of ungauged basins is an application for which it would be better not to have to rely on model calibration at all, since there is no data to use for calibration at the basin of interest. For ungauged applications, we would like our models to represent hydrologic processes so well that model fitting to observations would be unnecessary. And, in a world of perfect understanding of hydrologic processes, perfect input data, and no scale discrepancy between modeled and measured data, it might be possible to avoid distributed hydrologic model calibration. However, an important result from the Distributed Model Intercomparison Project (DMIP) [Smith *et al.*, 2004a] experiment was the acknowledgement that uncalibrated models do not have the benefit of accounting for the known biases in the rainfall archives over the calibration period. Only in the absence of rainfall biases might uncalibrated models be able to outperform calibrated models [Reed *et al.*, 2004]. Additionally, the process of model calibration is complex because of limitations in input and output data, the mathematical structure of the models, the quantitative methods used to calibrate, as well as imperfect knowledge of basin characteristics [Schaake, 2003].

This research examines a way to improve the use of spatially distributed hydrologic information within a watershed during model calibration to improve model performance at ungauged locations. During multi-objective calibration, streamflow prediction statistics are used as a measure of model performance. But in addition to attention to statistical performance, we also address how the calibration process can be

used to understand how to optimize the model with respect to the spatial heterogeneity of the hydrologic system in an attempt to learn about the unique locations that are modeled.

The Multi-Objective Shuffled Complex Evolution Metropolis (MOSCEM) [Vrugt *et al.*, 2003a] global optimization algorithm was chosen as the multi-objective calibration algorithm because of the Pareto ranking information provided about the tradeoff involved in optimizing to multiple objectives simultaneously. Implemented carefully, automatic calibration techniques that employ multiple objectives and estimates of distributions of watershed parameters may be a step towards both improving models as well as understanding hydrologic processes. For a recent assessment of state-of-the-art evolutionary algorithms for multi-objective calibration of hydrologic models, the reader is directed to *Tang et al.* [2006] and *Vrugt* [2007]. Here we use calibration at gauged basins as a way to conduct diagnostic analysis of model performance at specific locations in order to improve our understanding of how to best model ungauged basins. The aim is to use the framework as part of the model improvement process.

Many existing hydrological modeling procedures do not make best use of available information [*Wagner et al.*, 2001]. The calibration problem should be formulated using a general multi-objective framework that allows for specific calibration criteria tailored to the specific model application under consideration [*Madsen and Kristensen*, 2002]. For example, to address a watershed specific question such as “Do all sub-basins in the modeled catchment have similar dominant streamflow generation processes?” multi-objective calibration can be designed using temporal data from multiple sites and provide results on parameter interactions at each location and the trade-offs at each location when simultaneously calibrating at multiple locations. Parameter

values controlling dominant physical processes represented in the model may converge to the same value at all locations or different values at each. In this way, calibration results can contribute to the understanding of the physical system.

### **3.1.1 Calibration and The Multi-Objective Framework**

The calibration process involves choosing a measure or objective function to compare parameter sets and selecting the preferred parameter set to apply to the model. Early calibration techniques were notorious for converging to local optimal solutions and did not reliably find the global optimum [*Schaake*, 2003]. A complete review of optimization methods was presented by *Duan* [2003]. The Shuffled Complex Evolution (SCE) optimization method was a significant improvement in addressing the problem of convergence to local optima and has been shown to reliably find global optimal solutions [*Duan et al.*, 1992, 1994; *Duan*, 2003]. Current research on the calibration problem primarily focuses on uncertainty analysis and consideration of multiple objectives.

Equifinality of models recognizes that there may be no single, correct set of parameter values for a given model and that different parameter sets may give acceptable model performance [*Beven*, 2001]. The generalized likelihood uncertainty estimation (GLUE) method [*Beven and Binley*, 1992] addresses the equifinality issue by using prior distributions of parameter sets and a method for updating these distributions to make probabilistic estimates of model outputs. Multiple objective methods [*Gupta et al.*, 1998] used to address the equifinality issue are the focus of the remainder of this section.

Multi-objective calibration techniques traditionally merge multiple criteria into a single function for optimization [*Hill*, 1998; *Madsen et al.*, 1995]. However, *Gupta et al.*

[1998] made the case for maintaining independence of the multiple criteria to identify Pareto optimal solutions that capture information about parameter tradeoffs [*Gupta et al.*, 2003; *Boyle et al.*, 2000; *Schoups et al.*, 2005b]. A Pareto optimal solution is one where each objective function is minimized (in this case, statistics such as root mean square error, bias, or standard deviation) such that value of the other objectives functions are not increased. The objectives chosen should be those that are generally unrelated in order to extract complementary information from the data.

In *Gupta et al.* [1998], statistical functions such as daily root mean square error (RMSE), bias, or Nash-Sutcliffe efficiency are used as multiple objectives.

Complementary functions like RMSE, which tend to fit high flows, and bias, which weights high and low flows equally, used together in multiple objective calibration results in better overall model calibration than optimizing to RMSE or bias alone. The use of multiple objectives goes beyond minimization of statistical functions and includes:

- multi-statistic, i.e. root mean square error, bias, standard deviation;
- multi-variable measurements, i.e. groundwater level, surface runoff, soil moisture content, evapotranspiration [*Madsen and Kristensen*, 2002];
- weighted multi-site measurements, i.e. several measurement sites distributed within the catchment are merged into a single objective using a weighting function [*Madsen and Kristensen*, 2002];
- multi-response or process modes, i.e. various responses of hydrological processes, following *Boyle et al.* [2000], the hydrograph can be partitioned into components such as driven (immediate response to rain), nondriven quick (recession immediately after rain), and nondriven slow (baseflow);

- multi-resolution, i.e. using wavelet analysis to optimize to multiple time scales [Parada et al., 2003].

The result from pareto multi-objective calibration is not a single unique parameter set, but consists of a pareto set  $P(\theta)$  of solutions in the feasible parameter space. The location of the best parameter values ( $\theta$ ) within the parameter space, usually defined a-priori as a uniform distribution over the feasible space, correspond to the trade-offs between the objectives. Significant trade-offs in fitting multiple objectives may indicate an error in model structure such as a physical process not being represented in the model [Refsgaard and Henriksen, 2004].

A recent development in the field of multi-objective calibration is with the development of the Multi-Objective Shuffled Complex Evolution Metropolis (MOSCEM) [Vrugt et al., 2003a] global optimization algorithm which builds on the global optimization algorithm of Duan et al. [1992] by using the concept of Pareto dominance (lower values of Pareto rank are superior) to evolve the optimization and uses the Metropolis-Hastings algorithm [Kuczera and Parent, 1998; Metropolis et al., 1953; Hastings, 1970] to infer the posterior distribution of parameters. Using the Metropolis-Hastings algorithm within MOSCEM to update the search avoids the search collapsing to a single region of attraction (i.e. the global minimum) by using a distribution of parameters to direct the stochastic exploration of the parameter space [Vrugt et al., 2003b]. The result of the search is a Pareto set of parameters which allows for improved assessment of parameter uncertainty.

### 3.1.2 Recent Applications Using MOSCEM

*Schoups et al.* [2005a] used MOSCEM to calibrate a regional surface water-groundwater model of the Yaqui Valley in Mexico using hydraulic heads, canal seepage rates, and drainage volumes. The method allowed for better identification of the model parameters since the various objectives were sensitive to different parameters. Large parameter variation or uncertainty within the Pareto set of solutions was found to be symptomatic of the insensitivity of one of the objectives to the parameter and the shape of the trade-off curve was found to be a good indicator of model structural error. Results indicated that simulation of aquifer heads was sensitive to scaling factors (related to deep aquifer hydraulic conductivity and vertical hydraulic conductivity of the confining layer), so the model was refined by introducing spatially varying scaling factors by zones.

*Schoups et al.* [2005b] applied MOSCEM in the San Joaquin Valley of California to optimize a regional spatially-distributed subsurface water flow model using water table depth measurements, groundwater pumping, and subsurface drainage data. Using the prediction bounds created by the Pareto parameter set model outputs, they found larger uncertainty with water table predictions and lower uncertainty for drainage and pumping predictions. Because of the heterogeneity in the system, the optimal solution for predicting water level fit the data well for some locations, but severely under-predicted or over-predicted in other locations. We are not aware of any published results using MOSCEM with multi-site calibrations of distributed rainfall-runoff models.



### 3.2 Case Studies: Experimental Design

Two different distributed models used for different applications and at different locations were both calibrated using MOSCEM, see *Vrugt et al.* [2003a] for an algorithm description. For the first case, the Two-Zone Temperature and Solute model, referred to as the TZTS model [*Neilson, 2006*], is used to predict stream temperatures in the Virgin River, Utah, USA. Main channel streamflow and transient storage temperatures at two different sites are used to compare results of single and two-objective calibrations. Transient storage in the stream is considered to be hyporheic storage (subsurface storage), dead zones (surface storage), and/or other slow moving water relative to the main channel. Properties of the transient storage that are of interest include: 1) the exchange rates of energy or solute between the main channel and surface or subsurface transient storage, and 2) the size of the surface and subsurface transient storage zones. In this application, measured temperature of the dead zone and hyporheic zone are withheld during calibration and used to assess the predictive capacity of these components as ungauged model outputs.

For the second case, Topnet [see Chapter 2] is used to predict streamflow in the Illinois River at Tahlequah, Arkansas, USA. Topnet is a distributed rainfall-runoff model which predicts surface and near-surface hydrology and is used for flood forecasting and water resources management [*Ibbitt et al., 2001; Woods et al., 2003*]. Model output is provided at each sub-catchment delineated in the river network. Typically, the model is calibrated using the measured streamflow at the downstream outlet of a catchment, and sub-catchments upstream are modeled as ungauged. For this work, three different sites are used to compare results of single, two-objective, and three-objective

calibrations. For the single and two-objective calibrations, the sites not used for calibration are used for predictive tests of modeling of ungauged sub-catchments.

The Nash-Sutcliffe efficiency,  $E$ , (Equation 2) [Nash and Sutcliffe, 1970] is used as the objective statistic to compare observed ( $Q_o^t$ ) and modeled ( $Q_m^t$ ) simulations (at time  $t$ ) for both test cases, where  $\bar{Q}_o$  is the mean observed flow.

$$E = 1 - \frac{\sum_{t=1}^T (Q_o^t - Q_m^t)^2}{\sum_{t=1}^T (Q_o^t - \bar{Q}_o)^2} \quad (2)$$

The calibration algorithm minimizes the result of 1- $E$ , since the bounds of  $E$  are  $[1, -\infty]$ .

The normalization of the difference in error by the difference between the observed and the mean of the observed, allows comparison of results when the observations at different locations have different scales of variability.

To summarize the performance of the model at all locations, the arithmetic average of the Nash-Sutcliffe Efficiency,  $AE$ , (Equation 3) was calculated for  $n$  total locations where the model is predicting either temperature (Case I,  $n=2$ ) or streamflow (Case II,  $n=3$ ).

$$AE = \frac{1}{n} \sum_{i=1}^n E_i \quad (3)$$

### **3.2.1 Case I: An In-Stream Temperature Model And Two Locations**

#### **3.2.1.1. Study Area And Data**

Temperatures in the Virgin River, Utah, USA, have been a topic of study for a number of years because of two endangered fish species (Virgin River Chub (*Gila seminuda*) and woundfin (*Plagopterus argentissimus*)) and other native fishes unique to this river. The study reach has a dominantly sand channel and experiences extremely hot and dry summers with maximum air temperatures  $>100^{\circ}\text{F}$  ( $37^{\circ}\text{C}$ ) for the majority of July and August. Streamflow temperature data were collected in July and September 2005 to identify the energy balance components necessary to capture the temperature fluctuations in the Virgin River and for model calibration [Neilson, 2006]. The section of the Virgin River used in the study spans the towns of Hurricane and Washington near St. George (Figure 3.1).

This section of the Virgin River can be characterized in terms of two separate sections regarding slope and bed substrate. The upper section, approximately 7.5 km and hereafter referred to as ‘above Hurricane Bridge’ (HB), has an average bottom slope of 0.0039 and bed substrate consisting of sand (56%), gravel (26%), and cobble (14%). The lower section, approximately 10 km, and hereafter referred to as “above Washington Field Diversion” (WFD) has an average slope of 0.00124 and the bed substrate primarily consists of sand (72%), gravel (15%), and cobble (10%) and therefore, will likely behave differently in terms of hyporheic exchange and bed conduction than the upper section. Bottom sediments are highly transient in this section of the river.

Hobo® Water Temp ProV1 (Onset Corporation, Bourne, MA) temperature probes were used to measure temperature in the water column and in the sediments at three locations, 1) at Gould's Wash, the beginning of the study reach, 2) at Hurricane Bridge, and 3) at Washington Field Diversion. This observed temperature in the main channel of the river was used to calibrate the two-zone temperature and solute model using MOSCEM. Additional data for temperature in the surface and subsurface storage areas of the river (defined below in Section 2.1.2), which are generally modeled as ungauged and unique to this data collection effort, were used for model validation of these components. The sub-surface storage (SSS) model was compared to the measured data for the sediment using temperature probes placed at 3 cm, 9 cm and 12 cm depth. Sediment transport contributed to measurement error when probes were inconsistently covered and uncovered by shifting sands at Washington Fields Diversion.

### **3.2.1.2 Temperature Model**

The TZTS model [Neilson, 2006] separates transient storage into two zones, 1) surface storage or dead zone storage that represents the eddies, recirculating zones, and side pockets of water and 2) subsurface storage or hyporheic storage that represents the flow into or out of the stream substrate. Sources and sinks of heat in a river include fluxes across the air-water interface, bed conduction, conduction between the bed and deeper ground substrate, hyporheic exchange, dead zone exchange, and sediment warming due to radiation penetration to the bed substrate. To account for each of these sources or sinks, the TZTS model calculates energy and mass balances on the main

channel, surface storage zone (or dead zone storage), and subsurface storage (or hyporheic zone and/or sediments) for each reach or control volume.

Sources and sinks of heat in a river include fluxes across the air-water interface, bed conduction, conduction between the bed and deeper ground substrate, hyporheic exchange, dead zone exchange, and sediment warming due to radiation penetration to the bed substrate. To account for each of these sources or sinks, the TZTS model calculates energy and mass balances on the main channel, surface storage zone (or dead zone storage), and hyporheic storage zone and/or sediments for each reach or control volume. Figure 3.2 [taken from *Neilson, 2006*] shows the energy balance components that are considered in the model. The heat and solute is advected from one homogeneous stream reach to the next using kinematic wave routing [*Martin and McCutcheon, 1999; Chapra, 1997*] while accounting for external inflows.

Model assumptions include: reaches and storage zones are completely mixed, reaches have constant flow rate and volumes, advection longitudinally only occurs in the main channel, hyporheic and surface zone interaction with the main channel are adequately represented by first-order exchange, mass and heat exchange rates are equivalent, hyporheic exchange only occurs with the main channel, bed conduction occurs between the main channel water column and bed sediments and the dead zone water column and bed sediments, all zones have rectangular geometry, total width is the main channel width plus the dead zone width, hyporheic zone width is equal to the main channel width, and depth of the hyporheic zone is equal to the depth over which bed conduction occurs in both the main channel and dead zone.

Data inputs for the TZTS model include wind speed, air temperature, solar radiation, and relative humidity. Initial conditions for the model were set using measured streamflow and main channel water temperature. The model was run at a five minute time step for 1.6 days to coincide with a July 2005 data collection campaign [Neilson, 2006].

### **3.2.1.3 Case I Methods: Model Setup, Calibration And Experimental Design**

The two-zone temperature model was used to predict streamflow temperature at two separate cross-sections and three temperatures zones within each cross-section: the main channel, the surface storage, and the subsurface storage. The calibrated parameters included: total channel width, Manning's roughness coefficient, dead zone width, dead zone cross-sectional area, dead zone diffusivity, hyporheic storage advective transport coefficient, hyporheic storage sediment depth, and ground conduction depth. These eight parameters were calibrated at each cross-section, for a total of 16 calibrated parameters in each experiment. The parameter ranges used to define the a priori uniform distribution of the feasible parameter space are presented in Table 3.1.

The temperatures of the surface and subsurface transient storage were treated as ungauged variables at each cross-section location. Observed temperatures collected from the surface storage and sub-surface storage areas were withheld during calibration and used to compare model predictions.

Three calibration experiments were conducted: A) Single objective (SO) calibration using only main channel temperatures at Hurricane Bridge (HB) as calibration data, B) Single objective calibration using only main channel temperatures at Washington Field

Diversion (WFD) as calibration data, and C) Multi-objective (MO) calibration using two objectives; main channel temperature at Hurricane Bridge and Washington Field Diversion. Table 3.2 organizes the three experiments in rows A through C with the corresponding model outputs by location in columns 1 through 6 labeled by whether the experiment used data from that location for calibration (**C**) or as ungauged (**U**) model validation. Temperature data collected at each location were in the main channel (MC), surface storage (SS), and sub-surface storage (SSS).

The three temperature model experiments were calibrated using MOSCEM. The algorithm was run with a sample of 300 randomly sampled parameter sets that evolved using two complexes for a total of 3000 model runs. The modeled temperature at each location was compared to the observed temperature using the Nash-Sutcliffe efficiency (Equation 2) and an average Nash-Sutcliffe efficiency was calculated (Equation 3) for locations  $n=1$  through 6.

#### **3.2.1.4 Case I: Results**

The results for the single and multi-objective calibrations of the two –zone temperature and solute model are presented in Tables 3.3 which shows the results using the Nash-Sutcliffe Efficiency statistic at each of the two locations; Hurricane Bridge (HB) and Washington Field Diversion (WFD) and each zone modeled; main channel (MC), surface storage (SS) and sub-surface storage (SSS).

Comparing the results of the three experiments considering only the main channel temperatures, we see how choice of objective effects the optimization. The best result at Hurricane Bridge is  $E = 0.969$  from the single objective calibration (SO HB). The best

result at Washington Field Diversion is  $E = 0.905$  from the single objective calibration (SO WFD). For the third test, the multi-objective calibration (MO HB & WFD) uses main channel temperature at both locations. Figure 3.3 shows that the multiple objective results are a Pareto optimal solution by plotting the model results of the multi-objective calibration for the entire final sample of 300 parameter sets. The “best result” (black point, Figure 3.3) is considered the one that minimizes the trade-off between fitting the model to both locations simultaneously, with model results of  $E = 0.966$  at Hurricane Bridge and  $E = 0.902$  at Washington Field Diversion.

All the parameter sets with pareto rank one, or the pareto front (red points, Figure 3.3), were used to plot the uncertainty bounds in Figure 3.4. To simplify comparison of the tests, we have reported ‘best’ results in conjunction with the range of model results from multiple sets of parameters. The pareto rank one parameter sets are considered the behavioral set [Beven and Binley, 1992] of parameters which produce equally good model results considering the multiple objectives simultaneously.

Comparing the main channel results for the three calibration experiments, one can see in Table 3.3 that the best HB main channel result is from a single objective optimization at that location, and the best WFD main channel result is from the single objective optimization at that location. However, when either single objective model result is used to model the main channel temperature at the other location, the E results are lower. Using the AE statistic to assess the model performance over the spatial extent, or looking at performance at both main channel locations at the same time, Table 3.4, shows that the multi-objective result is higher,  $AE_{MO} = 0.934$ , than the single objective at either location,  $AE_{SO\ HB} = 0.904$ ;  $AE_{SO\ WFD} = 0.929$ . What is gained by using a multiple



objective calibration? In this case, a model calibrated using data from two locations performs better on average at both locations than a model calibrated with data from one location that is used to predict temperature at two locations.

The sub-surface storage (SSS) model results at Washington Field Diversion are difficult to compare numerically to the results at Hurricane Bridge since the measured data for the sediment was affected by the transport of sand. Sediment movement also contributed to the truncation of the SSS WFD observed temperatures. The 9 cm data was used as the SSS observed temperature for E and AE calculations. Although the E and AE results are poor compared to the other locations, the relative performance of the model between single objective and multi-objective calibrations is informative.

#### **3.2.1.5 Case I: Discussion**

The interesting results for this study are not only how the model predicts the main channel temperature, where data exists for calibration, but how the model results are affected in the ungauged transient storage components of the model output. In addition to predicting temperature in the main channel, the TZTS model decomposes the transient storage into two elements: the surface storage and the sub-surface storage. To analyze the results in the transient storage areas, AE values of the dead zone and hyporheic storage were considered in series of increasing complexity. Table 3.4 presents AE results considering a) the main channel at two locations, b) the main channel and surface storage at two locations, c) the main channel, surface storage, and subsurface storage at two locations. The overall model performance, as measured by AE for main channel predictions (Table 3.4.a) and main channel plus dead zone predictions (Table 3.2.b) at the

two locations, is improved by using the multi-objective calibration compared to using a single objective at either location to predict temperature at both locations.

However, the behavior of the hyporheic storage predictions are not improved by using main channel temperatures at both locations as objectives. In this case, the main channel temperature at Washington Field Diversion is the best predictor for the behavior of the hyporheic storage over the extent of the system (Table 3.4 c, AE=0.855). This makes sense due to the dominance of flow through hyporheic storage at this location with shifting sandy bottom compared to the Hurricane Bridge location with a more heterogeneous substrate. There is hyporheic storage at both locations, but it is a more dominant physical process at Washington Field diversion.

In summary, these results show that to best model main channel temperatures throughout the system, better sets of model parameters can be determined using data from two locations and a multi-objective calibration. Similarly, to predict both main channel and dead zone temperatures, a multi-objective calibration should be used. To best model hyporheic storage, using a calibration that uses only data where hyporheic storage is a dominant process relative to other locations gives the best model performance. This is consistent with qualitative observations of loose porous sand at WFD which is an indicator of the streambed to facilitate hyporheic storage.

Improving model performance in the Virgin River can be focused on data collection of hyporheic storage at Washington Field Diversion. With this additional information, multi-objective calibrations using main channel temperatures in addition to hyporheic storage at WFD may provide even better model calibrations than presented in this work.

### **3.2.1 Case II: A rainfall-runoff model and three locations**

#### **3.2.2.1 Topnet**

The rainfall-runoff model, Topnet, is a distributed version of TOPMODEL [*Beven and Kirkby, 1979; Beven et al., 1995*] with a DEM-based system for delimiting channels, model components, and estimation of model parameters. The implementation of TOPMODEL used is modified from the original [*Beven and Kirkby, 1979; Beven et al., 1995*] by the addition of a potential evapotranspiration component, a canopy storage component to model interception, and the inclusion of a soil zone component that provides infiltration excess runoff generation capability through a Green-Ampt like parameterization. Detailed model information is available in Chapter 2.

To parameterize the model using physical data, we used the soil texture from each of the 11 soil depth grid layers derived from Pennsylvania State University STATSGO data [*Soil Survey Staff, 2006*] provided by the Distributed Model Intercomparison Project (DMIP) [*Smith, 2002*], and soil hydraulic properties derived from texture using relationships provided by *Clapp and Hornberger [1978]*. We also used 1 km resolution Advanced Very High Resolution Radiometer (AVHRR) vegetation data processed through the NASA Land Data Assimilation Systems (LDAS) program with an International Geosphere-Biosphere Program (IGBP) classification system [*Eidenshink and Faundeen, 1994*]. There are a total of nine parameters that were derived from this soils and vegetation information. We used a GIS to spatially average the parameter values for each sub-basin model element.

### 3.2.2.2 Calibration of Spatially Distributed Parameters

The calibration procedure used is designed to retain the spatial pattern provided by estimating parameters from the GIS data, while still allowing an adjustment of parameters to match observed stream flow. Parameters are adjusted through a set of multipliers that scale the parameters while maintaining the relative differences between model elements indicated from the GIS information. There is one multiplier for each parameter that is the same across all sub-basins. Subgrid variability within sub-basins is not explicitly represented apart from the spatial distribution of soil moisture that is parameterized by distribution of the TOPMODEL wetness index.

*Ajami et al.* [2004] used a multi-objective (using statistics HRMS-hourly root mean-square and the log of low flows) SCE-based global optimization (MACS) [*Hogue et al.*, 2003] to look at the minimum level of spatial complexity required for simulation accuracy and the spatial details necessary to enable flow prediction at any point along the river network, or at ungauged locations. They found that increasing the spatial complexity of the parameter distribution from a semi-lumped (parameters are the same for all sub-basins but routing is distributed) to a semi-distributed calibration (parameters are calibrated for each sub-basin one-at-a-time from upstream to downstream) strategy did not improve simulations at the model outlet or at interior nested locations. This may have been due to the homogeneity in soil, vegetation and land use in the basin or the uncertainty in the a priori estimation of soil parameters [*Koren et al.*, 2003].

Lumped conceptual models have relatively few calibration parameters, generally on the order of 10. However, spatially distributed models can have many parameters that

limit the functionality of optimization techniques. They suffer the “curse of dimensionality.” Instead of calibrating sub-basins one-at-a-time [such as *Ajami et al.*, 2004], sub-basin a priori parameters can be scaled up or down using “super-parameters.” *Tonkin and Doherty* [2005] designed an approach for minimizing the dimensionality of a highly parameterized groundwater model. The method is based on constructing a highly parameterized base model, calculating base parameter sensitivities, and decomposing the base parameter normal matrix into eigenvector representing principal orthogonal directions in parameter space. The decomposition is used to construct super parameters. Super parameters are factors by which principal eigenvectors of the base parameter normal matrix are multiplied in order to minimize a composite least squares objective function. The method was found to effectively reduce the computational burden of the calibration problem, and resulted in a better model fit than following a lumped calibration scheme. The important result of their work with regards to the rainfall runoff model calibration shown in this paper is the idea that super parameters multiplied by the base parameter set is an effective method for optimizing numerous spatially distributed parameters in a parsimonious and effective way.

### **3.2.2.3. Study Area and Data**

The Illinois River at Tahlequah, Oklahoma, USA (Figure 3.5) was chosen as a demonstration dataset since it was used as a study basin in the Distributed Model Intercomparison Project (DMIP) [*Smith et al.*, 2004b] and had already been applied in Chapter 2. Two interior USGS gage locations are used: Illinois River at Savoy OK, (433 km<sup>2</sup>), Illinois River at Watts, OK (1,645 km<sup>2</sup>). The Tahlequah basin is mostly silt loam,

silty clay loam and silty clay. Approximately 90% of the Tahlequah basin is pasture and forest. The topography is gently rolling to hilly. The longest path length of river channel is 163.8 km, the longest path slope is 0.003 m/m. The annual rainfall averages 1157 mm. The annual runoff at Tahlequah is 300 mm, with a runoff coefficient of 0.26 [Smith *et al.*, 2004b].

The input data for modeling this basin is the same as the data used in the DMIP project [See Chapter 2]. The NEXRAD radar precipitation data is an hourly dataset with 4 km x 4 km grid cell resolution. A spatial average of raingages gave the average hourly rainfall at each sub-basin. The Tahlequah basin was divided into 21 sub-basins with the Terrain Analysis Using Digital Elevation Models (TauDEM is available at <http://hydrology.neng.usu.edu/taudem/>) and a 30m grid cell resolution digital elevation model (DEM). There is no data available to estimate the uncertainty of the radar rainfall estimates. For this reason, it is impossible to separate the errors in input data, parameter uncertainty, observed streamflow or model structure when trying to reduce the total error in the streamflow model.

#### **3.2.2.4 Case II Methods: Model Setup, Calibration and Experiments**

The approach for calibrating this model uses initial or base parameters based on spatially distributed physical information. We assume that the spatial distribution of initial parameters is representative and optimize parameter multipliers, or super parameters, using multiple stream flow locations to scale the base parameters over the extent of the watershed. Using super parameters for calibration instead of individual sub-basin parameters reduces the dimensionality of the optimization as well as retains the

spatial representation of the physically based spatially distributed parameters. The resulting calibrated multiplier set can be applied to model flow at ungauged locations within the watershed.

Nine spatially distributed sub-basin parameters were calibrated: saturated storage sensitivity, surface saturated hydraulic conductivity, drainable porosity, plant available porosity, depth of soil zone, wetting front suction, canopy capacity, intercepted evaporation enhancement factor, and albedo. Three parameters that were treated as spatially constant were also calibrated: soil zone drainage sensitivity, overland flow velocity, and Manning's  $n$ . A table of Topnet model parameters is presented in Table 3.5. The rainfall runoff model was run at an hourly time step for the calibration period of October 1998- May 1999. The beginning date for the calibration period was chosen to avoid incorporating the bias noted in the rainfall prior to 1997 [Seo *et al.*, 1997] and the end date was chosen in correspondence with the DMIP calibration period [See Chapter 2]. A total of 5800 hourly timesteps were included in the model setup.

Five calibration experiments were conducted (Table 3.6): a) single objective calibration using only observed streamflow at the watershed outlet, Illinois River at Tahlequah, as calibration data: b) single objective calibration using only observed streamflow data at an interior location, Illinois River at Watts, as calibration data, c) single objective calibration using only observed streamflow data at an interior location, Illinois River at Savoy, as calibration data, d) multi-objective calibration using two objectives; streamflow data at Illinois River at Tahlequah and at Watts as calibration data and e) multi-objective calibration using three objectives; streamflow data at Illinois River at Tahlequah, Watts, and Savoy as calibration data. The combination of multi-objective

locations were chosen to create a series from downstream to upstream: 1) single objective at Tahlequah, 2) multi-objective at Tahlequah plus Watts, 3) multi-objective at Tahlequah plus Watts plus Savoy. The additional single objective calibrations at Watts and Savoy are informative about the model performance at these locations independent of the multi-objective calibrations.

The five Topnet model experiments were calibrated using MOSCEM. For single objective experiments, the algorithm was run with a sample of 200 randomly sampled parameter sets that evolved using two complexes for a total of 5000 model runs. For multi-objective calibrations, the algorithm was allowed to extend the sampling for a total of 10,000 model runs. Since the range for  $E$  (Equation 2) is  $[1, -\infty]$ , the value of  $1-E$  was minimized in the algorithm. The parameter search space was defined as a uniform distribution between the lower and upper bounds of each calibrated parameter shown in Table 3.5 for all five model experiments. Although multi-objective calibrations have been improved by constraining the multi-objective parameter search space based on the results of the single objective optimization [Vrugt, 2007; Schoups *et al.*, 2005a], to objectively compare the results of single and multi-objective calibration we maintained a consistent initial search space for all experiments.

The experiments were designed to test the effect of including internal gauged points as multiple objectives in calibration (Tests d and e) compared to single objective results (Tests a, b, and c) at each location. All five calibration experiments produced model outputs used to compare results at the three locations: Illinois River at Tahlequah, Illinois River at Watts, Illinois River at Savoy. The modeled streamflow at each location was compared to the observed streamflow using the Nash-Sutcliffe efficiency (Equation 2)



and an average Nash-Sutcliffe efficiency was calculated (Equation 3) for locations  $n=1$  through

### 3.2.2.5 Case II: Results

Table 3.7 presents the range of results using the E statistic for each of the five calibration experiments. The Pareto set of parameters results in a minimum ( $E_{\min}$ ) and maximum ( $E_{\max}$ ) value for the resulting modeled streamflow. Locations used for objectives are shown in bold to differentiate between the experiments. Considering the single objectives (Table 3.7, a, b and c), the modeled streamflow at both Tahlequah and Watts (a and b) is acceptable ( $E > 0.7$ ) while the modeled streamflow at Savoy only approaches this level of performance when Savoy is the single objective (c) with the result that the performance at Tahlequah and Watts is severely compromised ( $E < 0$ ).

Considering the multi-objective results (Table 3.7, d and e), the two-objective experiment results are within the range of the single objective results for Tahlequah and Watts. The three-objective experiment results are slightly lower, but within close proximity to the values of the highest  $E_{\max}$  result of each of single objectives. However, the lowest  $E_{\min}$  results are lower than for the single objectives. Interestingly, the two-objective experiment resulted in a higher E at Tahlequah and Watts than the single objective experiments at those locations. We expected that the single objective optimization at Tahlequah would give better results than the multi-objective optimization using two locations. It may be that the tradeoff between fitting both objectives simultaneously prevented the algorithm from converging to a local (albeit close to the global) minimum in this case. However, the relatively greater tradeoff between fitting

the three objectives, where the model does not perform as well at Savoy, causes a slight deterioration in the highest  $E_{\max}$  values and a large deterioration in model performance considering the  $E_{\min}$  at Tahlequah and Watts.

The increased range in performance for the three-objective experiment can be seen in the tradeoff shown in Figure 3.6. For the single-objective calibrations, the MOSCEM algorithm converged to a limited range in the objective and resulted in less parameter uncertainty. For the multi-objective calibrations, the algorithm converged to 30 pareto rank one parameter sets (shown in red, Figure 3.6) for the both the two-objective and three-objective calibrations, out of 200 samples (shown in blue, Figure 3.6) evolved over 10,000 model runs. The black points in Figure 3.6 are the Pareto rank one point which minimizes the tradeoff, using a Euclidean distance from the origin.

Figure 3.6a shows the tradeoff between fitting the Illinois River at Tahlequah and Watts in the two-objective experiment. The shape of the Pareto tradeoff curve suggests that the model is more sensitive to the Tahlequah location compared to the Watts location; changes in parameter values result in more change in objective function at Tahlequah compared to Watts. Figure 3.6a shows the same tradeoff for the three-objective experiment, the third dimension of the tradeoff, the Illinois River at Savoy, is shown in Figures 3.6c and 3.6d, which shows that the model is relatively insensitive to the Savoy location compared to the Tahlequah and Watts locations.

To compare the calibration experiments over the extent of the watersheds, the AE statistic (Equation 2) was calculated for each of the five experiments. The  $AE_{\max}$  is the best average model performance over the extent of the watershed given a specific parameter set in the Pareto rank one set of parameters; the  $AE_{\min}$  is the worst model

performance that can be expected from the same set of Pareto rank one parameters. The difference between the  $AE_{\max}$  and  $AE_{\min}$ , calculated using the  $E_{\max}$  and  $E_{\min}$  values respectively, results in a range of uncertainty ( $U_{\text{range}}$ ). The  $U_{\text{range}}$  value was used to calculate an  $AE_{\text{midpoint}}$ . The  $AE_{\max}$  values are useful for interpreting the best model results that can be expected, these improve as multiple locations are used to calibrate the model. The  $AE_{\text{mid}}$  values are useful for quantifying the uncertainty that is added when multiple locations are incorporated in the calibration as objectives. The model performs best with less uncertainty when using the single objective calibration at the Watts location (Table 3.8b) and worst when using the single objective location at Savoy (Table 3.8c). The two-objective calibration (Table 3.8d) is an improvement on the single objective using only Tahlequah (Table 3.8a), but the three-objective calibration (Table 3.8e) is not as good because of the involvement of the Savoy location in the tradeoff.

The results of the single-objective calibrations at Tahlequah, Watts and Savoy locations are shown in Figure 3.7, 3.8, and 3.9 including the Nash-Sutcliffe Efficiency maximum ( $E_{\max}$ ) and minimum ( $E_{\min}$ ) results at each of the three locations as well as the Average Nash-Sutcliffe Efficiency maximum ( $AE_{\max}$ ) and minimum ( $AE_{\min}$ ) results. These values also appear in Tables 3.7 and 3.8, but are repeated within the graphs for clarity. Since the calibration converged to a minimum in the parameter space, the resulting bounds on the modeled streamflow and range on the resulting objective function is narrow.

Figures 3.10 and 3.11 present the modeled streamflow for the multi-objective calibration experiments using two and three locations. Because of the tradeoff that exists in modeling multiple locations simultaneously, the bounds on the modeled streamflow

and the range in model performance as measured by NSE and AE are wider than in the single objective experiments.

### **3.2.2.6 Case II: Discussion**

Comparing Figures 3.7 to 3.11 illustrates the effect of calibrating the model using only one location. When the model is fit to one location, the resulting parameter sets have limited applicability to other locations within the watershed. The actual uncertainty in the calibration, when applying the calibrated model to internal locations, is better captured by using information at multiple locations simultaneously.

When rainfall-runoff models are calibrated at one downstream location, the uncertainty inherent in applying the calibrated model parameters to other locations within the watershed is not captured. The result of Case II shows how different parameter sets are optimal for modeling streamflow at specific locations (single objective experiments), while applying a Pareto optimal set of multiple parameters derived by optimizing the model using streamflow at multiple locations gives an improved understanding of the uncertainty involved in applying the model at ungauged locations.

How can this information be used in a practical ‘ungauged’ model application? Which model calibration should be used depends on where the model performance is being assessed. For example, using the Case II dataset, a modeling application that aimed to scale a priori parameters simultaneously for the best fit over the extent of the modeling area, would benefit most from a multi-objective calibration using measured streamflow at all three locations. Using three objectives (Tahlequah, Watts, and Savoy) simultaneously would increase the uncertainty, but could be expected to improve the

predictions at smaller basins on the scale of Savoy, compared to using only the downstream location of the Illinois River at Tahlequah.

Using the calibration framework as a tool for improving models, we can see that the model does not perform as well at Savoy as the other two locations. Figures 3.7 through 3.11 show that the Savoy basin is flashier than further downstream at Watts and Tahlequah. In this case, it could be that the streamflow recession is more a function of travel time than soil properties. For Topnet, the  $f$  parameter which controls the sensitivity of the baseflow recession may better be determined a priori from channel length than from soil texture. Alternatively, different conceptual models for streamflow runoff in small catchments may need to be developed. Finally, it may be that data on channel width is required to properly model streamflow in the smaller catchments within the watershed so that channel hydraulic parameters can be modeled in a distributed way.

For model applications where streamflow at specific ungauged locations is the aim, single objective calibration using data from basins at the same scale as the basin of interest may provide better model predictions than multi-objective calibrations which will incorporate some tradeoff in performance between locations. However in watersheds other than in Case II, the tradeoff between locations seen may not exist. The benefit of using the multi-objective calibration framework is to gain understanding about the tradeoff that does exist before applying parameter sets that are a good fit to locations other than the ungauged location of interest.

### 3.3 Conclusions

This research examined the application of multiple objective calibration to distributed hydrologic models. An in-stream temperature model and a rainfall-runoff model were used for test cases. One benefit of using distributed hydrologic models for streamflow prediction is the ability to make predictions at upstream locations. This functionality is useful for modeling at ungauged basins, and is an alternative to calibration of models using data only at downstream locations when making predictions at upstream interior locations. This work compared calibration schemes to test whether model predictions at ungauged locations can be improved by using data from multiple locations in the watershed rather than calibrating the model using only one location.

The obvious aim in the calibration of any modeling effort is to use data that contains the most information for your system and the ungauged component that is the focus of the modeling effort. The multi-objective calibration framework used in this work, helps assess where that data is most important. Using the TZTS model in the Virgin River, Utah, USA, we show that main channel and surface storage temperatures are best modeled using temperatures from two locations, however, sub-surface storage is better represented using calibration at the location where sub-surface energy storage is a dominant process. Using Topnet, a rainfall-runoff model applied in the Illinois River, Arkansas, USA, we show that parameter sets that best predict flow at downstream locations do not necessarily predict flow well at upstream interior locations. In this case, when data at interior locations is not available, a calibration which includes a trade-off between fitting multiple locations in the watershed improves model predictions at interior locations while providing an improved assessment of the model uncertainty.

## References

- Ajami, N. K., H. V. Gupta, T. Wagener, and S. Sorooshian, (2004), Calibration of a semi-distributed hydrologic model for streamflow estimation along a river system, *J. Hydrol*, 298, 112-135.
- Beven, K., (2001), *Rainfall -Runoff Modelling: The Primer*, John Wiley & Sons, LTD, Chichester, England.
- Beven, K., and A. Binley, (1992), The Future of distributed models: Model calibration and uncertainty prediction, *Hydrol. Processes*, 6, 279-298.
- Beven, K., R. Lamb, P. Quinn, R. Romanowicz and J. Freer, (1995), Topmodel, *Computer Models of Watershed Hydrology*, Edited by V. P. Singh, 627-668, Water Resources Publications, Highlands Ranch, Colorado.
- Beven, K. J., and M. J. Kirkby, (1979), A Physically based variable contributing area model of basin hydrology, *Hydrol. Sci. Bull.*, 24(1), 43-69.
- Boyle, D. P., H. V. Gupta, and S. Sorooshian, (2000), Toward improved calibration of hydrologic models: Combining the strengths of manual and automatic methods, *Water Resour. Res.*, 36(12), 3663-3674.
- Chapra, S. C., (1997), *Surface Water Quality Modeling*, McGraw-Hill, Boston, MA.
- Clapp, R. B., and G. M. Hornberger, (1978), Empirical equations for some soil hydraulic properties, *Water Resour. Res.*, 14, 601-604.
- Duan, Q., (2003), Global Optimization for Watershed Model Calibration, *Calibration of Watershed Models*, Edited by Q. Duan, H. V. Gupta, S. Sorooshian, A. N. Rousseau and R. Turcotte, 89-104, American Geophysical Union, Washington D.C.
- Duan, Q., S. Sorooshian, and V. K. Gupta, (1992), Effective and efficient global optimization scheme for conceptual rainfall-runoff models, *Water Resour. Res.*, 28(4), 1015-1031.
- Duan, Q., S. Sorooshian, and V. K. Gupta, (1994), Optimal use of the SCE-UA global optimization method for calibrating models, *J. Hydrol*, 158, 265-284.
- Eidenshink, J. C., and J. L. Faundeen, (1994), The 1-Km AVHRR global land data set: First stages in implementation, *International Journal of Remote Sensing*, 15, 3443-3462.
- Gupta, H. V., L. A. Bastidas, J. A. Vrugt and S. Sorooshian, (2003), Multiple Criteria Global Optimization for Watershed Model Calibration, *Calibration of Watershed*

- Models*, Edited by Q. Duan, H. V. Gupta, S. Sorooshian, A. N. Rousseau and R. Turcotte, American Geophysical Union, Washington D.C.
- Gupta, H. V., S. Sorooshian, and P. O. Yapo, (1998), Toward improved calibration of hydrologic models: Multiple and noncommensurable measures of information, *Water Resour. Res.*, 34(4), 751-76.
- Hastings, W. K., (1970), Monte Carlo sampling methods using Markov Chains and their applications, *Biometrika*, 57, 97-109.
- Hill, M. C., (1998), Methods and guidelines for effective model calibration, Report 98-4005, USGS Water Resources Investigations.
- Hogue, T. S., H. V. Gupta, S. Sorooshian, and C. D. Tomkins, (2003), A Multi-Step Automatic Calibration Scheme for Watershed Models, *Calibration of Watershed Models*, Edited by Q. Duan, H. V. Gupta, S. Sorooshian, A. N. Rousseau and R. Turcotte, American Geophysical Union, Washington D.C.
- Ibbitt, R. P., R. D. Henderson, J. Copeland and D. S. Wratt, (2001), Simulating mountain runoff with meso-scale weather model rainfall estimates: A New Zealand experience, *J. Hydrol*, 239, 19-32.
- Koren, V., M. Smith, and Q. Duan, (2003), Use of *a Priori* Parameter Estimates in the Derivation of Spatially Consistent Parameter Sets of Rainfall-Runoff Models, *Calibration of Watershed Models*, Edited by Q. Duan, H. V. Gupta, S. Sorooshian, A. N. Rousseau and R. Turcotte, 239-254, American Geophysical Union, Washington D.C.
- Kuczera, G., and E. Parent, (1998), Monte Carlo assessment of parameter uncertainty in conceptual catchment models: The Metropolis algorithm, *J. Hydrol.*, 211, 69-85.
- Madsen, H., and M. Kristensen, (2002), A multi-objective calibration framework for parameter estimation in the Mike She integrated hydrologic modelling system, Proceedings of the 4th International Conference on Calibration and Reliability in Groundwater Modeling, ed. K. Kovar and Z. Hrkal, 270-277, Prague, Czech Republic, Acta Universitatis Carolinae - Geologica.
- Madsen, H., D. Rosbjerg, and P. Harremoes, (1995), Application of the Bayesian approach in regional analysis of extreme rainfalls, *Stochastic Hydraul. Hydrol.*, 9, 77-88.
- Martin, J. L., and S. C. McCutcheon, (1999), *Hydrodynamics and Transport for Water Quality Modeling*, Lewis Publishers, Boca Raton.



- Metropolis, N., A. W. Rosenbluth, M. N. Rosenbluth, and A. H. Teller, (1953), Equations of state calculations by fast computing machines, *J. Chem. Phys.*, 21, 1087-1091.
- Nash, J. E., and J. V. Sutcliffe, (1970), River flow forecasting through conceptual models Part 1 - A discussion of principles, *J. Hydrol.*, 10(3),282-290.
- Neilson, B. T., (2006), Dynamic Stream Temperature Modeling: Understanding the Causes and Effects of Temperature Impairments and Uncertainty in Predictions, Ph.D.,157, Civil and Environmental Engineering, Utah State University, Logan, Utah, USA.
- Parada, L. M., J. P. Fram and X. Liang, (2003), Multi-Resolution Calibration Methodology for Hydrologic Models: Application to a Sub-Humid Catchment, *Calibration of Watershed Models*, Edited by Q. Duan, H. V. Gupta, S. Sorooshian, A. N. Rousseau and R. Turcotte, American Geophysical Union, Washington D.C.
- Reed, S., V. Koren, M. Smith, Z. Zhang, F. Moreda, D. J. Seo, and DMIP Participants (2004), Overall distributed model intercomparison project results, *J. Hydrol.*, 298, 27-60.
- Refsgaard, J. C., and H. J. Henriksen, (2004), Modeling guidelines, terminology, and guiding principles, *Adv. Water Resour.*, 27, 71-82.
- Schaake, J., (2003), Introduction, *Calibration of Watershed Models*, Edited by Q. Duan, H. V. Gupta, S. Sorooshian, A. N. Rousseau and R. Turcotte, American Geophysical Union, Washington D.C.
- Schoups, G., C. L. Addams and S. M. Gorelick, (2005a), Multi-objective calibration of a surface water-groundwater flow model in an irrigated agricultural region: Yaqui Valley, Sonora, Mexico, *Hydrol. and Earth Sys. Sci.*, 9, 549-568.
- Schoups, G., J. W. Hopmans, C. A. Young, J. A. Vrugt, and W. W. Wallender, (2005b), Multi-Criteria Optimization of a Regional Spatially-Distributed Subsurface Water Flow Model, *J. Hydrol.*, 311, 20-48.
- Seo, D. J., R. A. Fulton, and J. P. Breidenbach, (1997), Final Report for Interagency Mou among the Nexrad Program, WSR-88D OSF and NWS/OH/HRL, NWS/OH/HRL, Silver Spring, MD.
- Sivapalan, M., K. Takeuchi, S. W. Franks, V. K. Gupta, H. Karambiri, V. Lakshmi, X. Liang, J. J. McDonnell, E. M. Mendiondo, P. E. O'Connell, T. Oki, J. W. Pomeroy, D. Schertzer, S. Uhlenbrook, and E. Zehe, (2003), IAHS Decade on Predictions in Ungauged Basins (PUB), 2003-2012: Shaping an Exciting Future for the Hydrological Sciences, *Hydrological Sciences Journal-Journal Des Sciences Hydrologiques*, 48(6), 857-880.

- Smith, M., (2002), Distributed Model Intercomparison Project (DMIP), National Weather Service, <http://www.nws.noaa.gov/oh/hrl/dmip/>, [Accessed November, 2001].
- Smith, M. B., K. P. Georgakakos, and X. Liang, (2004a), The Distributed Model Intercomparison Project (DMIP), *J. Hydrol.*, 298, 1-3.
- Smith, M. B., D. J. Seo, V. I. Koren, S. M. Reed, Z. Zhang, Q. Duan, F. Moreda, and S. Cong, (2004b), The Distributed Model Intercomparison Project (DMIP): Motivation and experiment design, *J. Hydrol.*, 298, 4-26.
- Soil Survey Staff, (2006), Soil Survey Geographic (SSURGO) Database for Survey Area, Natural Resources Conservation Service, United States Department of Agriculture, <http://soildatamart.nrcs.usda.gov> [Accessed January 26, 2005].
- Tang, Y., P. Reed, and T. Wagener, (2006), How effective and efficient are multiobjective evolutionary algorithms at hydrologic model calibration?, *Hydrol. and Earth Sys. Sci.*, 10, 289-307.
- Tonkin, M. J., and J. Doherty, (2005), A Hybrid Regularized Inversion Methodology for Highly Parameterized Environmental Models, *Water Resour. Res.*, 41.
- Vrugt, J. A., (2007), Comment On How Effective and Efficient Are Multiobjective Evolutionary Algorithms at Hydrologic Model Calibration? By Y.Tang et al., *Hydrol. Earth Syst. Sci.* 10, 289-307, 2006, *Hydrol. Earth Syst. Sci.* 11, 1435-1436.
- Vrugt, J. A., H. V. Gupta, L. A. Bastidas, W. Bouten, and S. Sorooshian, (2003a), Effective and efficient algorithm for multiobjective optimization of hydrologic models, *Water Resour. Res.*, 39(8).
- Vrugt, J. A., H. V. Gupta, W. Bouten, and S. Sorooshian, (2003b), A shuffled complex evolution metropolis algorithm for optimization and uncertainty assessment of hydrologic model parameters, *Water Resour. Res.*, 39(8).
- Wagener, T., D. P. Boyle, M. J. Lees, H. S. Wheater, H. V. Gupta, and S. Sorooshian, (2001), A framework for development and application of hydrological models, *Hydrol. and Earth Sys. Sci.*, 5(1), 13-26.
- Woods, R. A., R. D. Henderson, and Andrew Tait (2003), Surface Water Components of New Zealand's National Water Accounts, 1995-2001, Client Report No. CHC2003-074. , NIWA, 50.

**Table 3.1.** Calibrated Parameters for the TZTS Model

Parameter Description	Parameter Name	Parameter Range	
		Lower Bound	Upper Bound
Total Channel Width (m)	$B_{Tot}$	15	30
Manning's Roughness Coefficient	$n$	0.025	0.06
Dead Zone Width (% Total Channel Width)	$\%H_{Tot}$	5	30
Dead Zone CS Area (m <sup>2</sup> )	$A_{c,DZ}$	0.5	2.0
Dead Zone Diffusivity (cm <sup>2</sup> /s)	$\alpha_{DZ}$	2000	10,000
Hyporheic Storage Advective Transport Coefficient (cm <sup>3</sup> /s)	$Q_{HS}$	2000	10,000
Hyporheic Storage Sediment Depth (cm)	$Y_{HS}$	5	100
Ground Conduction Depth (m)	$Y_{gr}$	0.1	1.00

**Table 3.2.** Matrix of Calibration Experiments for Single Objective(SO) and Multi-Objective (MO) at Hurricane Bridge (HB) and Washington Field Diversion (WFD) for Corresponding Locations in the Main Channel (MC), Surface Storage (SS) and Sub-Surface Storage (SSS) Used for Calibration (C) and Model Validation of Ungauged Performance (U)

	<b>HB</b>	<b>WFD</b>	<b>HB</b>	<b>WFD</b>	<b>HB</b>	<b>WFD</b>
	<b>MC</b>	<b>MC</b>	<b>SS</b>	<b>SS</b>	<b>SSS</b>	<b>SSS</b>
<b>A – SO HB</b>	<b>C</b>	<b>U</b>	<b>U</b>	<b>U</b>	<b>U</b>	<b>U</b>
<b>B – SO WFD</b>	<b>U</b>	<b>C</b>	<b>U</b>	<b>U</b>	<b>U</b>	<b>U</b>
<b>C - MO HB &amp; WFD</b>	<b>C</b>	<b>C</b>	<b>U</b>	<b>U</b>	<b>U</b>	<b>U</b>

**Table 3.3.** Model Results for Nash-Sutcliffe Efficiency (E) for the ‘Best’ Parameter Set. Locations Used for Calibration Have Values Presented in Bold, While Those Results That Were Used for Ungauged Model Validation Are Not Emboldened

	<b>HB</b>	<b>WFD</b>	<b>HB</b>	<b>WFD</b>	<b>HB</b>	<b>WFD</b>
	<b>MC</b>	<b>MC</b>	<b>SS</b>	<b>SS</b>	<b>SSS</b>	<b>SSS</b>
<b>A – SO HB</b>	<b>0.969</b>	0.839	0.972	0.797	0.875	-0.292
<b>B – SO WFD</b>	0.952	<b>0.905</b>	0.956	0.869	0.856	0.589
<b>C - MO HB &amp; WFD</b>	<b>0.966</b>	<b>0.902</b>	0.969	0.857	0.864	0.467

**Table 3.4.** Average Nash-Sutcliffe Efficiency (AE) Results for the TZTS Model with AE Calculated Using a) Main Channel Temperatures; b) Main Channel Plus Surface Storage Locations; c) Main Channel, Surface Storage and Sub-Surface Storage Locations with Measurements at 9 cm Sediment Depth

	MC	MC+ SS	MC+ SS+ SSS
<b>a. SO HB</b>	0.904	0.894	0.693
<b>b. SO WFD</b>	0.929	0.921	0.855
<b>c. MO HB &amp; WFD</b>	0.934	0.924	0.838

**Table 3.5.** TOPNET Model Parameters

	Name	Estimation * = Multiplier calibrated	Parameter Range Lower Bound: Upper Bound	
<b>Spatially Distributed</b>				
f (m <sup>-1</sup> )	Saturated store sensitivity	From soils *	1	15
K <sub>o</sub> (m/hr)	Surface saturated hydraulic conductivity	From soils *	0.001	150
θ <sub>Δ1</sub>	Drainable porosity	From soils *	0.01	0.5
θ <sub>Δ2</sub>	Plant available porosity	From soils *	0.05	0.5
d (m)	Depth of soil zone	depth = 1/f From soils *	0.005	2
ψ <sub>r</sub> (m)	Wetting front suction	From soils*	0	0.5
CC (m)	Canopy capacity	From vegetation *	0	0.005
Cr	Intercepted evaporation enhancement	From vegetation *	0	2
α	Albedo	From vegetation *	0	1
<b>Spatially Constant</b>				
c	Soil zone drainage sensitivity	1 *	0	20
V (m/hr)	Overland flow velocity	360 *	100	1000
Lapse (°C/m)	Lapse rate	0.0065	NA	NA
<b>Channel Parameters</b>				
n	Mannings n	0.024 *	0.001	0.5
a	Hydraulic geometry constant	0.00011	NA	NA
b	Hydraulic geometry exponent	0.518	NA	NA
<b>State Variables</b>				
$\bar{Z}$ (m)	Average depth to water table	Initial observed flow	NA	NA
SR (m)	Soil zone storage	0.02	NA	NA
CV (m)	Canopy storage	0.0005	NA	NA

**Table 3.6.** Matrix of Calibration Experiments for Single Objective (SO) and Multi-Objective (MO) at Illinois River at Tahlequah (T), Watts (W) and Savoy (S) Locations Used for Calibration (C) and Model Validation of Ungauged Performance (U)

	<b>T</b>	<b>W</b>	<b>S</b>
<b>a. – SO Tahlequah</b>	<b>C</b>	<b>U</b>	<b>U</b>
<b>b. – SO Watts</b>	<b>U</b>	<b>C</b>	<b>U</b>
<b>c. – SO Savoy</b>	<b>U</b>	<b>U</b>	<b>C</b>
<b>d. - MO Tahlequah + Watts</b>	<b>C</b>	<b>C</b>	<b>U</b>
<b>e. - MO Tahlequah + Watts + Savoy</b>	<b>C</b>	<b>C</b>	<b>C</b>



**Table 3.7.** The Range of Model Results for Nash-Sutcliffe Efficiency (E) for Pareto Rank One Parameter Sets. Locations Used for Calibration Have Values Presented in Bold, While Those Results That Were Used for Ungauged Model Validation Are Not Emboldened

	Tahlequah		Watts		Savoy	
	E Max	E Min	E Max	E Min	E Max	E Min
a. SO Tahlequah	<b>0.843</b>	<b>0.843</b>	0.698	0.696	0.344	0.342
b. SO Watts	0.805	0.791	<b>0.739</b>	<b>0.738</b>	0.432	0.430
c. SO Savoy	-2.032	-2.252	-1.452	-1.594	<b>0.682</b>	<b>0.682</b>
d. MO T + W	<b>0.899</b>	<b>0.737</b>	<b>0.818</b>	<b>0.714</b>	0.399	0.251
e. MO T + W + S	<b>0.806</b>	<b>0.381</b>	<b>0.768</b>	<b>0.539</b>	<b>0.663</b>	<b>0.202</b>

**Table 3.8.** The Range of Model Results for Average Nash-Sutcliffe Efficiency (AE) for Pareto Rank One Parameter Sets

	AE r a x	AE r i r	U r a n g e	AE N i d
a. SO Tahlequah	0.628	0.627	0.001	0.628
b. SO Watts	0.659	0.653	0.006	0.656
c. SO Savoy	-0.935	-1.055	0.120	-0.995
d. MO T + W	0.675	0.621	0.054	0.648
e. MO T + W + S	0.694	0.461	0.233	0.578

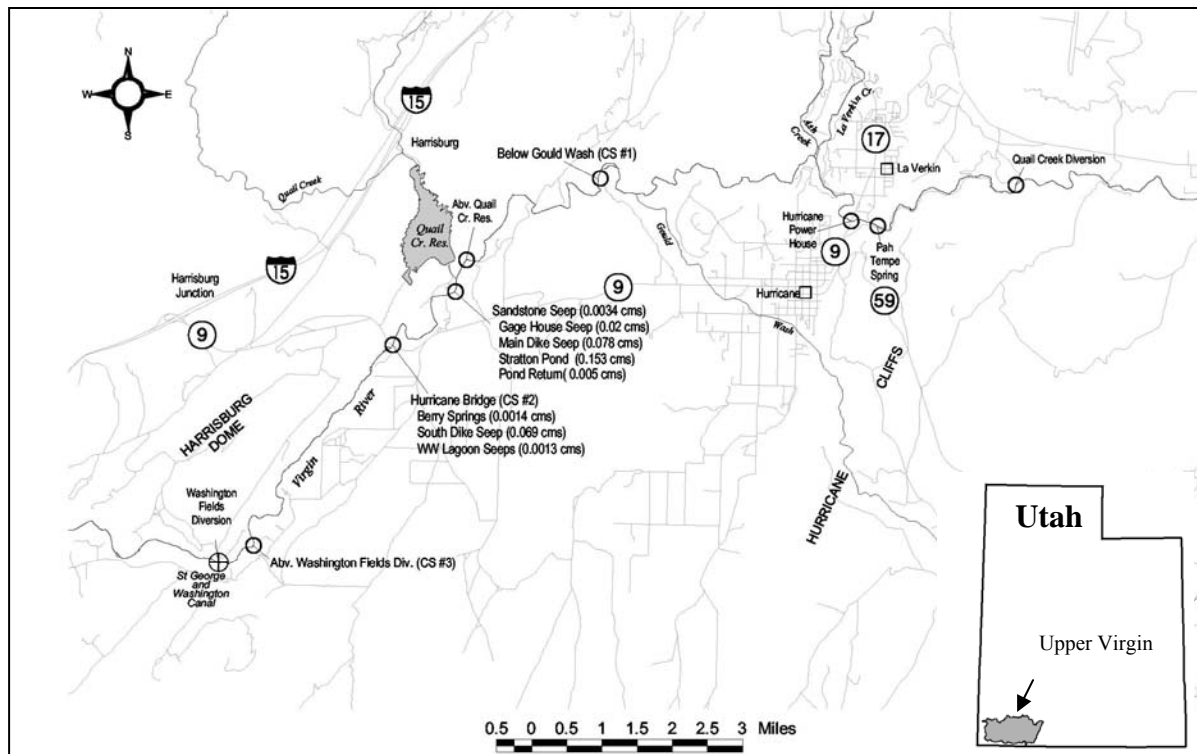


**Figure 3.1.** Layout of Upper Virgin hydrologic cataloging unit. The portion of the river studied is below Gould's Wash (CS #1) and above Washington Fields Diversion (CS #3). Flowrates associated with external inflows in September are included.

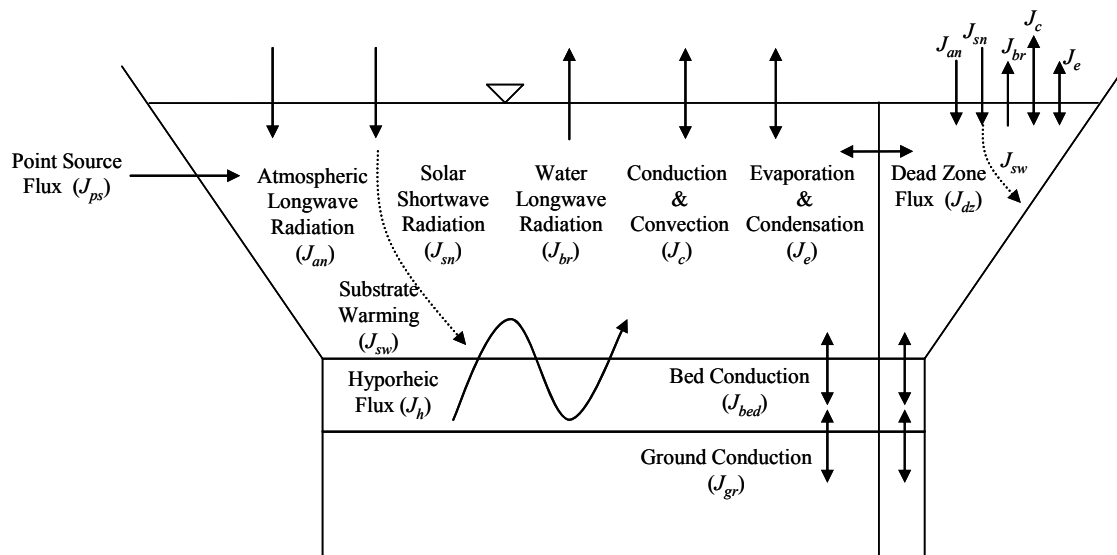


**Figure 3.2.** Energy balance components of the Two-Zone Temperature and Solute Model.

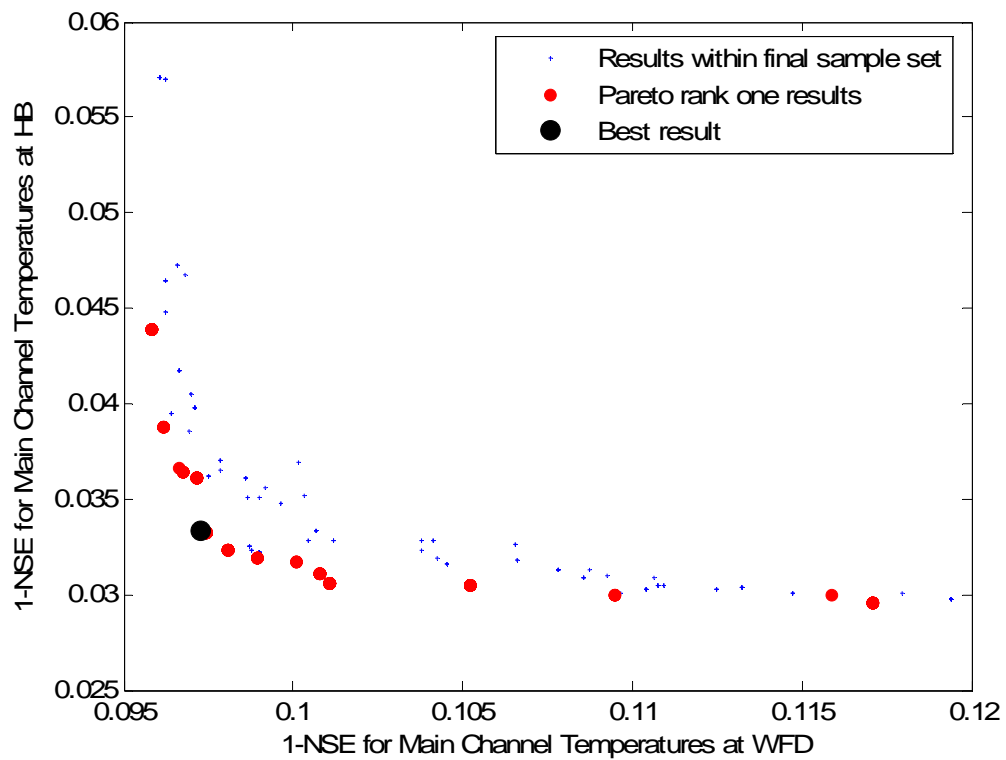


**Figure 3.3.** The tradeoff in the multi-objective calibration of the TZTS model using two main channel temperature locations. 1-NSE in the main channel was the objective minimized in the multi objective function.

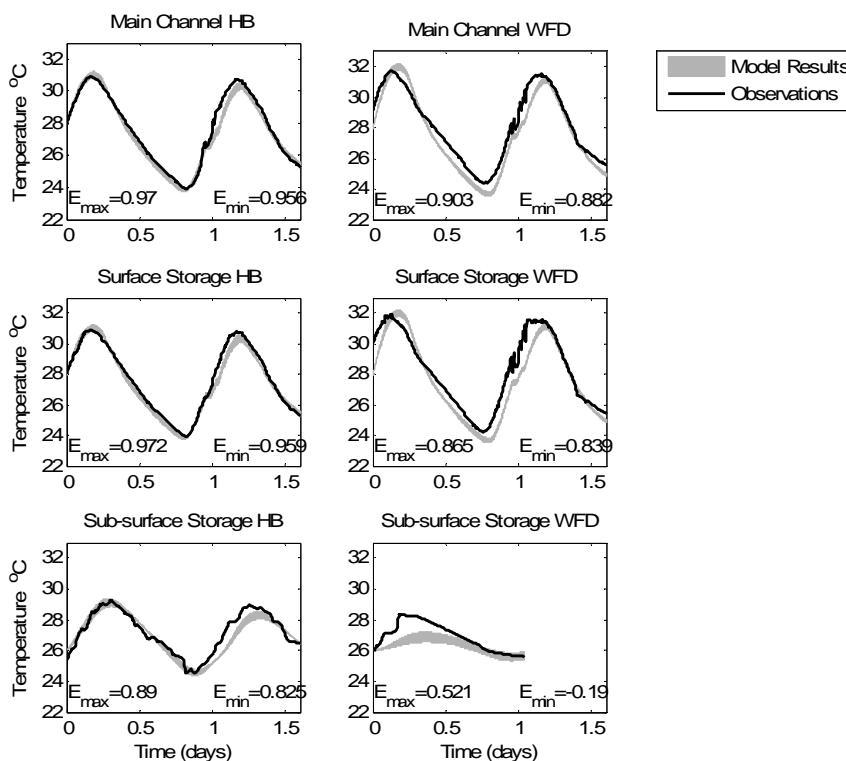


**Figure 3.4.** Multi-objective results for calibration using main channel temperatures at Hurricane Bridge (HB) and Washington Field Diversion (WFD). Model results include those modeled as gauged, main channel HB and main channel WFD, as well as those modeled as ungauged, surface storage HB, surface storage WFD, sub-surface storage HB, and sub-surface storage WFD. Model result bounds created using model results from all pareto rank one parameter sets.

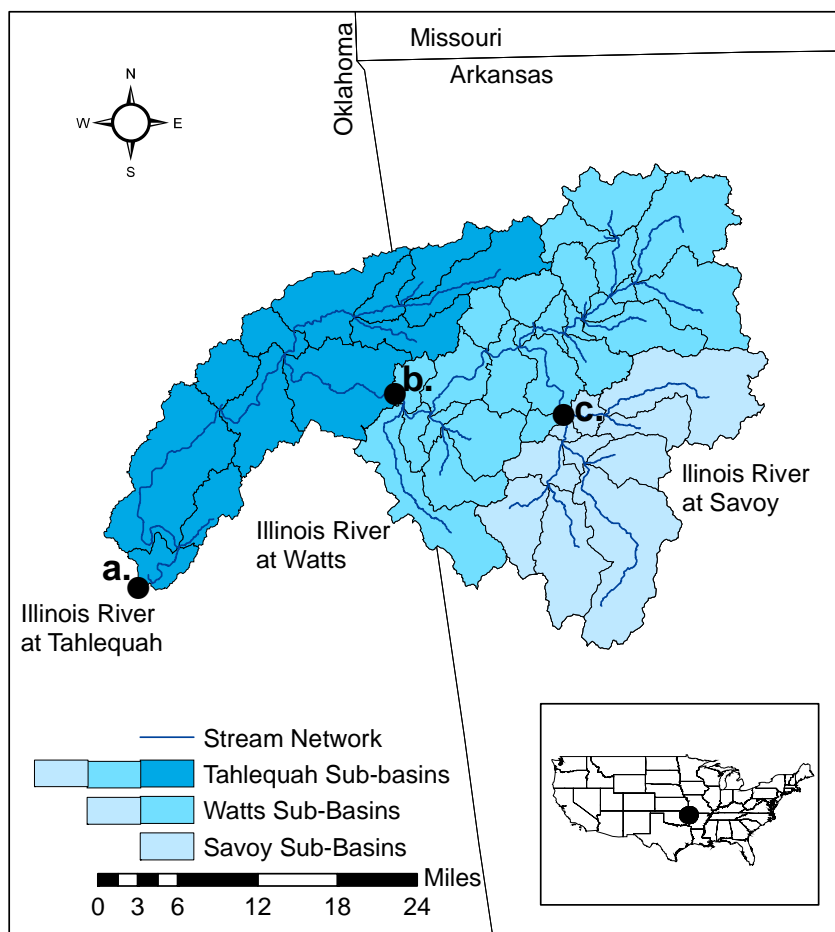


**Figure 3.5.** The (a) Illinois River at Tahlequah watershed and internal sub-basins used in the distributed modelling including output locations at (b) Illinois River at Watts and (c) Illinois River at Savoy.

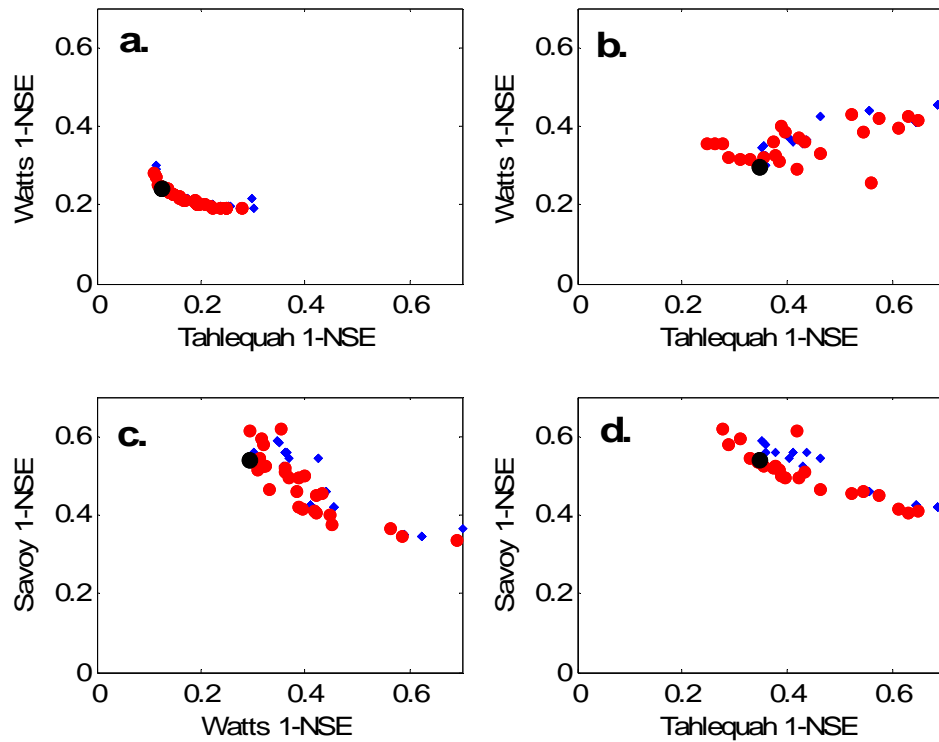


**Figure 3.6.** Calibration experiment results in two dimensional space for two objective test at a) Tahlequah and Watts, and the three-objective test using Tahlequah, Watts and Savoy comparing in two dimensions results at b) Tahlequah Watts and c) Watts and Savoy, and d) Savoy and Tahlequah. Red points indicate pareto rank one parameter sets, blue points indicate other points in the 200 point sample and the black point represents the ‘best’ result that minimizes the tradeoff between objectives.



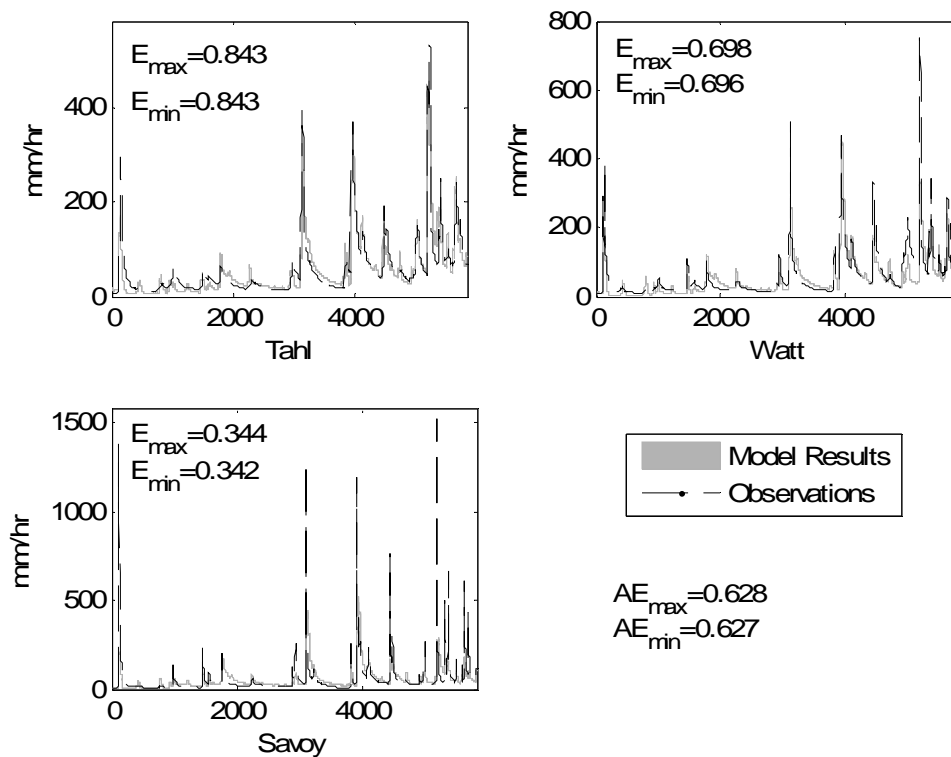


**Figure 3.7.** Single objective calibration results for the Illinois River at Tahlequah.

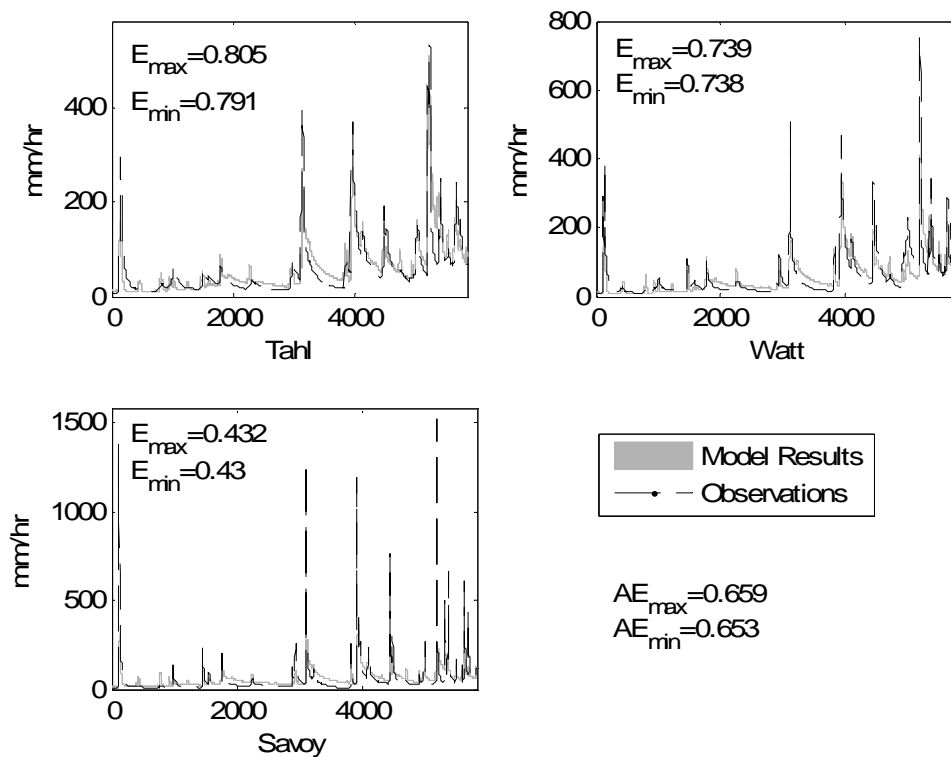


**Figure 3.8.** Single objective results for the Illinois River at Watts.

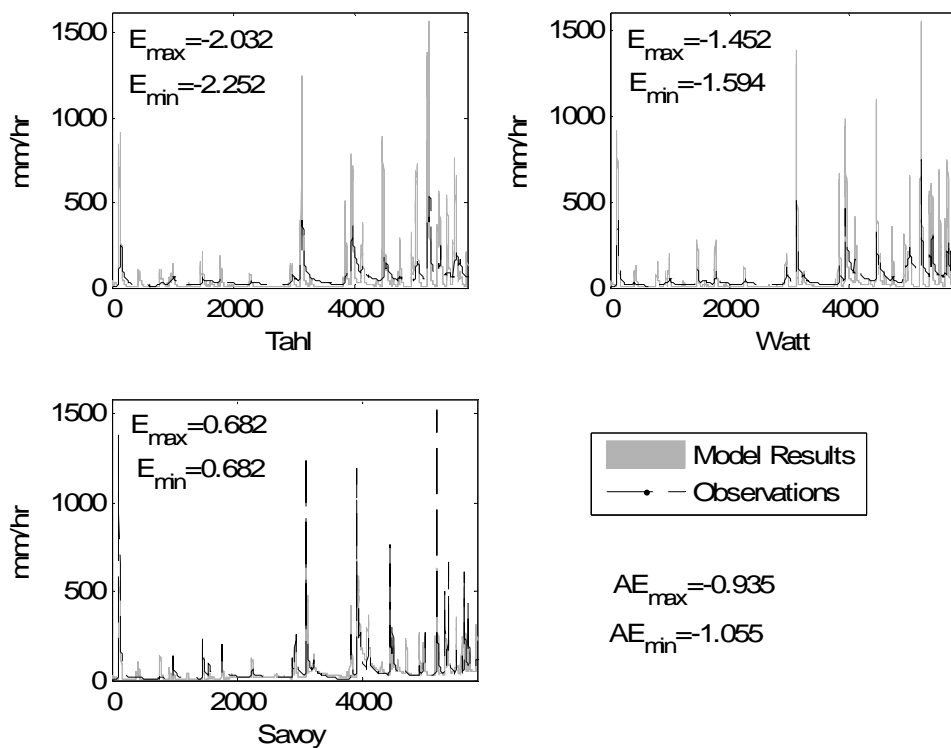


**Figure 3.9.** Single objective results for the Illinois River at Savoy.

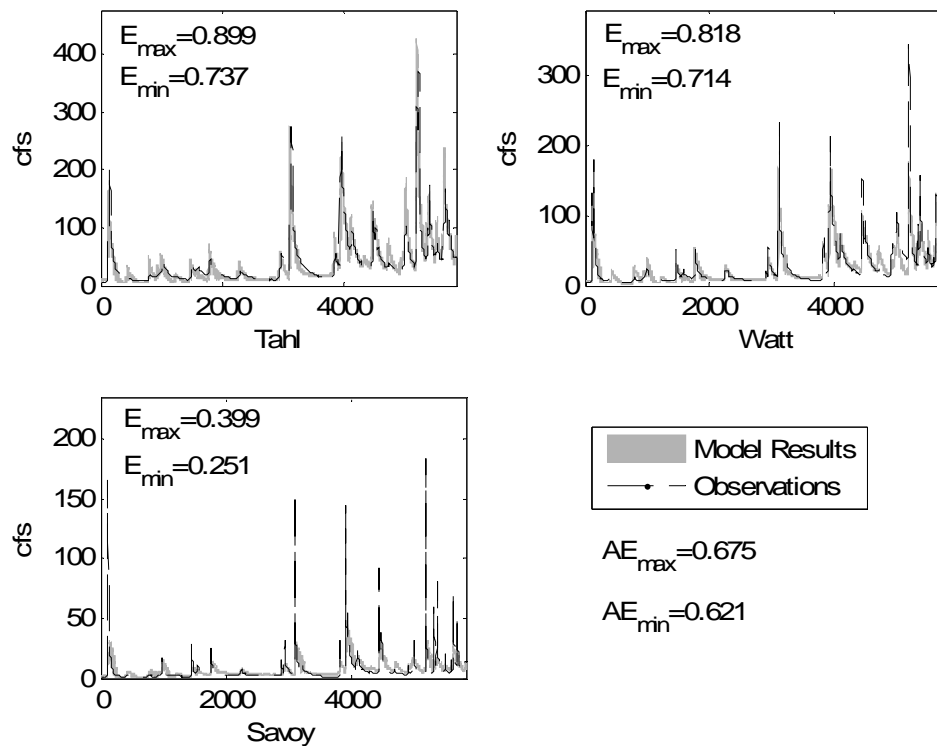


**Figure 3.10.** Results at three locations when using multi-objective calibration at two locations, Tahlequah and Watts, for the calibration period.

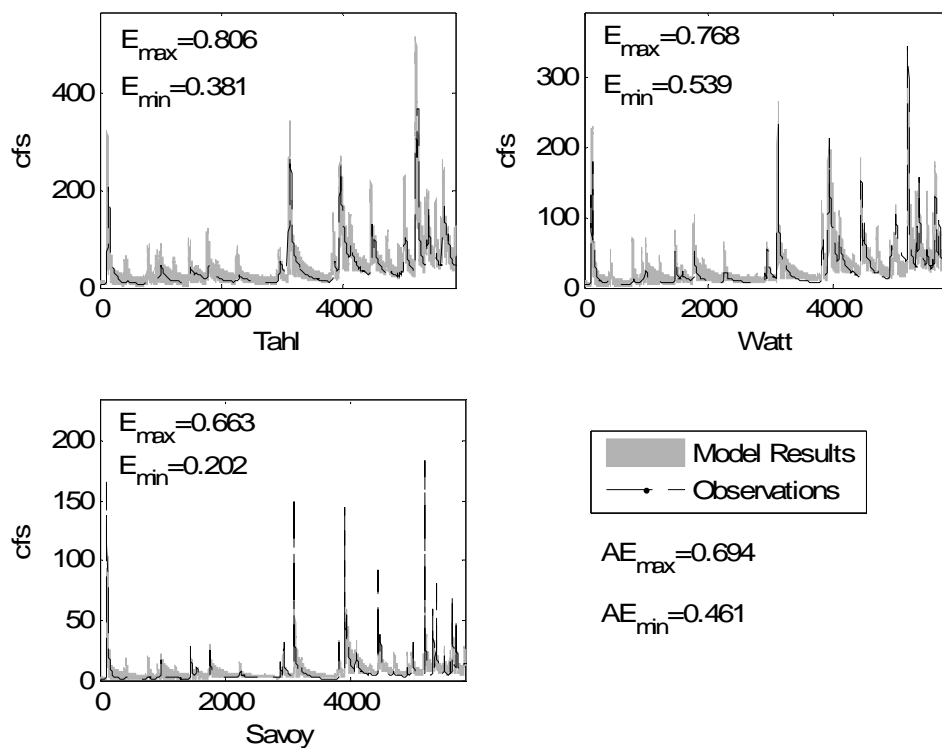


**Figure 3.11.** Results at three locations when using multi-objective calibration at three locations, Tahlequah, Watts and Savoy, for the calibration period.

**CHAPTER 4**  
**PREDICTING STREAMFLOW RECESSION**  
**FROM SOIL AND WATERSHED PROPERTIES<sup>1</sup>**

**Abstract**

This study examines the empirical relationship between streamflow recession data from USGS stream gauges and soil and watershed properties. We test the general hypothesis that a relationship exists between soil properties derived from Soil Survey Geographic (SSURGO) soil data integrated across a watershed and streamflow recession parameters. We also examine the roles that drainage density and slope play in this relationship. Using a random sample of 48 watersheds from across the continental United States, we found a significant correlation between streamflow recession parameters and soil sensitivity, which we quantified using a combination of hydraulic conductivity and porosity. We found that watershed average hydraulic conductivity is the most significant soil property correlated with recession and that the relationship with hydraulic conductivity statistically explains the majority of the recession relationship observed in our data. We also found that in some cases, drainage density has a strong negative correlation to watershed averaged saturated hydraulic conductivity. These correlations between streamflow recession and the

---

<sup>1</sup> Coauthored by David Tarboton, Ross Woods and Janis Boettinger

watershed averaged soil and watershed characteristics change between different geographic regions and climate regimes.

#### **4.1 Introduction**

In this paper we test the hypothesis that watershed averaged soil properties are related to water storage properties reflected in the streamflow recession. Specifically, we examine whether soil properties derived from SSURGO soil data and averaged over a watershed are related to water storage properties reflected in the recession relationship between the rate of decrease in streamflow ( $-dQ/dt$ ) and streamflow itself ( $Q$ ), here measured at the daily scale. This follows the suggestion by *Lin et al.* [2006], that soils and hydrology are related. Our specific interest is to see how watershed averaged soils information is related to the landscape water flux captured by the streamflow recession.

Spatially distributed hydrologic models have been designed, in part, to take advantage of spatially distributed input data such as topography, soils, vegetation and land use. The challenge is to use spatial data in a physically based way so that results are improved because the model is a better representation of reality, not because the model was optimized for good performance at one time period in one specific location. Or in other words, that we are getting the right answer for the right reasons [*Kirchner, 2006*].

Physically based models are intended to improve transferability of methods and parameters to other locations. However calibration is still required because of differences in scale between data and model and uncertainty in data to estimate a priori parameters. Improved spatial representation of a priori parameter estimates, together with calibration techniques

that maintain the spatial variability of a priori estimates, have the potential to improve calibrated streamflow predictions.

This paper starts with a discussion of the physical processes which determine streamflow recession (Section 4.1.1). Next, empirical recession theory (Section 4.1.2), and current a priori parameter estimation techniques applied in hydrologic modeling (Section 4.1.3) are reviewed. Methods for deriving watershed average soil parameters from spatially distributed SSURGO soil survey data and for deriving streamflow recession parameters from streamflow time series data are given in Section 4.2. This is followed by results relating the soil parameters to the streamflow recession parameters and interpretation of how the findings contribute to our knowledge of hydrologic processes in watersheds (Section 4.3).

#### **4.1.1. Controls on Streamflow Recession**

Soils are a determinant of hydrologic behavior because they influence water storage and flux. Measurable soils properties, such as texture, porosity, and depth, have been suggested as physical determinants of streamflow recessions [Lin *et al.*, 2006]. Soil forms as a result of environmental factors influencing natural processes [Buol *et al.*, 2003]. The hydrologic properties of the soils that exist in each watershed are a product of the long-term interplay of the five natural soil-forming factors defined by Jenny [1941]: climate, organisms, geology, topography, and time. Hydrology and soils are thus synergistic and this synergy underlies efforts to understand relationships between soils and hydrology. In particular the soil mapped at any particular location has properties that are assumed to affect the short-term hydrologic response to precipitation. This work is motivated by the idea that measurable properties of soils capture the general hydrologic characteristics of a watershed



that evolved over longer time scales and can be used to develop improved predictions of short-term hydrologic response.

The drainage network is also considered to be an expression of the interrelationship between climate, soils, and vegetation [Moglen *et al.*, 1998]. The drainage network has been shown to be an important measurable watershed property that can be used to understand the impact of overland and throughflow travel distances on hydrologic response [Horton, 1945]. The drainage network is a product of hydrologic processes that sculpt the landscape, while conversely the landscape affects hydrologic response reflecting a synergy between geomorphology and hydrology [Rodriguez-Iturbe, 1979; Gupta *et al.*, 1980, Gupta and Mesa, 1988]. Drainage density,  $D_d$  ( $m^{-1}$ ), the ratio of the total length of stream channels,  $L$  (m), to the area of the watershed,  $A$  ( $m^2$ ) [Horton, 1932], quantifies the basic hillslope length scale associated with the topography. Drainage density controls recession through this relationship to the length of hillslope flow paths. Low drainage density is generally found in areas with highly permeable soils, dense vegetation, and low relief, while high drainage density occurs with less permeable soils, less vegetation and higher relief [Strahler, 1964].

In the studies of Tague and Grant [2004] in Oregon, they found that geology is related to the hydrologic response through the direct effect on flow path, hydraulic gradient, conductivity, storage properties, and relief, and indirectly through its effect on meteorologic forcing.

#### 4.1.2. Recession Theory

Recession analysis, comprehensively reviewed in *Brutsaert* [2005], relates the rate of decrease of streamflow following a storm to soil and geomorphological characteristics of watersheds. The equation

$$-\frac{dQ}{dt} = f(Q) \quad (1)$$

expresses the recession slope as a function of discharge itself and can be considered to be characteristic for a given catchment. *Lamb and Beven* [1997] suggested ways to estimate  $f(Q)$  empirically, directly from recession curve data.

Much recession analysis has focused on a power law form of Equation 1, namely

$$-\frac{dQ}{dt} = aQ^b \quad (2)$$

This form was used by *Brutsaert and Nieber* [1977] who combined observed low streamflow data from six gauging stations in New York State with analytic solutions to the Boussinesq equation for free surface groundwater flow to estimate soil and geomorphic parameters. *Brutsaert and Nieber* showed that, with specific assumptions about the aquifer draining to the stream, parameter  $a$  can be related to watershed and soil properties, while the value of parameter  $b$  captures the general class of recession behavior and varies with specific forms of aquifer assumptions, but in the analysis done by *Brutsaert and Nieber* [1977] is not related to specific watershed and soil properties.

*Brutsaert* [2005] presents derivations for different values of parameter  $a$  and parameter  $b$  (Equation 2) based on different aquifer assumptions. These derivations are all

based on representing a hillslope as an unconfined aquifer with uniform hydraulic conductivity and effective porosity that drains to a stream at the downstream end and is bounded by an impermeable divide at the upstream end.

The parameter value  $b=3$  arises from assumptions of short term drainage of an initially saturated hillslope, where a short time after the peak flow, the influence of near stream drawdown has not yet reached the upstream bound. For a longer time after the peak flow when the recession drawdown reaches the upstream end of the aquifer, a value of  $b=1.5$  is obtained. This long term solution, originating with Boussinesq, assumes that the shape of the water table surface within the hillslope retains a constant functional form. Another long term solution, with a value of parameter  $b=1$ , is obtained by linearizing the Boussinesq equation for flow in an unconfined aquifer by approximating the variable water table position by an average value.

The short time solution for Equation 2 ( $b=3$ ) results in parameter  $a$  directly related to hydraulic conductivity ( $k$ , [m/s]), total channel length ( $L$ ,[m]), aquifer thickness (soil depth,  $D$ ,[m]), and effective porosity ( $n_e$ ) [Brutsaert, 2005]:

$$a = \frac{1.1336}{kn_e D^3 L^2} \quad (3)$$

The long term solution ( $b=1.5$ ) results in the parameter  $a$  having the value [Brutsaert, 2005]

$$a = \frac{4.8038k^{1/2}L}{n_e A^{3/2}} \quad (4)$$

where  $A$  is drainage area [ $\text{m}^2$ ]. The linearized solution ( $b=1$ ) results in the parameter  $a$  having the value [Brutsaert, 2005]

$$a = \frac{\pi^2 k \cdot p \cdot D \cdot L^2}{n_e A^2} \quad (5)$$

where  $p$  is a linearization factor that represents the effective water table position in the aquifer as a fraction of  $D$ .

*Tague and Grant* [2004] found a linear relationship between streamflow recession and geology in 27 watersheds in Oregon. They found that the relationship between  $\log(-dQ/dt)$  and  $\log(Q)$  (Equation 2) changed between different catchments and for different streamflow periods in the same catchment. They attributed this to the different processes that control streamflow generation: streams with similar climate and drainage areas have contrasting hydrologic regimes due to geologic differences.

*Hilberts et al.* [2007] reviews studies conducted on straight hillslopes, using linearized versions of the Boussinesq equation, and notes that these generally model outflow rates successfully, but do not capture the water table dynamics as well. *Hilberts et al.* [2005, 2007] address this problem by coupling the one-dimensional Richards equation for unsaturated flow and the one-dimensional hillslope-storage Boussinesq model [Troch et al., 1993] and show that the unsaturated zone plays an important role in influencing lateral saturated flow in complex hillslopes.

#### **4.1.3. A Priori Parameter Estimation Using Soils Data**

*Koren et al.* [2003] presents equations for estimating a priori parameter values for the Sacramento Soil Moisture Accounting (SAC-SMA) [*Burnash et al.*, 1973] model using soil properties derived from the State Soil Geographic Database (STATSGO). The soil properties-model parameter relationship is used as a quantitative measure of differences between parameters of neighboring watersheds and is used for rescaling calibrated parameters to ungauged watersheds. Their results suggest that soil derived parameters can improve the spatial and physical consistency of parameter estimates while maintaining hydrological performance.

STATSGO (now known as the US General Soil Map) [*Soil Survey Staff*, 2006] is a digital general soil association map developed by the National Cooperative Soil Survey and distributed by the Natural Resources Conservation Service of the U.S. Department of Agriculture [*Soil Survey Staff*, 2006]. STATSGO data was intended for multi-state and regional scale analyses with generalized soil polygons on the scale of 100-200 km<sup>2</sup>. Hydrologic modeling of distributed sub-watersheds less than 100 km<sup>2</sup> is limited by the resolution of STATSGO soil data [*Anderson et al.*, 2006].

More detailed information than STATSGO is now available in the Soil Survey Geographic (SSURGO) database [*Soil Survey Staff*, 2006]. SSURGO data is available at map scales ranging from 1:12,000 to 1:63,360, which is roughly 10 times the resolution of STATSGO. The datasets are developed and maintained by the Natural Resources Conservation Service (NRCS) [*Soil Survey Staff*, 2006]. Internet access to available

SSURGO data began in 2005, with full coverage of the United States scheduled for completion in 2008.

*Anderson et al.* [2006] showed that using higher resolution SSURGO soils data in the SAC-SMA model improved simulations of streamflow compared to simulations using STATSGO data. This suggests that there is a relationship between the observed streamflow and the hydrologic processes controlled by measurable soil properties available in the SSURGO database.

The Hydrology of Soil Types (HOST) classification is another application demonstrating that the physical properties of soils have a major influence on catchment hydrology [*Lilly*, 1998]. This classification of watersheds in Great Britain was created using 1: 250,000 scale soil maps along with hydrological indices of Base Flow and Standard Percentage Runoff. Conceptual hydrological response models were created (11 for the entire country) that describe the dominant pathways of water movement through the soil and substrate [*Lilly et al.*, 1998]. The HOST classification is used in Great Britain to predict river flows of ungauged watersheds, and may be used for predictions of water quality, land suitability and environmental assessments.

Hydrologic relationships applied to models should be shown to have some basis in empirical relationships applicable to a wide diversity of watershed types before the methods can be confidently used in ungauged basins. Issues to consider while exploring the empirical relationships include: 1) local heterogeneities at the model element scale (sub-watershed) may mean that averaged equations should be different from local or field scale descriptions, especially where there are coupled surface and subsurface flows [*Binley et al.*, 1989]; 2)

extremes of the local responses such as infiltration rates may be more important than the average; and 3) the use of pedotransfer functions to estimate a set of average soil parameters at the element scale of a distributed hydrological model should not be expected to give accurate results. This follows purely from considerations of nonlinear mathematics, even if Richards' equation is acceptable as a description of the local flow processes [Beven, 2001].

Hydrologically, it is understood that storage properties of a watershed, such as soil depth, porosity, and hydraulic conductivity, influence the streamflow recession. If SSURGO soil data is to be used to parameterize storage properties in hydrologic models in the United States, it would be useful to know if these properties are empirically related to the components of the streamflow hydrograph that the models aim to reproduce. To this aim, we examine the relationship between a watershed averaged parameterization of soils from the SSURGO database and the streamflow recession parameter  $a$  (Equation 2).

## 4.2 Data and Methods

In order to test the hypothesis that there is a relationship between soils and streamflow recession data, a cross-country sample was selected from Hydro-Climatic Data Network (HCDN) watersheds [Slack *et al.*, 1993] across the continental United States. These are watersheds with United States Geological Survey (USGS) streamflow records selected to be free from diversions and other human impacts. The dataset was selected as a stratified random sample of three watersheds from each of the principal National Ecological Observatory Network Climate Domains [NEON, 2006] in the continental United States. We did not sample from NEON domain 4, which is the southern tip of Florida where there are

no HCDN watersheds, so we ended up with a total of 48 watersheds from the remaining 16 domains (Figure 4.1, Table 4.1).

In our sample, the length of record ranged between 21 and 92 years of daily streamflow. The mean annual precipitation ranges from 250 to 2200 mm. The selection of sample watersheds was limited to those where greater than 90% of the watershed area has SSURGO data available and to sizes ranging between approximately 15 km<sup>2</sup> and 3000 km<sup>2</sup>. Methods for estimating watershed averaged soil and watershed properties are described in Sections 4.2.1 and 4.2.2. The combination of soils and watershed properties into a watershed sensitivity parameter is described in Section 4.2.3. Parameterization of streamflow recession is described in Section 4.2.4.

The high-resolution National Hydrography Dataset, NHD [*U.S. Geological Survey in cooperation with U.S. Environmental Protection Agency, 2007*] was used to calculate the total length of all streams in each watershed. Main channel length, channel slope, mean annual precipitation, and watershed area were obtained from the HCDN database [*Slack et al., 1993*]. The average hillslope and slope from the highest point in the watershed to the outlet was obtained from the HCDN Watershed Database compiled by *Kroll et al. [2004]*.

The data used to investigate the relationships between streamflow recessions and soil and watershed properties, are listed in Table 4.2. In the first column we list the physical attributes of interest in this work. The second column lists the aggregate parameter used to quantify each attribute. The third column gives the distributed data used to estimate aggregate parameters, either through a spatial or temporal aggregation process. Precipitation and streamflow data are temporally distributed and so are represented by aggregate



parameters over time, while soils, topography and network information are spatially distributed and represented by spatial aggregates. The fourth column gives the data source.

#### **4.2.1 Soil Properties Extracted from the SSURGO Database**

Soil components are unique types of soil that occur within each soil map unit. Values for saturated hydraulic conductivity, soil depth, horizon thickness, and soil texture are available for each horizon (layer) within the soil components comprising each map unit in the SSURGO database. Soil depth ( $d$ ) for each soil component is the sum of the thickness (m) of all horizons in the typical soil profile, where horizon thickness is measured from the upper to lower boundary of each soil horizon. For soil horizon depths, the value from the SSURGO database presented as representative was used; a low value and high value based on the expected range within the soil component are also available. Soil and horizon depths were used for depth averaging of horizon porosity and hydraulic conductivity values for each component.

Saturated hydraulic conductivity ( $K_{\text{sat}}$ ) for each soil horizon is available from the SSURGO data base, estimated based on texture, structure, pore size, bulk density, organic matter, and mineralogy [USDA, 2007]. Total porosity ( $f$ ) is the proportion of the soil volume that is not occupied by solids, which can be filled by water or air. Because total porosity is not directly available in the SSURGO database, we estimated the total porosity for each horizon from soil texture using empirical porosity values developed by *Clapp and Hornberger* [1978] and given in Table 4.3. From here on we refer to total porosity as “porosity.”

To aggregate soil properties from component to map unit, we used component percentages given in the SSURGO database for each map unit. The area of each map unit and the value of the soil properties for each map unit were used to calculate watershed averaged soil properties that were used in the calculation of recession sensitivity that follows.

Considering all 48 study watersheds, estimates for the hydraulic conductivity ranged from 0.02 to 1.14 mm/day; soil depth ranged from 0.7 to 2.0 m; and porosity ranged from 0.29 to 0.53. Figures 4.2 to 4.4 give examples of soil properties for three watersheds in the sample.

Figure 4.2 shows the hydraulic conductivity, soil depth and porosity maps for the San Casimiro Creek near Freer, Texas, in Webb County. This watershed has the highest drainage density and the lowest hydraulic conductivity values from the entire 48 watershed sample. In this soils map, the soils-hydrology interaction is apparent by the dense stream network pattern reflected by the soil properties. Figure 4.3 for the Cartoogechaye Creek near Franklin, North Carolina, in Macon County is an example in the mid-range of drainage density and hydraulic conductivity values. The soils-hydrology interaction is apparent, but the stream network pattern less dense than in Figure 4.2 and more dense than in Figure 4.4 which is for the Dismal River near Thedford, Nebraska, in Thomas, Hooker, Grant, and Arthur Counties. Figure 4.4 is at the opposite extreme compared to Figure 4.2, with the lowest drainage density and highest hydraulic conductivity value of the sample watersheds. In Figure 4.4 the stream network pattern is less apparent (see inset to show the drainage network pattern at a scale similar to Figures 4.2 and 4.3). These watersheds illustrate

varying degrees of alignment between soil patterns and the drainage network, believed to reflect the degree of hydrologic influence on the formation of soils [Buol *et al.*, 2003].

One limitation of the SSURGO dataset is that soil property values can change across survey boundaries in watersheds that span multiple survey areas. For example, in Figure 4.4b the survey area in the northwest of the watershed has a higher soil depth (shown in dark green) compared to the rest of the watershed (shown in tan). This is a problem believed to be due to sometimes inconsistent survey methods used in different survey areas. Four watersheds in the sample were affected by this, but they do not appear as outliers in the results.

#### **4.2.2. Watershed Data and Sample Stratification**

To quantify watershed geomorphology, we used drainage density values calculated using the channel length available in the National Hydrography Dataset (NHD) high resolution data [U.S. Geological Survey in cooperation with U.S. Environmental Protection Agency, 2007]. We used the mean annual precipitation and watershed area reported in the HCDN database [Slack *et al.*, 1993]. Three measures of slope from the HCDN Watershed Database [Kroll *et al.*, 2004] were included: (1) the main channel slope reported in the HCDN database; (2) average topographic hillslope from the national elevation dataset Digital Elevation Model (<http://seamless.usgs.gov/>); and (3) slope calculated from the peak elevation to the outlet.

To further explore the information available in our 48 watershed dataset, we calculated correlations for subsets of the watersheds classified by geography, topography and climate. The geographic classification selected the first subset as watersheds from

NEON Climate Domains 1 to 11, the eastern half (30 watersheds), and the second subset from climate domains 12-17, the western half (18 watersheds). The topographic classification was based on average hillslope: the third subset is of sample watersheds with the lowest average hillslope, less than 0.02 m/km (13 watersheds), and the fourth subset is of the sample watersheds with the highest average hillslope, between 0.06 and 0.18 m/km (13 watersheds). The climate classification split the 48 watershed dataset based on mean annual precipitation. The 24 “wet” watersheds (>1000 mm) have between 1030 mm and 2270 mm of mean annual precipitation. The 24 “dry” watersheds (<1000 mm) range between 290 mm and 936 mm of mean annual precipitation.

#### **4.2.3 Watershed Sensitivity Parameter**

A conceptual model for the sensitivity of streamflow recession rates to soil properties is to consider streamflow to be supplied by horizontal drainage through the soil profile. As the soil drains, a smaller fraction of the soil profile is active in draining water resulting in a decrease in the soil drainage rate. The capacity of the soil to store water relative to the capacity of the soil profile to transmit water laterally provides a measure of the sensitivity of soil water drainage that supplies streamflow to changes in soil water storage.

The soil storage capacity is represented by the area averaged porosity,  $f$  (dimensionless), multiplied by the area averaged soil depth,  $d$  (m). The ability of water to move through the soil horizontally, or the lateral drainage capacity, is quantified by transmissivity. This is calculated from the area and depth averaged saturated hydraulic conductivity,  $K_{\text{sat}}$  (m/day), multiplied by the area averaged soil depth. The relative change in

drainage capacity per unit change in stored water, determines the soil sensitivity that we postulate should be related to streamflow recession. The ratio of transmissivity,  $K_{sat}d$ , to storage capacity,  $fd$ , is defined as soil sensitivity,  $S$ , and simplifies to:

$$S = \frac{K_{sat}}{f} \quad (6)$$

With this definition, clayey soils, which drain slowly because of low  $K_{sat}$  but have high porosity, are expected to have a small  $S$  value, indicating a relatively small change in drainage rate between them being wet and dry. In contrast sandy soils, with high  $K_{sat}$  and low porosity, will have a large  $S$  value.

Steeper topography is generally associated with higher drainage densities [Knighton, 1984; Leopold *et al.*, 1964; Dunne and Leopold, 1978], implying a more developed stream channel network with shorter hillslope flow distances that may influence the streamflow recession. The sensitivity of the soils,  $S$  (Equation 6), can be extended to capture the sensitivity for a watershed,  $W$ , by looking at a ratio of flow rate to watershed storage capacity.

Integrating transmissivity,  $K_{sat}d$ , along both sides of the channels draining the soil mantle with total channel length,  $L$ , and multiplying by the slope gradient,  $g$ , that drives lateral flow results in soil mantle drainage capacity of  $2K_{sat}dLg$ . The multiplier of 2 represents the two hillslopes, one draining into each side of each channel. Integrating storage capacity,  $fd$ , over the watershed area ( $A$ ), watershed storage capacity is  $fdA$ . Taking the ratio we have Equation 7.

$$W = \frac{2 \cdot K_{sat} \cdot d \cdot L \cdot g}{f \cdot d \cdot A} \quad (7)$$

This watershed sensitivity,  $W$ , has units of  $T^{-1}$ . Now, recognizing that  $L/A$  is drainage density,  $D_d [L^{-1}]$ , we have Equation 8

$$W = \frac{2 \cdot K_{sat} \cdot D_d \cdot g}{f} \quad (8)$$

Further recognizing that hillslope length,  $h$ , is on average  $1/2D_d$  [*Horton*, 1945] we have

$$W = \frac{K_{sat} \cdot g}{f \cdot h} \quad (9)$$

Watershed sensitivity combines the soil sensitivity defined in equation 6 with the geomorphologic quantities of slope and drainage density or hillslope length. Watersheds characterized by longer hillslopes (reflected by lower drainage densities) are predicted to have lower sensitivity because they take longer to drain; shorter hillslopes have higher sensitivity. Steeper slopes drain more quickly, and are thus more sensitive than gentle slopes.

It is instructive to examine watershed sensitivity in the context of a linear system characterized by

$$Q = rZ \text{ or } \frac{dQ}{dZ} = r \quad (10)$$

where  $Z$  denotes the storage in the system and  $r$  is a storage-discharge coefficient. Under recession, when the only change in storage is discharge, we have

$$\frac{dZ}{dt} = -Q \quad (11)$$

Combining this with (10) we get

$$-\frac{dQ}{dt} = rQ \quad (12)$$

This is equivalent to Equation 2 with parameter  $b=1$  and shows that the constant  $a$  in the linear form of Equation 2 is equivalent to a linear storage discharge coefficient. The justification for  $W$ , presented above, quantified sensitivity as the change in discharge from hillslopes to streams as soil storage is depleted. This is an approximation for  $dQ/dZ$ . Watershed sensitivity  $W$  may therefore be expected to be equivalent to parameter  $a$  when parameter  $b=1$ .

Comparing  $W$  to the theoretical results for parameter  $a$  from *Brutsaert* [2005] presented above, Equation 5 (the solution for parameter  $b=1$ ) can be written

$$a = \frac{\pi^2 k \cdot p \cdot (D/h)}{4n_e \cdot h} \quad (13)$$

where  $2h=1/D_d=A/L$  is used to represent drainage density in terms of hillslope length. Equation (13) is similar in form to Equation (9). Hillslope length  $h$  appears in the denominator and effective porosity,  $n_e$ , is comparable to porosity,  $f$ . The numerator of both equations includes hydraulic conductivity and the term  $D/h$  is akin to slope because it provides a ratio of parameters that quantify vertical and horizontal scales.

When parameter  $b$  is not equal to 1, such as the solutions when  $b=3/2$  or  $b=3$ , Equations 3 and 4 can also be related to  $W$ . Because the sensitivity,  $W$ , derived above was expressed in terms of discharge per unit area, comparison to Equations 3 and 4 require recasting Equation 2 on a per unit area basis. Using  $q=Q/A$ , results in

$$-\frac{dq}{dt} = (aA^{b-1})q^b = a'q^b \quad \text{where } a' = (aA^{b-1}) \quad (14)$$

Now using  $a$  from Equation 4 where  $b=3/2$ , results in

$$a' = (aA^{1/2}) = \frac{2.4019 \cdot k^{1/2}}{n_e \cdot h} \quad (15)$$

Although this has different units from Equation 9, the sensitivities are similar with  $k$  appearing in the numerator and  $n_e$  and  $h$  appearing in the denominator.

Using parameter  $a$  from Equation 3 where  $b=3$  results in

$$a' = (aA^2) = \frac{4.53 \cdot h^2}{kn_e D^3} \quad (16)$$

In this case, the short time solution predicts an inverse relationship between parameter  $a$  and  $k$ ,  $n_e$ , and  $D$ , and a positive relationship to  $h$ .

This theory suggests that recession curve sensitivity should be related to hydraulic conductivity and slope, and inversely related to porosity and hillslope length a long time after the peak when the influence of the stream drawdown has reached the upstream boundary. A short time after the peak, or when the influence of the stream drawdown has not yet reached the upstream boundary, the recession parameter  $a$  is expected to be inversely related to hydraulic conductivity, porosity and aquifer depth, and related to hillslope length.

#### **4.2.4. Streamflow Data**

##### **4.2.4.1. Methods For Selecting Recession Points From Daily Streamflow**

There are many ways that recession points have been selected from streamflow time series [Brutsaert and Nieber, 1977; Brutsaert and Lopez, 1998; Mendoza et al., 2003; Tague and Grant, 2004]. We were concerned that identification of recession points may impact



results and are not aware of any work that tests the effect of the recession selection methods on the resulting parameters ( $a$  and  $b$ ) derived from the recession points. We therefore evaluated the sensitivity using three approaches. After normalizing the streamflow by drainage area, recession points were first selected as all flow values occurring more than two days after a streamflow peak, up until the next increase in flow. We then identified summertime recession points as the subset from these recession points that occurred between July and October. Thirdly, we tried eliminating the recessions above the median streamflow to identify lower baseflow recessions. The method for recession selection only had a significant effect on the resulting recession parameters for five of the watersheds. We consequently settled on the first method which selected recessions throughout the year occurring more than two days after a streamflow peak, since this resulted in a greater number of recession points for analysis.

#### 4.2.4.2 Streamflow Recession Analysis

Recession points were selected from the daily USGS streamflow data [Wahl *et al.*, 1995] over the historical record of each watershed. After normalizing the streamflow by the watershed area, streamflow recession analysis was performed using Equation 2 [Brutsaert and Nieber, 1977]. Horizontal striations in the  $\log(-dQ/dt)$  versus  $\log(Q)$  scatterplot occur when the difference in flow values between daily time steps is less than the precision with which the flows are measured. To avoid these data artifacts, our recession point selection method included precision averaging following Rupp and Selker [2006], also used by Kroll *et al.* [2004]. Average flow values are calculated over the length of time required for a change in flow greater than the precision of the measurements. See Kroll *et al.* [2004] for

more details on applying this procedure with USGS streamflow data that has varying precision.

Two sets of recession analyses were carried out. First we plotted  $\log(-dQ/dt)$  versus  $\log(Q)$  relationships for all recession periods and fit a linear least squares regression model to determine the slope, parameter  $b$ , and intercept, parameter  $a$ , for each site. This analysis quantifies the recession at each site empirically according to Equation 2. However the parameter  $a$  values resulting from these analyses are not comparable because they have different units, the units of parameter  $a$  being dependent on parameter  $b$ . We are generally more interested in the parameter  $a$ , because while the parameter  $b$  characterizes the general class of behavior of a streamflow recession, the parameter  $a$  is expected to vary from place to place and to be related to watershed and soil attributes. To have comparable parameter  $a$  values, the second set of recession analyses used fixed parameter  $b=1$ . This corresponds to the selection of a linear model which has been widely used [*Brutsaert, 1994; Verhoest and Troch, 2000; Serrano, 1995*].

Figure 4.5 shows a histogram of the empirically based parameter  $b$  values for the 48 watersheds in the dataset. Without the constraint of parameter  $b=1$ , the distribution of parameter  $b$  values across the 48 sample watersheds ranges between 0.28 and 2.38 with a peak near 1, indicating that parameter  $b=1$  is not a poor choice. Figure 4.6 shows the regression lines fit to the recession data for each watershed in our study set. Each line extends over the range of the data for that watershed and passes through the centroid which is also plotted. A line with  $b=1$  through the cluster of centroids is shown for illustration.

Figures 4.5 and 4.6 show that for the most part, empirically based parameter  $b$  values are close to  $b=1$  lines, but in some cases the watersheds do not behave linearly. In some cases, the regression line through the scatterplot was limited by the available data. This was the case for three of the watersheds in the sample that gave rise to negative values for parameter  $b$ . These negative values were not included in Figure 4.5.

For the remainder of this paper we focus on the results where the regression through recession data has been constrained by  $b=1$ . This is for a number of reasons: 1) the simplicity of linear methods; 2) the need for one value for parameter  $b$ , so that the values of parameter  $a$  are comparable; 3) the dimensional consistency that results in units of  $1/T$  for parameter  $a$ ; 4) the empirical finding in Figures 4.5 and 4.6 that parameter  $b=1$  is generally a reasonable approximation; 5) of the theoretical values for parameter  $b$  (1, 1.5 and 3) from prior work [Brutsaert, 2005], the value  $b=1$  is reasonably close to the peak in the histogram shown in Figure 4.5. Figure 4.7 shows the regression lines fit to streamflow recessions for the entire dataset with the constraint of parameter  $b=1$ . The similarity of the general pattern of this figure to Figure 4.6 gives further support to the choice of the constraint of parameter  $b=1$ .

When parameter  $b$  is assumed to be 1, the parameter for the least squares line through  $\log(-dQ/dt)$  versus  $\log(Q)$  data can be shown to be given by Equation 17.

$$a^* = \frac{\text{geometricmean}\left(\frac{-dQ}{dt}\right)}{\text{geometricmean}(Q)} \quad (17)$$

We use the notation  $a^*$  to denote the recession parameter  $a$  calculated with the constraint  $b=1$ . This equation is a manifestation of the fact that a regression line goes through the centroid of the data. The parameter  $a^*$  has units of inverse time [ $T^{-1}$ ] and can be compared to watershed sensitivity (Equations 7 to 9) which also has units of inverse time.

To illustrate the methods described in this section, we continue with examples of our streamflow recession analysis applied to three sample watersheds.

Figures 4.8 to 4.10, show the hydrographs and  $\log(-dQ/dt)$  versus  $\log(Q)$  scatterplots from three watersheds from the sample dataset chosen to illustrate the recession point selection process and the range of hydrologic behaviors captured in the dataset. In Figures 4.8a, 4.9a, and 4.10a, three years of streamflow data are shown in log scale with blue and cyan points where recessions were selected. Cyan points indicate precision averaged recession points; blue points are those which are not averaged. In Figures 4.8b, 4.9b and 4.10b, the recession points from the entire length of record are shown; these are used to determine the  $\log(Q)$  vs  $\log(-dQ/dt)$  relationship using simple linear regression.

Figure 4.8 shows streamflow from a watershed from an arid area with quick recessions and no flow between precipitation events (or flow less than 0.01 cubic feet per second, which is reported by the USGS as 0.00). The annual precipitation is 546 mm. This watershed in Texas is also shown in Figure 4.2 as an example watershed with clay soils characterized by low hydraulic conductivity and higher porosity. A highly developed drainage network is also apparent from the soils map. The average recession behavior is very close to linear with parameter  $b=1$ . Figure 4.9 is an example from a more humid

region in North Carolina with higher average streamflow, longer recessions, and less flow rate variability compared to the watershed shown in Figure 4.8. The annual precipitation is 1550 mm per year. The soil properties from this watershed were shown in Figure 4.3 as an example of a watershed with a mid-range of hydraulic conductivity and drainage network development. Figure 4.10 shows streamflow from a watershed in the Yosemite National Park in California which has annual precipitation of 1372 mm. This watershed had high hydraulic conductivity and low drainage density with soil property patterns similar to the Nebraska watershed shown in Figure 4.4.

In the San Casimiro Creek, Texas, the quick streamflow recession with no measurable baseflow (Figure 4.8a) contrasts with the apparent baseflow recession in the Cartoogechaye Creek in North Carolina (Figure 4.9a) and the strong effects of annual cycles in the Merced River, California (Figure 4.10a). Figures 4.8b, 4.9b and 4.10b, which show the scatterplots of  $\log(-dQ/dt)$  versus  $\log(Q)$ , are plotted on with axis scales the same to distinguish differences between watersheds in the range of flow rates over which recessions occur.

## **4.3 Results**

### **4.3.1 Relating Streamflow Recession and Watershed Sensitivity**

For the 48 study watersheds, we calculated correlation statistics using the log transform of each variable in the dataset. Correlation statistics for the relationship between the logs of the streamflow recession parameter  $a^*$  and soil and watershed parameters are given in Table 4.4. Soil sensitivity,  $S$ , is from Equation 6 and watershed sensitivity,  $W$ , is

from Equations 7 to 9. Correlation statistics between logs of the streamflow recession parameter  $a^*$  and logs of the factors that comprise S and W are also shown. The components of S comprising the spatially averaged values of: saturated hydraulic conductivity ( $K_{\text{sat}}$ ), soil depth (d), and porosity (f) are described in Section 4.2.1. The components of W are high resolution drainage density ( $D_d$ ) from the NHD [*U.S. Geological Survey in cooperation with U.S. Environmental Protection Agency, 2007*], channel slope (channelslope) from the HCDN database [*Slack et al., 1993*], average hillslope (aveslope) and slope from the highest elevation to outlet (peakslope) from the HCDN Watershed Database [*Kroll et al., 2004*] described in Section 4.2.2. The significance of the correlation was tested using the student's t distribution and the significant correlations ( $p < 0.05$ ) are highlighted in grey shading in Table 4.4. Although there are many alternatives to statistical inference, we are using this significance test and p-value as a baseline for which to highlight the strongest correlations and assess the evidence in our data.

The largest three significant correlations presented in Table 4.4 (bolded) are between the streamflow recession parameter  $a^*$  and S,  $K_{\text{sat}}$  and W calculated using channel slope.  $K_{\text{sat}}$  is a factor in the estimation of both S and W and the high correlation with  $K_{\text{sat}}$  suggests that it alone can account for the majority of the correlation between  $a^*$  and S and W. Additionally, there is a significant correlation between  $a^*$  and channel slope.

Examination of the data shows that the correlation between streamflow recession parameterized by  $a^*$  and soils data parameterized with S, is strongly affected by two points with  $\log(S) < -9.5$ . Although the relationship remains statistically significant if these two watersheds are removed, those with larger  $\log(S)$  values do not appear to be as strongly

correlated. This suggests that these entire dataset correlations may not be an appropriate generalization for some watersheds. The results for correlations with data from watersheds classified by geography, topography and climate (as defined in Section 4.2.2) follow to address this issue.

#### **4.3.2 Watersheds Classified by the Geography, Topography, and Climate**

Table 4.5 gives the correlation value between parameter  $a^*$  and the soil and watershed properties for subsets of the data based on geography, topography and climate as described above. Statistically significant correlation ( $p < 0.05$ ) highlighted in grey and with the strongest correlations in each subset bolded.

The strongest correlation for the eastern watersheds is between parameter  $a^*$  and soil sensitivity (Equation 6) where  $R = -0.712$ . For the western watersheds, which include all 13 of the watersheds from the highest slope subset, the hydraulic conductivity correlation is most significant, but in this case is positively correlated with  $R = 0.413$  as opposed to the negative correlation of the eastern subset. In this western watershed case, the hydraulic conductivity is more strongly related to parameter  $a^*$  than the aggregate soil sensitivity parameter. For the lowest slope set, soil sensitivity and the watershed sensitivity calculated with the channel slope are both very strongly correlated with the streamflow recession, with the porosity positively related and the channel slope inversely related. Porosity is significantly correlated to parameter  $a^*$  only in the lowest slope and eastern subsets.

Perhaps most interesting is that the relationship between parameter  $a^*$  and S changes from negative ( $R = -0.786$ ) when looking at the class of lowest slope watersheds to positive

( $R=0.402$ ) when looking at the class of western (dominated by highest slope) watersheds. Based on the theory presented earlier, we expected a positive correlation between recessions parameterized by  $a^*$  and S and W which all have dimensions of  $T^{-1}$ . This was only the case for watersheds in the western and highest slope subsets. Figure 4.11 shows the six data subsets plotted by a) geography, b) average hillslope, and c) mean annual precipitation, where the difference in the positive correlation between parameter  $a^*$  and S for western and highest slope watershed subsets compared to the negative correlation for eastern and lowest slope watershed subsets is notable. There is little difference in the negative parameter  $a^*$  and S correlation for watersheds classified by precipitation.

It is also interesting to note the difference in relationships between  $a^*$  and individual components of S and W. In the eastern and lowest slope subsets, the streamflow recession can be shown to be correlated to individual parameters of  $K_{sat}$ , porosity and channel slope; while in the western subset,  $K_{sat}$  is the only individual component that is significantly correlated to  $a^*$ . For all subsets where hydraulic conductivity is significantly correlated, streamflow recession is captured as well by  $K_{sat}$  alone as when looking at the variables in aggregates using S and W.

Comparing watersheds classified by climate, the relationship between the streamflow recession parameter  $a^*$  and the soil sensitivity is most strongly correlated in the wet watersheds. As with other subsets, the strength of this correlation is almost solely due to the role of hydraulic conductivity. In fact, addition of other variables degrades the strong correlation between streamflow recession parameter  $a^*$  and  $K_{sat}$ . The correlation between the streamflow recession parameter  $a^*$  and the soil sensitivity is weaker in the subset of dry



watersheds where the recession parameter is more strongly correlated to the watershed sensitivity calculated using peak to outlet slope, so in this case, addition of information about the slope from the peak elevation to the outlet does improve the correlation slightly.

### **4.3.3. Relating Hydraulic Conductivity to Drainage Density and Slope**

One explanation for the negative correlation between streamflow recession [1/T] and soil sensitivity [1/T] for the total sample and subsets of east, low slope, wet and, to a lesser extent, dry, may be the inverse relationship between hydraulic conductivity and drainage density shown in Table 4.6 where the correlation value between hydraulic conductivity and watershed properties are presented with significant relationships ( $p < 0.05$ ) highlighted in grey with the strongest correlation in each watershed subset bolded.

Results in Table 4.6 show that when parameterizations of slope do not have a significant positive correlation to  $K_{sat}$  (as with the west and high slope subsets),  $D_d$  has a negative correlation to  $K_{sat}$ . This is the case for the sets All, East, Lowest slope, Wet, and Dry. For example, in the eastern subset, average hillslope has a significant inverse correlation to  $K_{sat}$  ( $R=-0.319$ ), and the relationship to drainage density is also negative ( $R=-0.568$ ). The data for this relationship is shown in Figure 4.12. When a parameterization of slope has a significant positive correlation to  $K_{sat}$ , the  $D_d$  is not significantly correlated to  $K_{sat}$ . This is the case for the West and Highest slope subsets. Figure 4.13 shows the positive correlation between average hillslope and  $K_{sat}$  for the western subset.

The last three columns in Table 4.6 show results where  $D_d$  values and slope values are multiplied, because in the aggregate watershed sensitivity parameter derived in Equation

8 they occur together as a product. These show positive correlations for the steep and west subsets that appear to be dominated by the positive correlation between  $K_{sat}$  and average hillslope, while for the remaining subsets there are negative or insignificant correlations. The negative correlations are associated with negative correlations with both  $D_d$  and slope.

#### 4.4 Discussion

The statistically significant empirical correlations ( $p < 0.05$ ) found for the different watershed subsets (Tables 4.5 and 4.6) can be summarized as follows:

Lowest slope:  $a^* \sim -K_{sat}$ ,  $f$ ,  $-g$  and  $K_{sat} \sim -D_d$

East:  $a^* \sim -K_{sat}$ ,  $f$ ,  $-g$  and  $K_{sat} \sim -D_d$

West:  $a^* \sim K_{sat}$

Wet:  $a^* \sim -K_{sat}$ ,  $-g$  and  $K_{sat} \sim -D_d$

Dry:  $a^* \sim -K_{sat}$ ,  $-g$  and  $K_{sat} \sim -D_d$

The notation "~" above indicates correlation that is positive when the variable is unsigned, or negative when a "-" sign is used. In the above  $g$  denotes channel slope. There was no statistically significant correlation for the highest slope watersheds. However, the correlation between recession and  $K_{sat}$  is positive in the western watersheds, which includes the 13 highest slope watersheds and likely includes younger and more tectonically active landscapes, and negative elsewhere. Both the Brutsaert and Nieber long time scale recession theory and sensitivity parameters we developed would predict a positive correlation with  $K_{sat}$ . The Brutsaert and Nieber short time scale recession predicts a negative correlation with  $K_{sat}$ , but this was for  $b=3$ .

There are a number of possible physical explanations for this negative recession correlation. These include: (A) short time scale aquifer recession; (B) a negative correlation between drainage density and hydraulic conductivity that offsets the direct effect of hydraulic conductivity on the recession; (C) the recession being an overland flow recession, with overland flow more likely with smaller  $K_{sat}$ ; and (D) soil drainage being governed by the unsaturated hydraulic conductivity, which is likely to be larger for fine soils than coarse soils at low moisture contents. These are each discussed in turn.

A. To discuss the short time scale aquifer recession we present a definition sketch (Figure 4.14) for the Dupuit-Boussinesq aquifer model that is the basis for the recession analysis of *Brutsaert and Nieber* [1977]. This depicts schematically how the shape of the free groundwater surface is expected to change with drainage through time following initial saturation of the aquifer. In Figure 4.14,  $B$  is the breadth of the aquifer,  $D$  is the depth of the aquifer, and  $h(x,t)$  gives the elevation of the free groundwater surface at distance  $x$  from the stream at time  $t$ . In this conceptualization water held by capillary effects above the groundwater table is neglected. Early in the recession at  $t_1$ , the influence of streamflow drawdown has not reached the upstream bound and  $h(x,t) < D$  only when  $x$  is small. At  $t_1$  the short time solution (Equation 3) is valid. This has  $b=3$  and  $a$  inversely proportional to  $K_{sat}$ . Over time, the influence of the stream drawdown eventually reaches the upstream bound (at  $t_2$  in Figure 4.14) and  $h(x,t) < D$  everywhere (for  $t > t_2$ , as illustrated by  $h(x,t_3)$  in Figure 4.14). This is when the long time solutions (Equations 4 and 5) are expected to hold and  $b$  is reduced to 1 or 1.5 and  $a$  becomes proportional to  $K_{sat}$ .

In this conceptualization, watersheds with low slope are much more likely to have shallow water tables that are closer to the surface, such as depicted at  $t_1$  and tend to follow the short time scale recession with recession coefficient inversely related to  $K_{sat}$ . Whereas steeper watersheds are likely to have deeper water tables resembling those depicted at  $t_2$  or  $t_3$  with recession coefficient directly related to  $K_{sat}$ . This suggests that flatter watersheds should have a larger  $b$ , close to 3, while steeper watersheds should have smaller  $b$ , closer to 1 or 1.5. We examined the  $b$  parameters from Figure 4.5 versus each of the slope measures (channelslope, aveslope and peakslope), and although we found a decreasing trend in  $b$  with an increase in each slope measure, none was statistically significant. Also, the short time scale recession predicts  $b=3$ , but we are finding parameter  $b$  consistently less than 3 (Figure 4.5).

B. A second possible explanation for the inverse relationship between the recession coefficient and  $K_{sat}$  is the effect of drainage density. When  $K_{sat}$  is small, drainage density is large due to the synergy between channel network development and runoff. Small  $K_{sat}$  leads to slower infiltration which results in more overland flow. More overland flow leads to the development of a denser network of channels with shorter hillslopes that have quicker recessions. Large  $K_{sat}$  leads to faster infiltration, less overland flow, and comparatively less development of channel networks.

C. Thirdly, the inverse relationship between the recession coefficient and  $K_{sat}$  may be a direct overland flow effect. Since small  $K_{sat}$  may result in more overland flow, the streamflow recession in this case may really be an overland flow recession rather than a

subsurface drainage recession. Overland flow is generally expected to be quicker than subsurface flow, and so would recede more quickly.

D. A fourth possible explanation for the inverse relationship is the importance of the effect of unsaturated hydraulic conductivity, highlighted in the work of *Hilberts et al.* [2005, 2007]. Soil moisture characteristic curves show that sandy soils have high  $K_{sat}$ , but as their moisture content decreases, the hydraulic conductivity reduces dramatically. The reduction of  $K_{sat}$  of sandy soils at low moisture content, may reduce the component of drainage supplied by the unsaturated zone. Clayey soils have a low  $K_{sat}$  that does not necessarily reduce as much given a loss of the same volume of water [*Buckingham, 1907*].

#### 4.5 Conclusions

This paper explored the empirical relationship between streamflow recession data from USGS streamgauges and soils properties from high-resolution SSURGO soil data to test the general hypothesis that a relationship exists between plot scale soils data integrated across a catchment and catchment scale streamflow recession parameters. We compiled a dataset of soils and watershed data for a random sample of HCDN watersheds from across the continental United States and conducted our analysis with subsets classified based on geography, topography, and climate.

In our analysis, we have found that relationships between water storage and transmissivity properties of the soil derived from SSURGO soil data and the streamflow recession, parameterized following *Brutsaert and Nieber* [1977] using daily USGS data, vary based on geography, topography and climate. In watersheds with the lowest slopes and in the East, those with soils characterized by low hydraulic conductivity have been shown to

have quicker streamflow recession compared to watersheds with high hydraulic conductivity. In western watersheds, which included the highest slopes, this relationship is the inverse. Our results show that hydraulic conductivity dominates the relationship between streamflow recession and soils and watershed properties. Surprisingly, we did not find a statistically significant correlation between drainage density and recession, although hillslope length appears in theoretical recession parameterizations. This may be due to the offsetting effect of the significant inverse correlation between hydraulic conductivity and drainage density (Table 4.6).

Most recession theory suggests that the relationship between hydraulic conductivity and recession rate should be positive. This was the case for western watersheds, which included the steepest slopes. However, when the watersheds do not have high slopes, such as with our subsets of low slope and eastern watersheds, we found an inverse relationship between recessions and hydraulic conductivity. We believe that this may be influenced by one or more of: (1) the effect of the short time recession solution [Brutsaert, 2005], (2) correlation between drainage density and hydraulic conductivity, (3) overland flow drainage, and (4) unsaturated hydraulic conductivity effects.

## References

- Anderson, R. M., V. I. Koren, and S. M. Reed, (2006), Using SSURGO data to improve Sacramento Model a priori parameter estimates, *J.Hydrol.*, 320, 103-116.
- Beven, K., (2001), How far can we go in distributed hydrological modelling?, *Hydrol.Earth Sys. Sci.*, 5(1), 1-12.
- Binley, A., K. Beven and J. Elgy, (1989), A physically based model of heterogeneous hillslopes .2. Effective hydraulic conductivities, *Water Resour. Res.*, 25(6), 1227-1233.

- Brutsaert, W., (1994), The unit response of groundwater outflow from a hill slope, *Water Resour. Res.*, 30(10), 2759-2763.
- Brutsaert, W., (2005), *Hydrology: An Introduction*, Chapter 10, Cambridge University Press.
- Brutsaert, W. and J. P. Lopez, (1998), Basin-Scale Geohydrologic Drought Flow Features of Riparian Aquifers in the Southern Great Plains, *Water Resour. Res.*, 34(2), 233-240.
- Brutsaert, W., and J. L. Nieber, (1977), Regional drought flow hydrographs from a mature glaciated plateau, *Water Resour. Res.*, 13(3), 637-643.
- Buckingham, E. (1907). Water retention in soil. *Soil Bulletin* (38). U.S. Department of Agriculture.
- Buol, S. W., R. J. Southard, R. C. Graham, and P. A. McDaniel, (2003), *Soil Genesis and Classification*, The Iowa State University Press, Ames.
- Burnash, R. J. C., R. L. Ferral, and R. A. Maguire, (1973), A generalized streamflow simulation system: Conceptual models for digital computers, Joint Federal State River Forecast Center, Sacramento, CA.
- Clapp, R. B. and G. M. Hornberger, (1978), Empirical equations for some soil hydraulic properties, *Water Resour. Res.*, 14, 601-604.
- Dunne, T. and L. B. Leopold, (1978), *Water in Environmental Planning*, W H Freeman and Co, San Francisco, 818 p.
- Gupta, V. K., and O. J. Mesa, (1988), Runoff generation and hydrologic response via channel network geomorphology: Recent progress and open problems, *J. Hydrol.*, 102, 3-28.
- Gupta, V. K., E. Waymire, and C. T. Wang, (1980), A representation of an instantaneous unit hydrograph from geomorphology, *Water Resour. Res.*, 16(5), 855-862.
- Hilberts, A. G. J., P. A. Troch, and C. Paniconi (2005), Storage-dependent drainable porosity for complex hillslopes, *Water Resour. Res.*, 41.
- Hilberts, A. G. J., P. A. Troch, C. Paniconi, and J. Boll (2007), Low-dimensional modeling of hillslope: Relationship between rainfall, recharge, and unsaturated storage dynamics, *Water Resour. Res.*, 43.
- Horton, R. E., (1932), Drainage basin characteristics, *Trans. Am. Geophys. Union*, 13, 350-361.

- Horton, R. E., (1945), Erosional development of streams and their drainage basins: Hydrophysical approach to quantitative morphology, *Geol. Soc. Amer. Bull.*, 56, 275-370.
- Jenny, H., (1941), *Factors of Soil Formation*, McGraw-Hill, New York, 281.
- Kirchner, J. W., (2006), Getting the right answers for the right reasons: Linking measurements, analyses, and models to advance the science of hydrology, *Water Resour. Res.*, 42.
- Knighton, D., (1984), *Fluvial Forms and Processes*, Edward Arnold.
- Koren, V., M. Smith, and Q. Duan, (2003), Use of *a Priori* Parameter Estimates in the Derivation of Spatially Consistent Parameter Sets of Rainfall-Runoff Models, *Calibration of Watershed Models*, Edited by Q. Duan, H. V. Gupta, S. Sorooshian, A. N. Rousseau and R. Turcotte, 239-254, American Geophysical Union, Washington D.C.
- Kroll, C. N., J. G. Luz , T. B. Allen, and R. M. Vogel, (2004), Developing a watershed characteristics database to improve low streamflow prediction, *J. Hydrolog. Eng.*, 9(2), 116-120.
- Lamb, R., and K. Beven, (1997), Using interactive recession curve analysis to specify a general catchment storage model, *Hydrology and Earth Systems Sci.*, 1, 101-113.
- Leopold, L. B., M. G. Wolman, and J. P. Miller, (1964), *Fluvial Processes in Geomorphology*, W. H. Freeman, San Francisco, 522.
- Lilly, A., (1998), Institute of Hydrology Report No. 126, Hydrology of Soil Types: a hydrologically based classification of the soils of the UK, The Macaulay Institute, Wallingford, 137.
- Lilly, A., D. B. Boorman, and J. M. Hollis, (1998), The development of a hydrologic classification of UK soils and the inherent scale changes, *Nutrient Cycling in Agroecosystems*, 50, 299-302.
- Lin, H., J. Bouma, Y. Pachepsky, A. Western, J. Thompson, R. van Genuchten, H.-J. Vogel, and A. Lilly, (2006), Hydropedology: Synergistic integration of pedology and hydrology, *Water Resour. Res.*, 42.
- Mendoza, G. F., T. S. Steenhuis, M. T. Walter, and J. Y. Parlange, (2003), Estimating basin-wide hydraulic parameters of a semi-arid mountainous watershed by recession-flow analysis, *J. Hydrol.*, 279, 57-69.



- Moglen, G. E., E. A. B. Eltahir, and R. L. Bras, (1998), On the sensitivity of drainage density to climate change, *Water Resour. Res.*, 34(4), 855-862.
- NEON, (2006), Integrated Science and Education Plan, Washington, DC, <http://www.neoninc.org/documents/ISEP2006Feb2.pdf> [Accessed November 2006].
- Rodriguez-Iturbe, I., G. Deuto, and J. B. Valdes, (1979), Discharge response analysis and hydrologic similarity: The interrelation between the geomorphologic IUH and storm characteristics, *Water Resour. Res.*, 15(6), 1435-1444.
- Rupp D., and J. Selker (2006), Information, artifacts, and noise in  $dQ/dt - Q$  recession analysis, *Adv. Water Res.*, 29, 154-160.
- Serrano, S., (1995), Analytical solutions of the nonlinear groundwater flow equations in unconfined aquifers and the effect of heterogeneity, *Water Resour. Res.*, 31, 2733-2742.
- Slack, J. R., A. M. Lumb and J. M. Landwehr, (1993), U.S. Geological Survey Hydro-Climatic Data Network (HCDN): Streamflow Data Set, 1874 - 1988, USGS Water-Resources Investigations Report 93-4076, <http://water.usgs.gov/pubs/wri/wri934076/>. [Accessed December 2007].
- Soil Survey Staff, (2006), Soil Survey Geographic (SSURGO) Database for Survey Area, Natural Resources Conservation Service, United States Department of Agriculture, <http://soildatamart.nrcs.usda.gov> [Accessed January 26, 2005].
- Strahler, A. N., (1964), Quantitative geomorphology of drainage basins and channel networks, in *Handbook of Applied Hydrology*, Edited by V. T. Chow, 439-476, McGraw-Hill Book Co., New York.
- Szilagyi, J., M. B. Parlange, and J. D. Albertson, (1998), Recession flow analysis for aquifer parameter determination, *Water Resour. Res.*, 34(7).
- Tague, C. and G. E. Grant, (2004), A geological framework for interpreting the low-flow regimes of cascade streams, Willamette River Basin, Oregon, *Water Resour. Res.*, 40(4).
- Troch, P. A., F. D. Troch and W. Brutsaert, (1993), Effective water table depth to describe initial conditions prior to storm rainfall in humid regions, *Water Resour. Res.*, 29(2), 427-434.
- U.S. Geological Survey in cooperation with U.S. Environmental Protection Agency, U. F. S., and other Federal, State and local partners (2007), *National Hydrography Dataset (NHD) - High-Resolution*, <http://nhd.usgs.gov>, [Accessed July, 2007]

U.S. Department of Agriculture, Natural Resources Conservation Service, (2007), National Soil Survey Handbook, title 430-V, <http://soils.usda.gov/technical/handbook>, [Accessed January, 2008].

Verhoest, N. E. C., and P. A. Troch, (2000), Some analytical solutions of the linearized boussinesq equation with recharge for a sloping aquifer, *Water Resour. Res.*, 36, 793-800.

Wahl, K. L., J. W. O. Thomas, and R. M. Hirsch, (1995), Stream-gaging program of the U.S. Geological Survey. Circular 1123, Reston, Virginia.

**Table 4.1.** The Stratified Random Sample of HCDN Watersheds from NEON Climate Domains 1 Through 17, Excluding Domain 4 which is the Southern Tip of Florida. The USGS Code is the Streamgauge Identifier, the SSURGO Code Indicates the Soil Survey Area. Some Watersheds Required Soils Data from Multiple Surveys for Complete Spatial Coverage

Climate Domain	Random Selection 1		Random Selection 2		Random Selection 3	
	USGS Code	SSURGO Code	USGS Code	SSURGO Code	USGS Code	SSURGO Code
1	1142500	VT017	1399500	NJ027	1170100	VT025
2	1408000	NJ025	1471000	PA011;PA075	2053200	NC091;NC131
3	2175500	SC005;SC665;SC009	2324000	FL067	8010000	LA039;LA097
5	4063700	WI037;WI041	5394500	WI069;WI067	4078500	WI115
6	5419000	IL085	5466000	IL073	5414000	WI043
7	3500240	NC113	3298000	KY211;KY185	3248500	KY641
8	7187000	MO145;MO009	7247000	AR127	7056000	AR129;AR101
9	6775900	NE171;NE091;NE075;NE005	5060500	ND602;ND610	6334500	MT011;WY011
10	6841000	NE111;NE063	6783500	NE041;NE163	6876700	KS123;KS105;KS143
11	8194200	TX479	8064800	TX213;TX001	8198500	TX463;TX019
12	13075000	ID711	13200500	ID661	12414900	ID608
13	8283500	NM650	8269000	NM670	7208500	NM007
14	8405500	NM614	11058500	CA777	10258500	CA680;CA777
15	12500500	WA677	10329500	NV777	10172700	UT608,UT611
16	14193000	OR679	14325000	OR011	14301000	OR 009; OR007; OR067; OR057
17	11264500	CA790	11475560	CA694	10308200	CA729

**Table 4.2.** Data Used to Investigate the Relationships Between Streamflow Recessions and Soil and Watershed Properties

Physical Attribute	Aggregate Parameter	Distributed Data	Data Source
Climate	Annual Rainfall	Precipitation	HCDN database
Soils	Watershed averaged porosity, hydraulic conductivity, soil depth	Soil depth, hydraulic conductivity, soil texture	NRCS SSURGO database
Topography	Watershed averaged hillslope, channel slope	Elevation	HCDN Watershed Database [Kroll et al., 2004]
Stream channel network	Drainage density	Stream channel length, watershed area	NHD High Resolution, HCDN database
Streamflow Recession	Recession parameter	Recessions from daily streamflow	Historical USGS daily streamflow

**Table 4.3.** Porosity Based on Soil Texture from *Clapp and Hornberger* [1978]

Soil Texture	Porosity [-]
Sand <sup>1</sup>	0.395
Loamy sand <sup>2</sup>	0.41
Sandy loam <sup>3</sup>	0.435
Silt loam <sup>4</sup>	0.485
Loam	0.451
Sandy clay loam	0.42
Silty clay loam	0.477
Clay loam	0.776
Sandy clay	0.426
Silty clay	0.492
Clay	0.482

<sup>1</sup> Includes fine sand and coarse sand; <sup>2</sup> includes loamy fine sand and loamy coarse sand; <sup>3</sup> includes coarse sandy loam, fine sandy loam, and very fine sandy loam; <sup>4</sup> includes silt.

**Table 4.4.** Correlation Statistics (R, R<sup>2</sup>, t and p) Between Natural Logarithms of Soil and Watershed Properties and Streamflow Recession Parameter  $a^*$ . Grey Shading Denotes Correlations That Are Statistically Significant at the 0.05 Level,  $p < 0.05$ . The Three Largest Correlation Coefficients Are Shown in Bold

	df=48	R	R <sup>2</sup>	t	p
S	$K_{sat} / f$ [m/day]	<b>-0.586</b>	0.343	3.827	0.0003
S components	$K_{sat}$ [m/day]	<b>-0.575</b>	0.331	3.719	0.0004
	Soil depth [m]	0.272	0.074	1.496	0.073
	Porosity (f) [-]	0.283	0.080	1.561	0.064
	W; g=channelslope [day]	<b>-0.581</b>	0.338	3.777	0.0004
W	W; g=aveslope [day]	-0.295	0.087	1.634	0.056
	W; g=peakslope [day]	-0.474	0.225	2.848	0.004
	D <sub>d</sub> [1/km]	0.083	0.007	0.441	0.331
W components	channelslope [m/km]	-0.432	0.187	2.535	0.008
	aveslope [m/km]	-0.154	0.024	0.825	0.208
	peakslope [m/km]	-0.291	0.085	1.609	0.059

**Table 4.5.** Correlation Values (R) Between Log Transformed Soil and Watershed Properties and the Log of Streamflow Recession Parameter  $a^*$  for Watershed Data Stratified by Geography, Topography and Climate. The Strongest Correlation for Each Watershed Subset Is Shown in Bold

Correlation value (R)		East	West	Lowest Slope	Highest Slope	Wet	Dry
	Watershed count (df)	30	18	13	13	24	24
S	$K_{sat} / f$ [m/day]	<b>-0.712</b>	0.402	<b>-0.786</b>	0.360	-0.723	-0.483
S components	$K_{sat}$ [m/day]	-0.697	<b>0.413</b>	-0.784	0.340	<b>-0.723</b>	-0.466
	Soil depth [m]	0.139	0.065	-0.014	0.001	0.253	0.219
	Porosity (f) [-]	0.410	-0.066	0.598	-0.261	0.273	0.261
W	W; g=channelslope [day]	-0.673	0.278	-0.734	0.098	-0.702	-0.474
	W; g=aveslope [day]	-0.036	0.377	0.119	-0.024	-0.350	-0.323
	W; g=peakslope [day]	-0.334	0.211	0.089	0.035	-0.421	<b>-0.519</b>
W components	$D_d$ [1/km]	0.259	-0.049	0.363	-0.194	0.220	-0.053
	channelslope [m/km]	-0.389	-0.039	-0.512	-0.003	-0.530	-0.318
	aveslope [m/km]	0.110	0.177	0.255	0.092	-0.125	-0.196
	peakslope [m/km]	0.061	-0.143	0.179	-0.170	-0.242	-0.335

**Table 4.6.** Correlations Between Log Hydraulic Conductivity and Logs of Drainage Density, Channel Slope, Average Slope, and Slope from the Peak Elevation to the Outlet for the Entire Dataset (All) and Classified Subsets. Strongest Correlation for Each Set of Watersheds Is in Bold. Drainage Density Multiplied by each Slope Factor Is Given in the Final Three Columns

	D <sub>d</sub> [1/km]	Channel slope [m/km]	aveslope [m/km]	peakslope [m/km]	D <sub>d</sub> * channel slope	D <sub>d</sub> * aveslope	D <sub>d</sub> * peakslope
All	<b>-0.374</b>	0.239	-0.029	0.185	0.119	-0.027	0.145
East	<b>-0.568</b>	0.113	-0.319	-0.145	-0.219	-0.371	-0.283
West	-0.097	0.177	<b>0.613</b>	0.471	0.169	0.570	0.469
Lowest Slope	-0.514	0.158	-0.509	-0.355	-0.226	-0.539	<b>-0.551</b>
Highest Slope	0.080	0.029	<b>0.614</b>	0.384	0.050	0.588	0.456
Wet	<b>-0.401</b>	0.313	-0.080	0.111	0.210	-0.072	0.031
Dry	<b>-0.373</b>	0.182	-0.029	0.239	0.045	-0.037	0.235

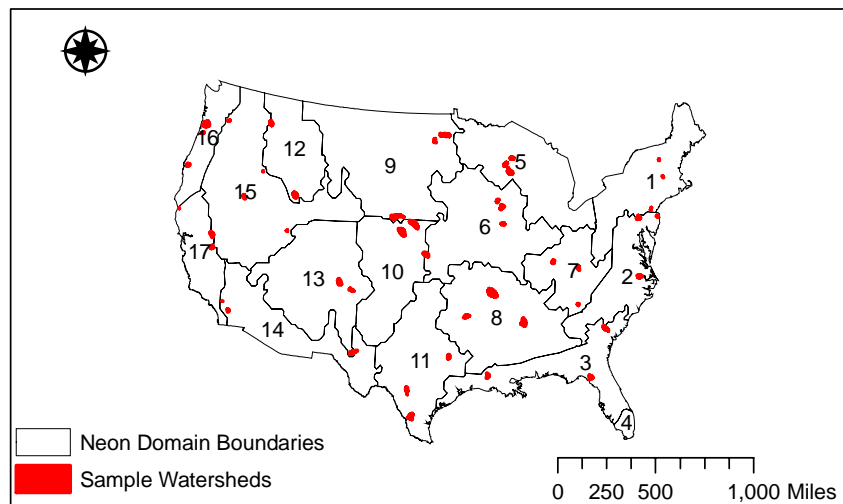


**Figure 4.1.** Sample of three HCDN watersheds from each National Ecological Observatory Network (NEON) domain across the continental United States.



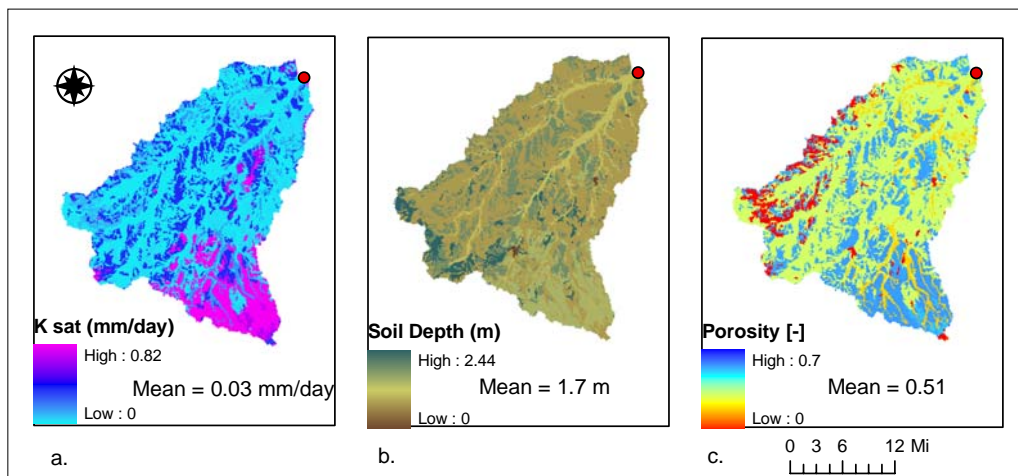


**Figure 4.2.** Hydraulic conductivity (a), soil depth (b) and porosity (c) maps for the San Casimiro Creek near Freer, Texas, in Webb County. This is an example of a strong soils-hydrology interaction apparent in the stream network pattern of the soil map.

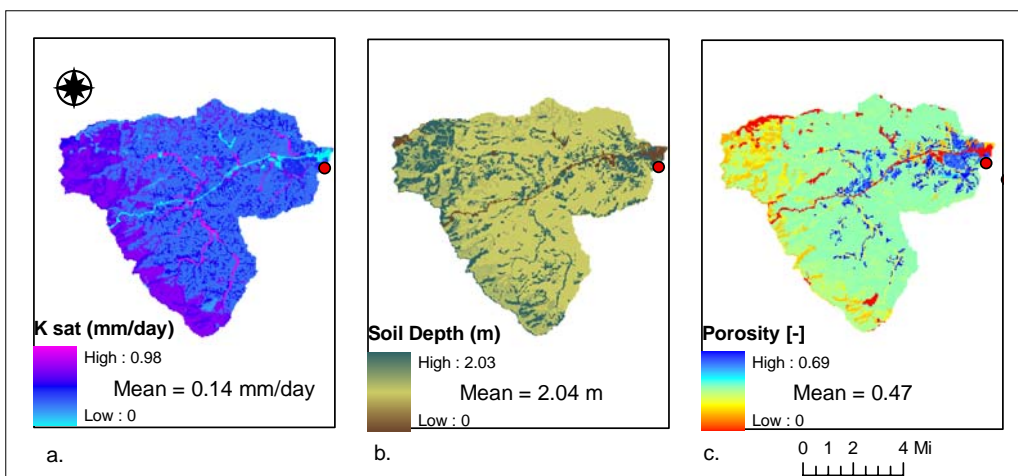


**Figure 4.3.** Hydraulic conductivity (a), soil depth (b) and porosity (c) maps for the Cartoogechaye Creek near Franklin, North Carolina, in Macon County. The soils-hydrology interaction apparent in the stream network pattern of the soil map is in the mid-range for the sample watersheds.

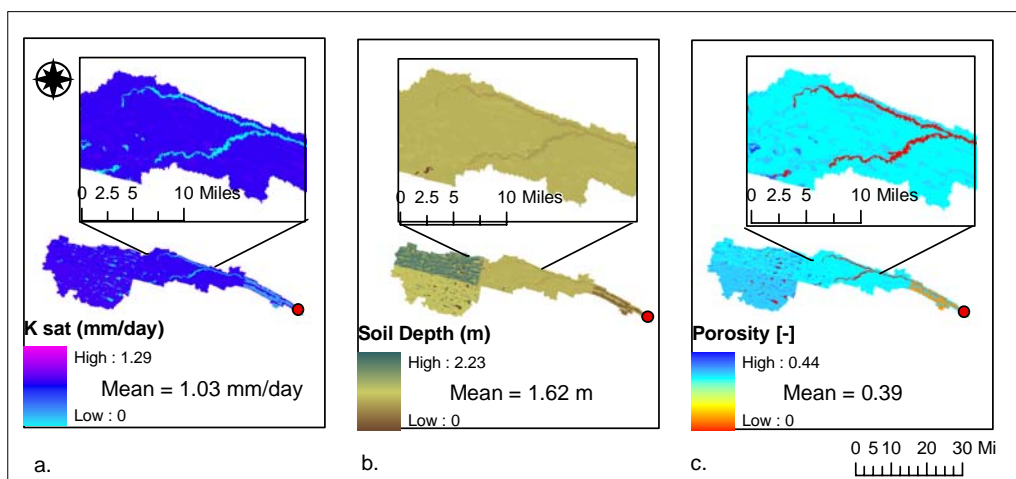


**Figure 4.4.** Hydraulic conductivity (a), soil depth (b) and porosity (c) maps for Dismal River near Thedford, Nebraska, in Thomas, Hooker, Grant, and Arthur Counties. This is an example of a weak soils-hydrology interaction apparent in the less dense stream network pattern of the soil map illustrated in the inset boxes compared to Figures 4.2 and 4.3.

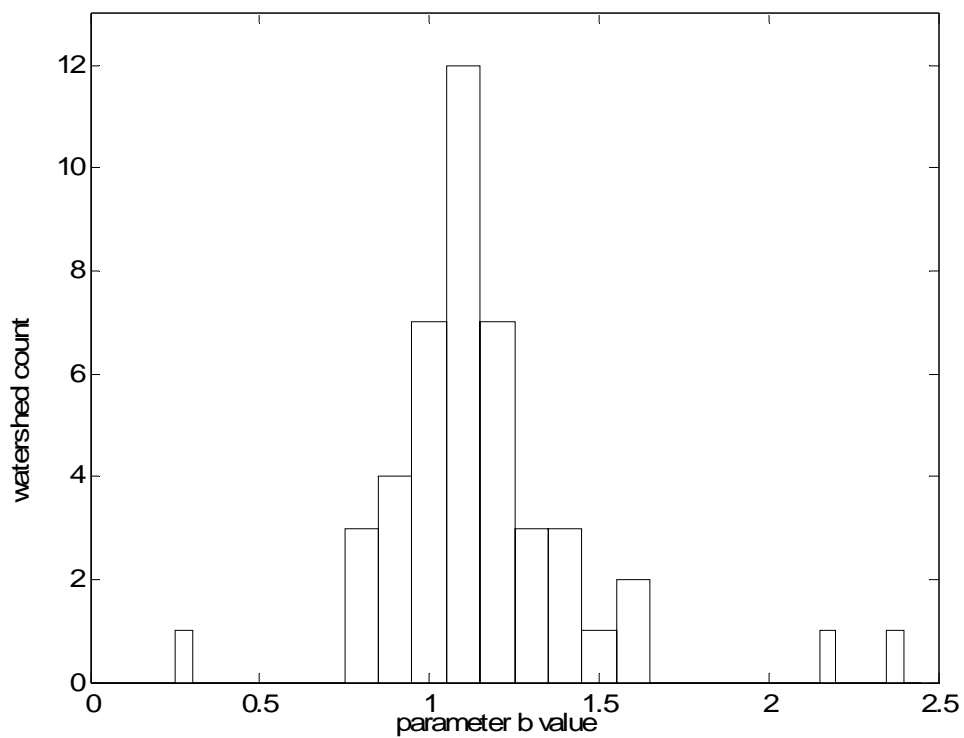


**Figure 4.5.** The distribution of the empirically based parameter  $b$  across the watersheds in the sample. The parameter  $b$  is the slope of the regression line through the  $\log(-dQ/dt)$  vs  $\log(Q)$  scatterplot.

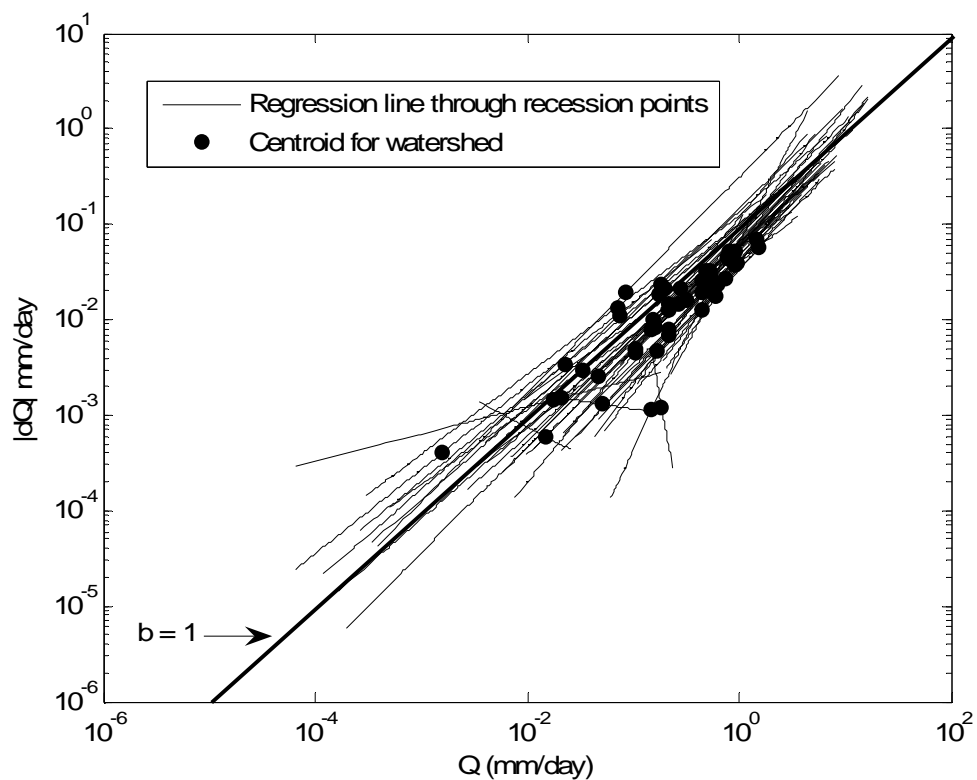


**Figure 4.6.** Regression lines fit to streamflow recession for all 48 watersheds studied. The line when parameter  $b=1$  is included as a reference. Each line extends over the range of the data for the particular watershed.

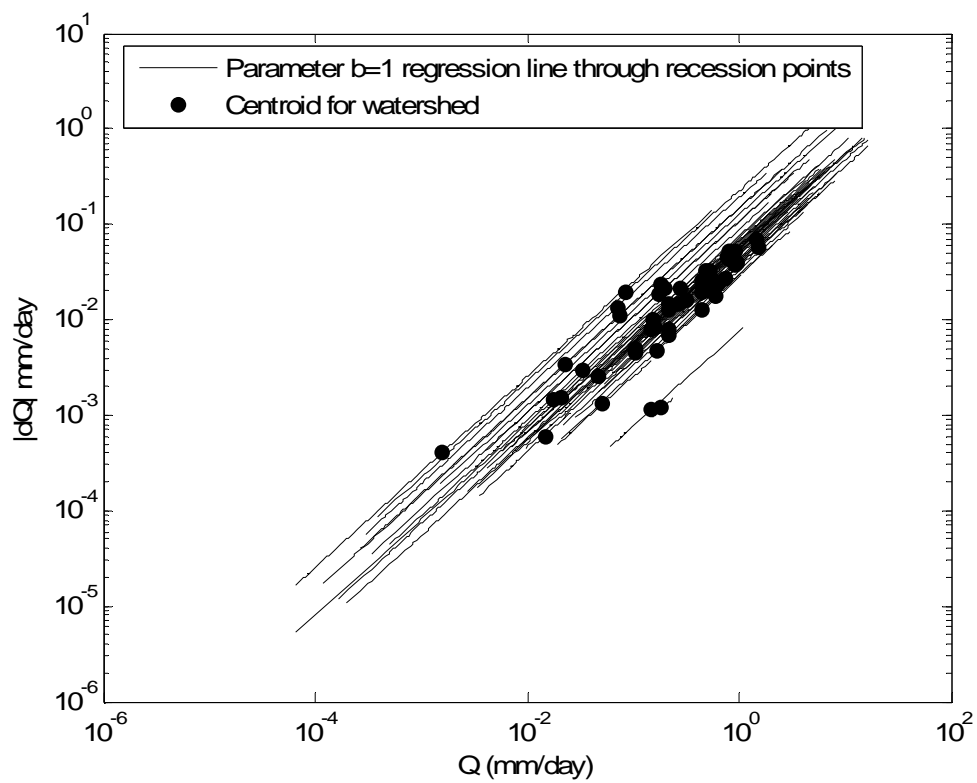


**Figure 4.7.** Regression lines fit to streamflow recessions for all 48 watersheds, with the constraint  $b=1$ . Each line extends over the range of the data for the particular watershed.

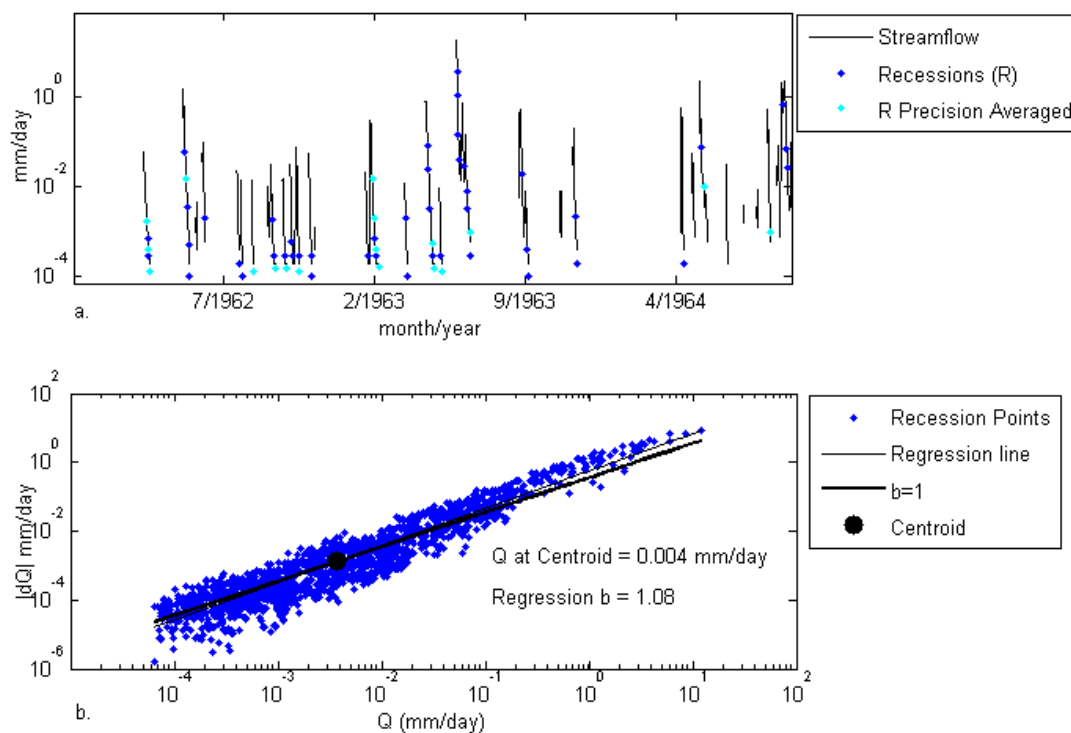


**Figure 4.8.** Recession information extracted from USGS station 08194200, for the San Casimiro Creek near Freer, Texas in Webb County, with Figure 4.8a showing 1000 days of streamflow data on a log scale with points where recessions were selected (blue and cyan) and averaged (cyan only). In Figure 4.8b, the selected recession points from the entire length of record (1962-2004; 15613 days) are plotted on log scale and a regression line fit to  $\log(-dQ/dt)$  versus  $\log(Q)$ .

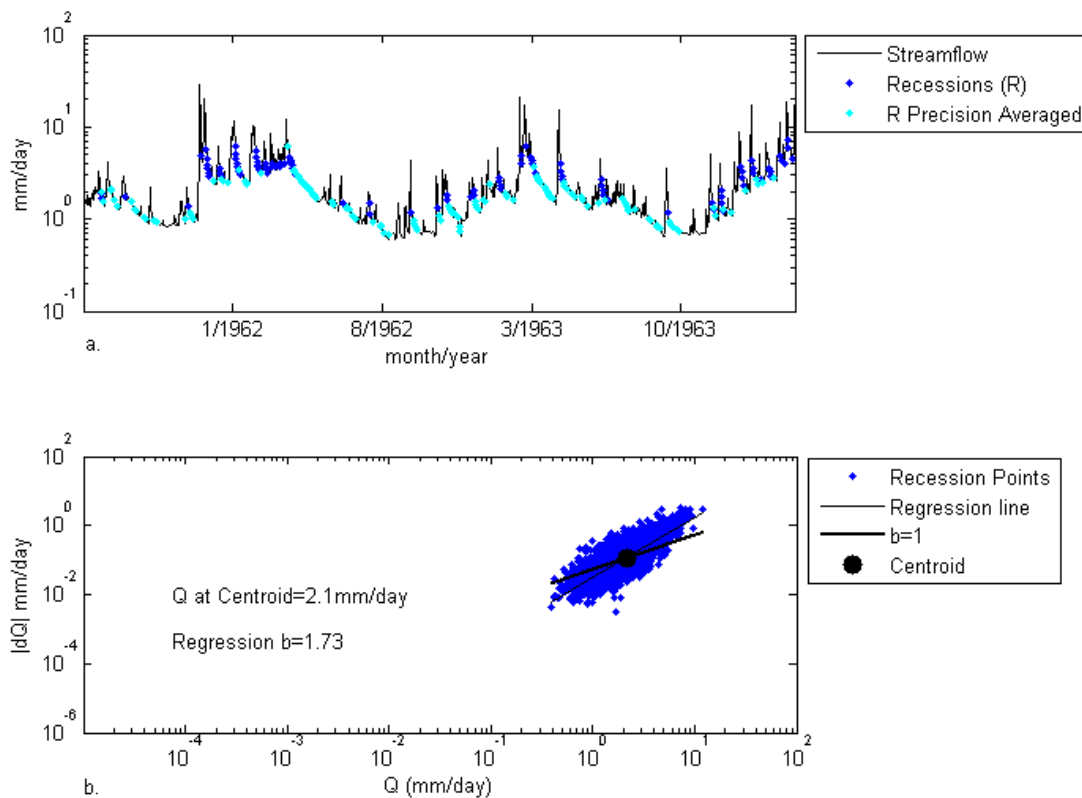


**Figure 4.9.** Recession information extracted from USGS station 03500240, for the for the Cartoogechaye Creek near Franklin, North Carolina in Macon County, with Figure 4.9a showing the first 1000 days of streamflow data on a log scale with points where recessions were selected (blue and cyan) and averaged (cyan only). In Figure 4.9b, the selected recession points from the entire length of record (1961-2005; 16162 days) are plotted on log scale and a regression line fit to  $\log(-dQ/dt)$  versus  $\log(Q)$ .

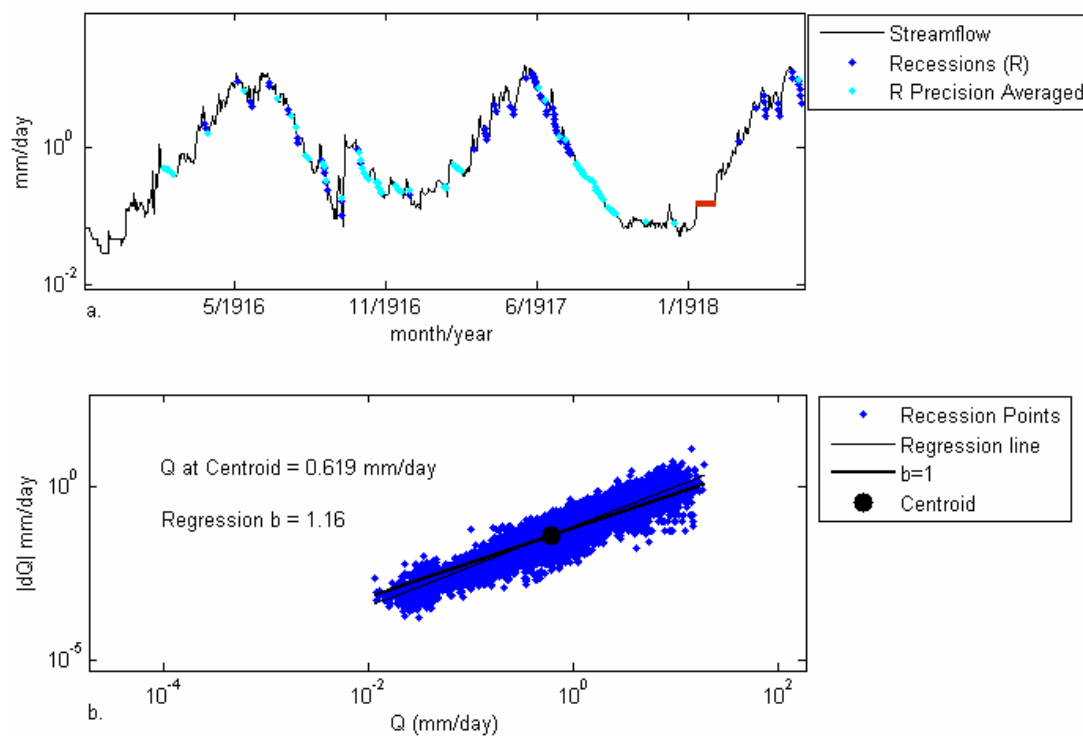


**Figure 4.10.** Recession information extracted from USGS station 11264500, for the Merced River at Happy Isles Bridge near Yosemite California in the Yosemite National Park soil survey area, with Figure 4.10a showing three years of streamflow data on a log scale with points where recessions were selected (blue and cyan) and averaged (cyan only). In Figure 4.10b, the selected recession points from the entire length of record (1915-2007; 33515 days) are plotted on log scale and a regression line fit to  $\log(-dQ/dt)$  versus  $\log(Q)$ . Missing data (February, 1918) is shown with a red line.



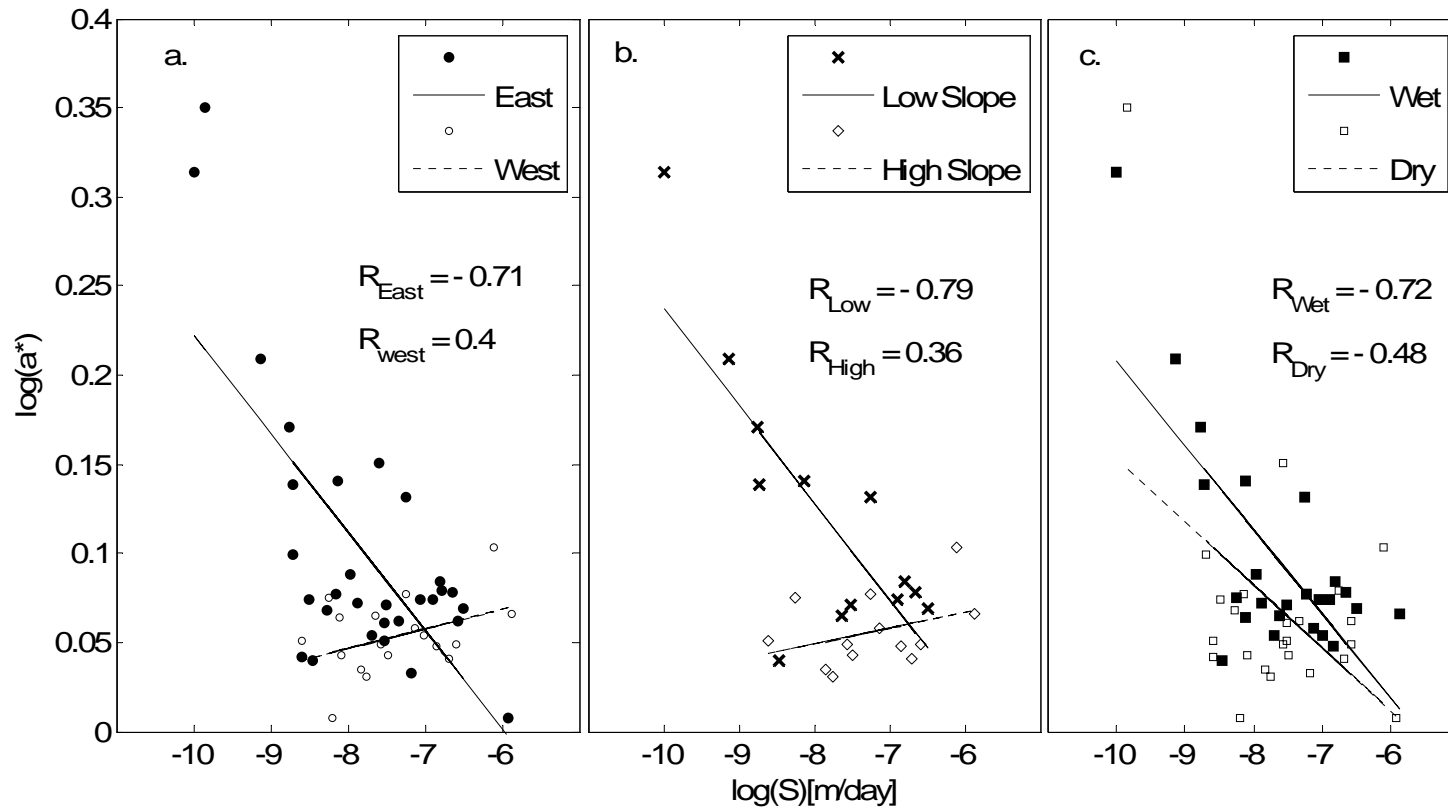


**Figure 4.11.** Log of streamflow recession parameter  $a^*$  [ $\text{day}^{-1}$ ] versus the log of soil sensitivity,  $S = K_{sat}/f$  [m/day], for the sample watersheds classified into a) East and West, b) Low and high average hillslope (hillslope  $< 0.02$  m/km and hillslope  $> 0.06$  m/km), and c) wet and dry (Annual precipitation threshold 1000 mm).



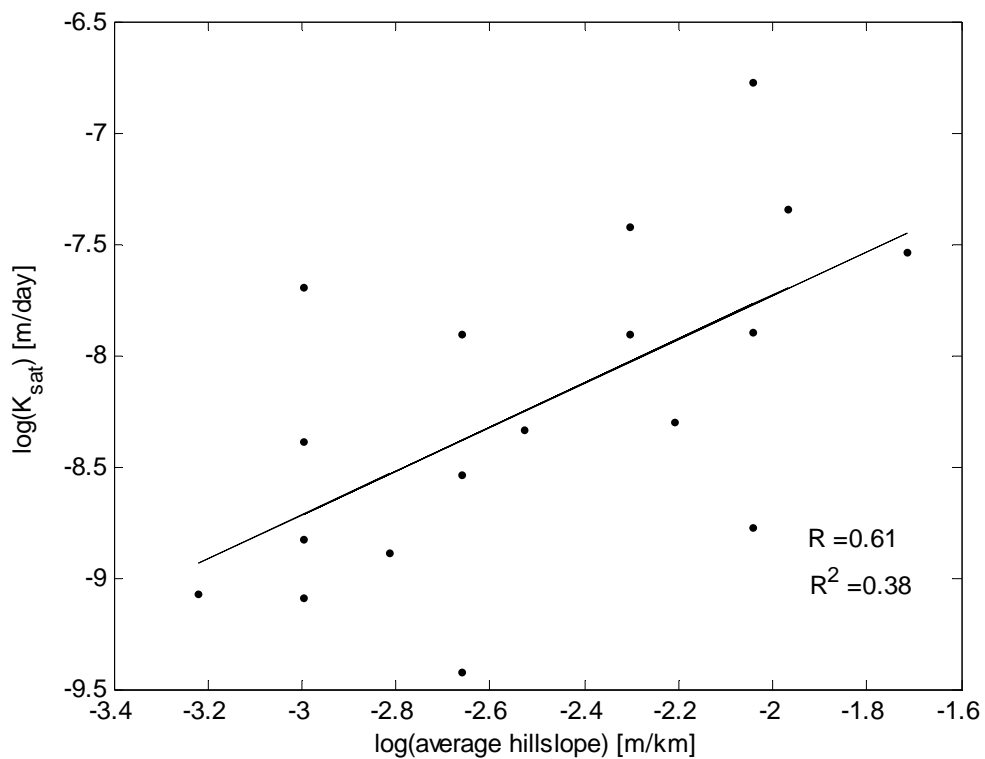


**Figure 4.13.** Log of watershed averaged saturated hydraulic conductivity versus the log of average hillslope for the sample subset from the western United States.

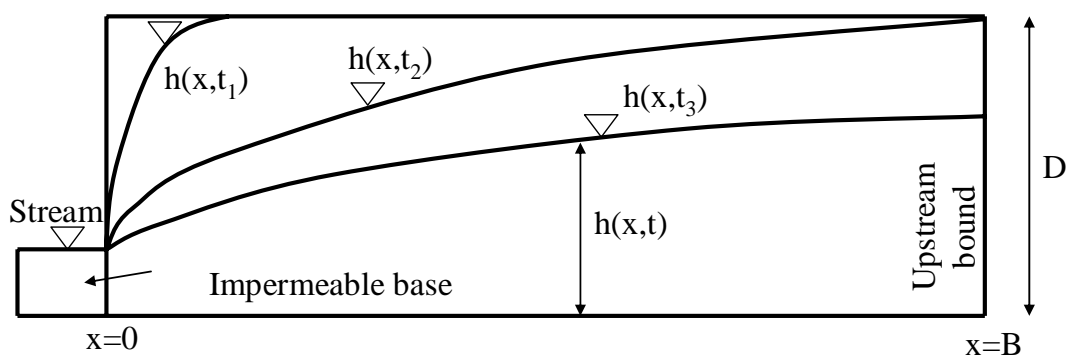


**Figure 4.14.** Definition sketch for the Dupuit-Boussinesq aquifer model depicting the changing shape of the free groundwater surface through time,  $h(x,t)$ , starting from saturation [adapted from Szilagyi *et al.*, 1998, Figure 1].

## CHAPTER 5

### SUMMARY, CONCLUSIONS, AND RECOMMENDATIONS

This research approaches distributed modeling as an opportunity to advance understanding of natural systems and addresses questions relevant to predicting streamflow in ungauged basins. Chapters 2 through 4 present the main results of this dissertation. The important conclusions and recommendations of the work are summarized in this chapter. Streamflow prediction of ungauged basins is an unsolved scientific problem that is important for developing policies for more efficient water resources management, flood forecasting, and land use management. Advanced methods in hydrology are required to learn how to best use the hydrologic information that is available for streamflow prediction.

This dissertation focuses on three topics related to distributed hydrologic modeling in ungauged basins. The first topic uses spatially distributed hydrologic models with distributed radar precipitation inputs to show the potential for distributed models to be useful operationally. The second topic uses advanced multi-objective calibration techniques that estimate parameter uncertainty to improve the model performance over the spatial extent of the watershed compared to a traditional calibration approach (manual or automatic) of calibrating the model at one measurement location. The third topic examines the relationship between high-resolution soils data and streamflow recession in order to improve the understanding of streamflow generation processes in different watersheds as well as the implications of using a priori parameters developed with high resolution soils data for distributed hydrologic modeling. The results of the research are

a contribution to the recently introduced field of hydrogeology [Lin *et al.*, 2006] with the vision that soils data can be used to improve hydrologic model predictions at the landscape level.

In the first paper (Chapter 2), we calibrated the rainfall-runoff model, Topnet, using the mean square error function. This improved the matching of the peak streamflows at the cost of over-predicting the low flows and introducing bias into the cumulative water balance. Single objective calibration does not use as much available data as is possible with multi-objective calibration, which is addressed in part with studies in Chapter 3. The use of a distributed model, Topnet, to simulate flow at ungauged interior locations was highlighted with the model results in Peacheater Creek at Christie, Oklahoma. Our model simulations with calibration were as good at interior locations, especially during the validation period, as in the larger scale basins. The small difference between calibrated and uncalibrated results for Topnet showed that, in some basins, flows could be predicted well with little or no calibration.

Participation in DMIP 1 (Chapter 2) was an important contribution in the collaborative effort initiated by the National Weather Service to move from lumped to distributed rainfall-runoff models that make better use distributed radar rainfall data for flood forecasting. However, as nice as it is to make good flow predictions, we do not know, for the watersheds studied in Chapter 2, how much of the model behavior is representative of reality. Distributed modeling studies like this stimulate questions and hypotheses that were pursued further in Chapters 3 and 4 in an effort to better understand and model the hydrologic response of watersheds. In Chapter 2 we confirmed that for TOPNET, with TOPMODEL controlling subsurface flow, the parameter  $f$  is highly

sensitive and its derivation from GIS soils information and careful calibration of the multiplier value is important for accurate streamflow simulations. In Chapter 3 we explored a method of improved model calibration and in Chapter 4 we assessed new ways to use soils information for parameter derivation. Future work related to distributed modeling comparison projects should be designed so that streamflow prediction uncertainties can be related to their source: radar rainfall, soils and vegetation data, sub-basin distribution, or network delineation.

In Chapter 3 we examined the application of multiple objective calibration to distributed hydrologic models using an in-stream temperature model and a rainfall-runoff model for test cases. This work compared calibration schemes to show that model predictions at ungauged locations can be improved by using data from multiple locations in the watershed rather than calibrating the model using only one location. When optimizing distributed models, we want to utilize available data that contains the most information for the modeled system, especially the ungauged component that is the focus of the modeling effort. The multi-objective calibration framework presented in Chapter 3 helps assess which data is most important.

For example, using a two-zone temperature and solute model in the Virgin River, Utah, USA, we show that main channel and surface storage temperatures are best modeled using temperatures from two locations, however, sub-surface storage is better represented using calibration at the location where sub-surface energy storage is a dominant process. Using Topnet, a rainfall-runoff model applied in the Illinois River, Arkansas, USA, we show that parameter sets that best predict flow at downstream locations do not necessarily predict flow as well at upstream interior locations. In this

case, when data at interior locations is not available, a calibration which includes a trade-off between fitting multiple locations in the watershed improves model predictions at interior locations while providing an improved assessment of the model uncertainty.

In both cases, incorporating information from multiple locations in the calibration scheme improves the model performance over the spatial extent of the watershed compared to an optimization approach of calibrating the distributed model at one downstream location while making predictions at multiple locations upstream. This is an important demonstration considering the challenges of calibrating distributed models, especially for applications where the model will be used for predictions at ungauged locations. The use of multiple locations in a multi-objective calibration is relevant regardless of the optimization algorithm that is selected. For example, multiple locations could be used with the multi-algorithm, genetically adaptive multi-objective method (AMALGAM), [Vrugt and Robinson, 2007] or other state-of-the-art multi-objective evolutionary algorithms [Tang *et al.*, 2006]. Future work could compare Case I or II with the AMALGAM optimization framework using additional watersheds (Case I) or field data (Case II).

In Chapter 4, we explored the empirical relationship between streamflow recession data from USGS streamgauges and high-resolution SSURGO soil data to test the general hypothesis that a relationship exists between plot scale soils data integrated across a catchment and catchment scale streamflow recession parameters. Using a random sample of watersheds from across the continental United States, we found a significant positive correlation between streamflow recession parameters and soil and watershed properties in steep watersheds. For less steep watersheds we found an inverse

relationship between recessions and hydraulic conductivity. A number of potential explanations for this covariation were presented in Chapter 4.

The research presented in Chapter 4 provides a new direction for developing a priori parameters developed with high resolution soils data for distributed hydrologic modeling and streamflow prediction at ungauged basins. The parameter values used to examine the relationships between soils and streamflow recession can be directly input to distributed rainfall-runoff models that use GIS derived soils data to parameterize soil depth, saturated hydraulic conductivity, and porosity – such as the rainfall runoff model used in Chapters 2 and 3. Future work should test streamflow predictions using parameters based on SSURGO data and assess the applicability of the general relationship between soils and streamflow recession developed in Chapter 4 to individual ungauged watersheds.

This research has approached spatially distributed hydrologic modeling with three complementary components: 1) spatially distributed inputs, 2) multi-objective calibration techniques, and 3) a priori parameter estimation. Each of these foci aim to reduce the predictive uncertainty in streamflow prediction at ungauged basins. Prediction of streamflow, sediment and water quality is most difficult at ungauged locations. Chapter 2 has shown how spatially distributed hydrologic modeling improves prediction of streamflow at ungauged basins compared to traditional modeling techniques. Advanced methods in hydrology are required to learn how to best use the hydrologic information that is available for streamflow prediction. Chapter 3 has shown that multi-objective calibration using multiple streamgauge locations improves prediction of streamflow at ungauged basins within or near the catchment compared to single-objective calibration at



a single downstream location. To reduce predictive uncertainty in streamflow models, especially at ungauged basins, improved knowledge and understanding of hydrologic processes is needed. Chapter 4 has shown relationships between soil properties from high-resolution soils data and streamflow recession parameters that can inform a priori parameter estimation for spatially distributed hydrologic models.

This research contributes to the broad quest to reduce uncertainty in predictions at ungauged basins (Chapter 2) by integrating developments of innovative modeling techniques (Chapter 3) with analysis that advances our understanding of natural systems (Chapter 4).

**References**

- Lin, H., J. Bouma, Y. Pachepsky, A. Western, J. Thompson, R. van Genuchten, H.-J. Vogel, and A. Lilly, (2006), Hydropedology: Synergistic integration of pedology and hydrology, *Water Resour. Res.*, 42.
- Tang, Y., P. Reed, and T. Wagener, (2006), How effective and efficient are multiobjective evolutionary algorithms at hydrologic model calibration?, *Hydrology and Earth System Sci.*, 10, 289-307.
- Vrugt, J. A., and B. A. Robinson, (2007), Improved evolutionary search from genetically adaptive multi-method search, *Proceedings of the National Academies of Science, USA*, 104(3), 708-711.

APPENDICES

## Appendix A

This appendix presents John Godfrey Saxe's (1816-1887) version of the famous

Indian legend [Saxe, 1963].

It was six men of Indostan  
To learning much inclined,  
Who went to see the Elephant  
(Though all of them were blind),  
That each by observation  
Might satisfy his mind.

The First approached the Elephant,  
And happening to fall  
Against his broad and sturdy side,  
At once began to bawl:  
"God bless me! but the Elephant  
Is very like a wall!"

The Second, feeling of the tusk  
Cried, "Ho! what have we here,  
So very round and smooth and sharp?  
To me `tis mighty clear  
This wonder of an Elephant  
Is very like a spear!"

The Third approached the animal,  
And happening to take  
The squirming trunk within his hands,  
Thus boldly up he spake:  
"I see," quoth he, "the Elephant  
Is very like a snake!"

The Fourth reached out an eager hand,  
And felt about the knee:  
"What most this wondrous beast is like  
Is mighty plain," quoth he;

"'Tis clear enough the Elephant  
Is very like a tree!"  
The Fifth, who chanced to touch the ear,  
Said: "E'en the blindest man  
Can tell what this resembles most;  
Deny the fact who can,  
This marvel of an Elephant  
Is very like a fan!"

The Sixth no sooner had begun  
About the beast to grope,  
Than, seizing on the swinging tail  
That fell within his scope.

"I see," quoth he, "the Elephant  
Is very like a rope!"

And so these men of Indostan  
Disputed loud and long,  
Each in his own opinion  
Exceeding stiff and strong,  
Though each was partly in the right,  
And all were in the wrong!

Moral:  
**So oft in theologic wars,  
The disputants, I ween,  
Rail on in utter ignorance  
Of what each other mean,  
And prate about an Elephant  
Not one of them has seen**

**References**

Saxe, J. G., (1963), *The Blind Men and the Elephant; John Godfrey Saxe's Version of the Famous Indian Legend*. Pictures by Paul Galdone, Whittlesey House, New York.

## Appendix B

This appendix presents a solution for recession parameter  $a^*$  based on linear regression. Brutsaert and Nieber [1977] used observed low streamflow data from six gauging stations in New York State and analytic solutions to the Boussinesq equation for nonlinear free surface groundwater flow to estimate soil and geomorphic parameters. They used the recession equation (B1)

$$-\frac{dQ}{dt} = aQ^b \quad (\text{B1})$$

where  $Q$  is flow from an unconfined, horizontal aquifer. The dimensions of parameter  $a$  depend on the value of the dimensionless parameter  $b$ . With  $Q$  in units of  $L^3T^{-1}$ , when  $b=1$ , parameter  $a$  has units of  $T^{-1}$ .

Equation A1 can also be written as Equation B2,

$$\log\left(-\frac{dQ}{dt}\right) = \log a + b \log Q \quad (\text{B2})$$

with  $Y$  and  $X$  defined as

$$Y = \log\left(-\frac{dQ}{dt}\right) \quad (\text{B3})$$

$$X = \log Q \quad (\text{B4})$$

equation B2 becomes:

$$Y = \log a + bX \quad (\text{B5})$$

Linear Regression solves for parameters  $\log(a)$  and  $b$  by minimizing the sum of square errors in this equation with observed  $X$  and  $Y$  values,  $X_i$  and  $Y_i$

$$SS = \sum (Y_i - (\log a + bX_i))^2 \quad (\text{B6})$$

To find the slope and constant that minimizes SS results in two equations (Equations B7 and B8) and two unknowns with

$$\frac{dSS}{d(\log a)} = 0 \quad (\text{B7})$$

$$\frac{dSS}{db} = 0 \quad (\text{B8})$$

However, if the slope is fixed at  $b=1$ , only Equation B7 remains. This equation, is solved as follows:

$$\frac{dSS}{d(\log a)} = \sum 2(Y_i - (\log a + bX_i))(-1) \quad (\text{B9})$$

$$\frac{dSS}{d(\log a)} = -\sum (2Y_i - 2\log a - 2bX_i) \quad (\text{B10})$$

$$\frac{dSS}{d(\log a)} = -2(\sum Y_i - n\log a - b\sum X_i) \quad (\text{B11})$$

Setting  $\frac{dSS}{d(\log a)}$  to zero and solving for  $\log(a)$  results in

$$0 = \sum Y_i - n\log a - b\sum X_i \quad (\text{B12})$$

$$\log a = \frac{\sum Y_i - b\sum X_i}{n} \quad (\text{B13})$$

$$\log a = \frac{1}{n}\sum Y_i - b\frac{1}{n}\sum X_i \quad (\text{B14})$$

$$\log a = \bar{Y} - b\bar{X} \quad (\text{B15})$$

Replacing Y and X with Equations B3 and B4

$$\log a = \text{arithmeticmean}\left(\log\left(\frac{-dQ}{dt}\right)\right) - b * \text{arithmeticmean}(\log(Q)) \quad (\text{B16})$$

These arithmetic means of the log transformed data represent the centroid of data, confirming the fact that regression lines pass through the centroid. With the assumption  $b=1$  and using logarithmic identities we can solve for parameter  $a$ .

$$\log(a) = \log(\text{geometricmean}\left(\frac{-dQ}{dt}\right)) - \log(\text{geometricmean}(Q)) \quad (\text{B17})$$

$$a = \frac{\text{geometricmean}\left(\frac{-dQ}{dt}\right)}{\text{geometricmean}(Q)} \quad (\text{B18})$$



Appendix C

Coauthor Approval Letters

# Utah State UNIVERSITY

DEPARTMENT OF CIVIL AND  
ENVIRONMENTAL ENGINEERING  
4110 Old Main Hill  
Logan UT 84322-4110  
Telephone: (435) 797-2932  
FAX: (435) 797-1185

Bethany Neilson  
Department of Civil and Environmental Engineering  
Utah State University  
Logan, UT 84322-4110

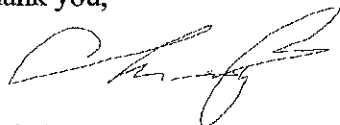
Dear Beth,

I am in the process of preparing my dissertation in the Civil and Environmental Engineering Department at Utah State University. I hope to complete my degree in May of 2008.

I am requesting your permission to include the attached paper, of which you are a coauthor, as a chapter in my dissertation. I will include acknowledgements to your contributions as indicated. Please advise me of any changes that you require.


Please indicate your approval of this request by signing in the space provided, attaching any other form or instruction necessary to confirm permission. If you have any questions please let me know.

Thank you,



Christina Bandaragoda

I hereby give permission to Christina Bandaragoda to use and reprint all of the material that I have contributed to Chapter 3 of her dissertation.



Dr. Bethany Neilson

# Utah State UNIVERSITY

DEPARTMENT OF CIVIL AND  
ENVIRONMENTAL ENGINEERING  
4110 Old Main Hill  
Logan UT 84322-4110  
Telephone: (435) 797-2932  
FAX: (435) 797-1185

Janis Boettinger  
Department of Plants, Soils, and Biometerology  
Utah State University  
Logan, UT 84322-4110

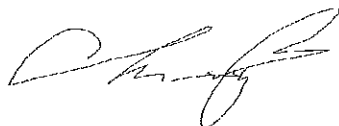
Dear Janis,

I am in the process of preparing my dissertation in the Civil and Environmental Engineering Department at Utah State University. I hope to complete my degree in May of 2008.

I am requesting your permission to include the attached paper, of which you are a coauthor, as a chapter in my dissertation. I will include acknowledgements to your contributions as indicated. Please advise me of any changes that you require.

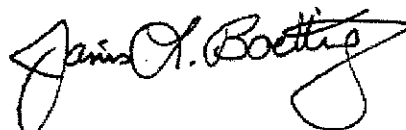
Please indicate your approval of this request by signing in the space provided, attaching any other form or instruction necessary to confirm permission. If you have any questions please let me know.

Thank you,



Christina Bandaragoda

I hereby give permission to Christina Bandaragoda to use and reprint all of the material that I have contributed to Chapter 4 of her dissertation.



---

Dr. Janis Boettinger

# Utah State UNIVERSITY

DEPARTMENT OF CIVIL AND  
ENVIRONMENTAL ENGINEERING  
4110 Old Main Hill  
Logan UT 84322-4110  
Telephone: (435) 797-2932  
FAX: (435) 797-1185

Ross Woods  
Department of Civil and Environmental Engineering  
Utah State University  
Logan, UT 84322-4110

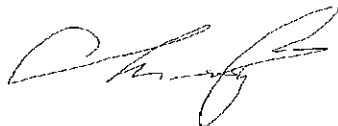
Dear Ross,

I am in the process of preparing my dissertation in the Civil and Environmental Engineering Department at Utah State University. I hope to complete my degree in May of 2008.

I am requesting your permission to include the attached paper, of which you are a coauthor, as chapters in my dissertation. I will include acknowledgements to your contributions as indicated. Please advise me of any changes that you require.

Please indicate your approval of this request by signing in the space provided, attaching any other form or instruction necessary to confirm permission. If you have any questions please let me know.

Thank you,



Christina Bandaragoda

I hereby give permission to Christina Bandaragoda to use and reprint all of the material that I have contributed to Chapters 2 and 4 of her dissertation.



---

Dr. Ross Woods

**CURRICULUM VITAE****Christina J. Bandaragoda****(August 2007)**10623 56<sup>th</sup> Ave W, Mukilteo, WA, 98275

Phone: 425-493-6502

Email: [christinamay@yahoo.com](mailto:christinamay@yahoo.com)**Education:**

Ph.D., Civil &amp; Environmental Engineering, Utah State University, Logan, Utah, 2007.

Concentrations: Hydrology, rainfall-runoff modeling, model calibration, water resources

Dissertation Title: Distributed Hydrologic Modeling for Streamflow Prediction at Ungauged Basins. Advisor: David G. Tarboton

M.B.A., Business Administration, Utah State University, Logan, Utah, 2006.

Concentrations: Economics, Environmental Economics

M.S., Biological &amp; Agricultural Engineering, Utah State University, 2001.

Concentrations: Remote sensing, geographic information systems, irrigation engineering, spatial data management for irrigation resources in development.

Thesis Title: "Mapping riparian resources in semi-arid watersheds using airborne multispectral imagery in the Escalante River corridor." Advisor: Christopher M. U. Neale

B.S. Wheaton College, Wheaton, Illinois, 1995.

Concentrations: Biology, Development Studies

**Areas of Interest:**

Hydrologic modeling for flood forecasting, economic development, and environmental and water resources management

Applying remote sensing and GIS technology for resource management

**Experience:**

CEO, Silver Tip Solutions, LLC. 2006 to present. Manage private consulting business for engineering software development and applications.

GAANN fellow, 2005-2007, Department of Civil &amp; Environmental Engineering, Utah State University, Logan, UT

Research intern, USGS EROS Data Center, International Program, Sioux Falls, SD, 2004 to 2005, Integrated Calibration and Sensitivity Analysis programs for Famine Early Warning System (FEWS) geospatial flood forecasting model (GeoSFM).

Graduate Research Assistant, Utah State University, Utah Water Research Laboratory, Logan, UT, from 2001 to 2004.. Participant in Distributed Model Intercomparison Project, National Weather Service.

Graduate Research Assistant, Utah State University, Remote Sensing Services Laboratory, Biological and Irrigation Engineering Department, from 1998 to 2001. Worked in the Dominican Republic creating survey questionnaire and developing hydro-agricultural database for irrigation resource development project. Managed large datasets used in image processing, data calibration, and classification, natural resource evaluation and ecosystem analysis.

Biological Technician, National Park Service, assisted in resource management projects including vegetation mapping and hydrology work for the Division of Water Rights (NPS). 1996-1998

**Teaching experience:**

Water Resources Engineering (CEE 5460/6460), Department of Civil and Environmental Engineering, Utah State University. Fall 2006

**Recognitions:**

Outstanding Student Paper with Bethany Neilson, *Data Collection Methodology for Dynamic Temperature Modeling, Testing, and Corroboration*, AGU Fall Conference 2005.

**Publications:**

**Thesis:**

May, Christina. 2000. Mapping Riparian Resources in Semi-Arid Watersheds Using Airborne Multispectral Imagery. Masters Thesis. Biological and Irrigation Engineering. Utah State University. Logan, UT.

**Refereed Papers:**

Artan, G., H. Gadain, J. L. Smith, K. Asante, C. Bandaragoda and J. Verdin, (2007), "Adequacy of Satellite Derived Rainfall Data for Stream Flow Modeling," Natural Hazards, May, 10.1007/s11069-007-9121-6

Bandaragoda, C., D. Tarboton, D. Maidment (2006), Hydrology's Efforts Toward the Cyberfrontier, *Eos Trans. AGU*, 87(1), 2, 10.1029/2006EO010005.

Bandaragoda, C, D.G. Tarboton, and R.Woods. (2004) "Application of Topnet in the Distributed Intercomparison Modeling Project", *Journal of Hydrology*, 298: 178-201, doi:10.1016/j.jhydrol.2004.03.038

May, Christina and Neale, Christopher M.U., (2000), "Mapping Riparian Resources in Semi-Arid Watersheds Using Airborne Multispectral Imagery", *Proceedings of Remote Sensing and Hydrology 2000 Symposium*, IAHS publication #267, Santa Fe, NM, April 2-7, pp.539-541.

Neilson, B. and C. Bandaragoda, (2007), " Data Collection Methodology for Dynamic Temperature Modeling, Testing, and Corroboration," *Journal of the North American Benthological Society*, In Review.

#### **Online material:**

Tarboton, D.G., Bandaragoda, C.B., Kaheil, Y., Zachry, M., Hult, C., (2003) Rainfall Runoff Processes. An online module developed for the National Weather Service COMET outreach program. <http://media.engineering.usu.edu/RRP/>

#### **Conference Proceedings & Posters:**

Neilson, B. T., Stevens, D. K., Chapra, S. C., Bandaragoda, C.J., Hardy, T.B., (2006), Model Development for Mass and Energy Transfer Between Main Channel Flows, Dead Zones, and the Hyporheic Zones in High Gradient Systems, *Eos Trans. AGU*, 87(36), Jt. Assem. Suppl. H22C-07.

Bandaragoda, C., Tarboton, D., (2006), Examination of the Relationship Between Plot Scale Soil Properties and Catchment Scale Streamflow Recession Properties, *Eos Trans. AGU*, 87(36), Jt. Assem. Suppl. H41A-02.

Artan, G., Gadain, H., Bandaragoda, C., Asante, K., Verdin, J., (2006), Utility of Satellite Derived Rainfall Data for Flood Risk Monitoring, *Eos Trans. AGU*, 87(36), Jt. Assem. Suppl.: H32A-02.

Neilson, B.T., C. Bandaragoda, D.K. Stevens, S.C. Chapra, T. B. Hardy, M. McKee. November 2006. Multiobjective Dynamic Stream Temperature Model Calibration: Understanding the Causes and Effects of Temperature Impairments and Uncertainty in Predictions. 2006 Annual Water Resources Conference. American Water Resources Association. Baltimore, MD.

Neilson, B.T., C. M. Bandaragoda, and D.K. Stevens. March 2006. Virgin River Temperature and Endangered Species. Water Environment Association of Utah 2006 Annual Conference. St. George, UT.

Neilson, B. T., Bandaragoda, C.J., (2005), Data Collection Methodology for Dynamic Temperature Modeling, Testing, and Corroboration, *Eos Trans. AGU*, 87(52), Fall Meet. Suppl. H13B-1332.

Tarboton, D. G., C. Bandaragoda and D. R. Maidment, (2005), "User Needs for a Community Hydrologic Information System," *Eos Trans. AGU*, 86(52): Fall Meet. Suppl., Abstract H23F-1498.

Bandaragoda, C., Artan, G., (2005), A Framework for the Calibration of a Spatially Distributed Hydrologic Model Using Multiple Streamgage Locations, *Eos Trans. AGU*, 87(52), Fall Meet. Suppl., Abstract H43A-0487.

Tarboton, D. G., C. Bandaragoda, Y. Kaheil, M. Zachry and W. Reed, (2003), "An Online Module on Rainfall Runoff Processes," *Eos Trans. AGU*, 84(47): Fall Meet. Suppl., Abstract ED32C-1213.

Bandaragoda, C., D. G. Tarboton and R. Woods, (2003), "Application of TOPNET to DMIP," AGU Hydrology Days, March 31-April 2. Fort Collins, CO.

Bandaragoda, C., D. G. Tarboton and R. Woods, (2002), "Application of TOPNET to DMIP," Presentation at National Weather Service Distributed Modeling Intercomparison Project Workshop, Silver Spring, Maryland, August 21

Bandaragoda, C, D.G. Tarboton, and R.Woods., (2002) "Towards model applications without calibration – the use of spatial and temporal data to estimate parameter values of physically based distributed models." AGU spring meeting poster, Washington D.C., May 28-31.

May, Christina and Neale, Christopher M.U., (1999), "Mapping Resources in the Escalante River Corridor using Airborne Multispectral Imagery"; Proceedings of the 17<sup>th</sup> Workshop on Color Photography and Videography in Resource Management, Reno NV, May 5-7, pp. 208-216.

### **SERVICE:**

Reviewer for *Advances in Water Resources* – 2006

Graduate Student Senate, 2002-2003; Organized Intermountain West Graduate Student Symposium.

EFICOR, New Delhi India. 1994; 1998, Ten months with non-profit organization in



India, research analysis of rural health center, water resource management and economic development projects.

**PROFESSIONAL DEVELOPMENT:**

Research Intern, National Institute of Water and Atmospheric Research (NIWA), Christchurch, New Zealand, Spring 2006. Worked on a priori parameter estimation studies for distributed models.

Modular Modeling System (MMS) Workshop - Utah State University - 2003

**OTHER RELATED SKILLS:**

Models/Modeling Packages

- TopNet/TopModel
- GeoSFM
- DAMBRK
- HEC-RAS

Field Work Experience

- Cross section/discharge measurements
- Temperature probe deployment
- Multi-probe deployment and use
- Tracer study tests
- Pebble counts
- Socio-economic questionnaire development and field survey

Software/Programming Languages

- Microsoft Word, Excel, Powerpoint
- C/C++
- Matlab
- ESRI ArcGIS

**PROFESSIONAL SOCIETIES:**

American Geophysical Union – 2001-current

American Society of Civil Engineers – 2001-current